Higgs Properties ATLAS

Nikos Karastathis
N.T.U. Athens & NIKHEF

On behalf of the
ATLAS Collaboration

LHC and ATLAS

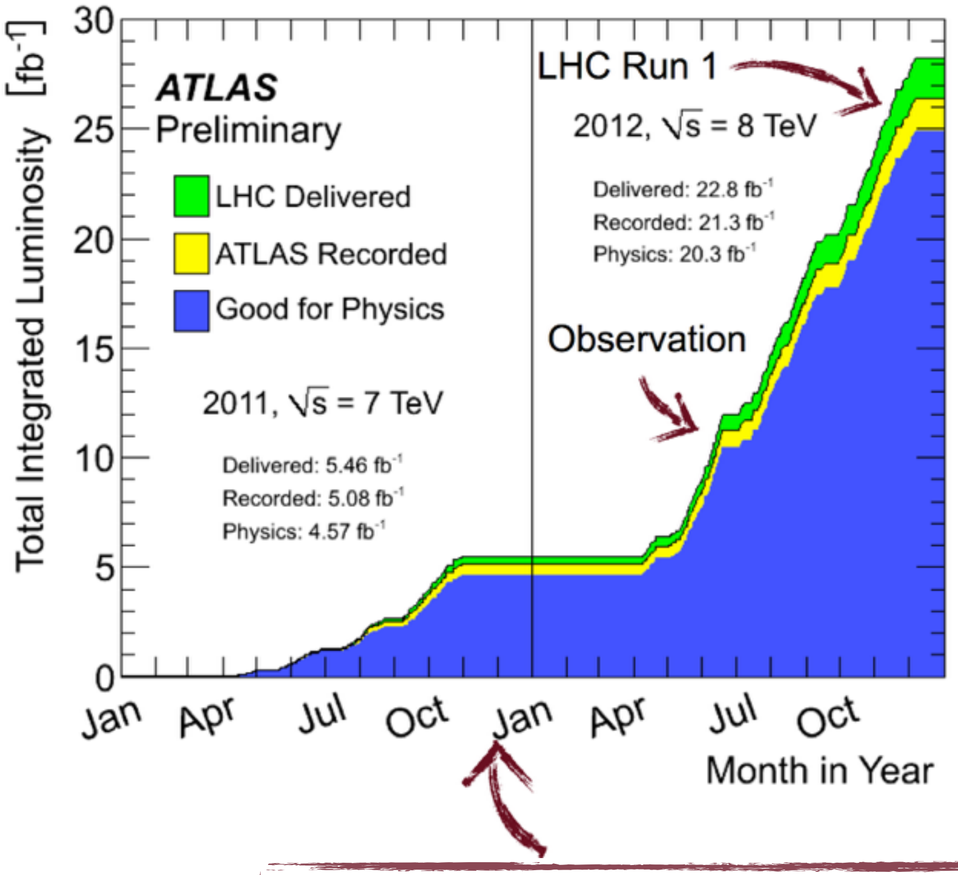

Excellent LHC & ATLAS Operations
Overall efficiency 90%

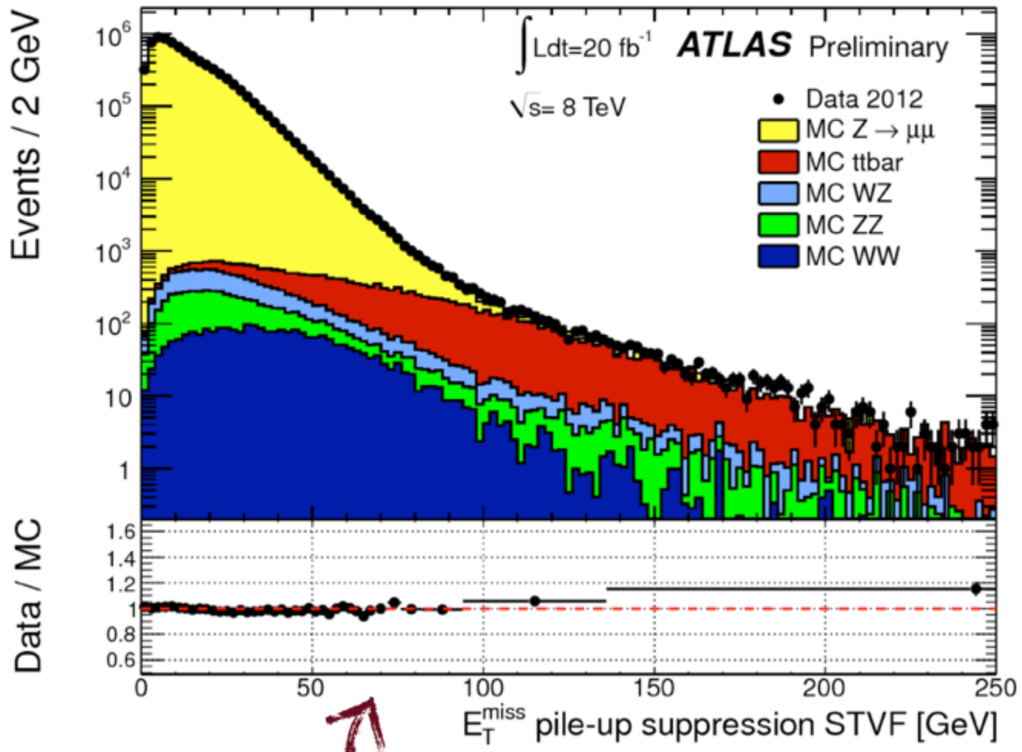

Excellent understanding of detector performance!

The amount of high quality data allows for detailed studies of the properties of the higgs boson!

Higgs Production & Decays

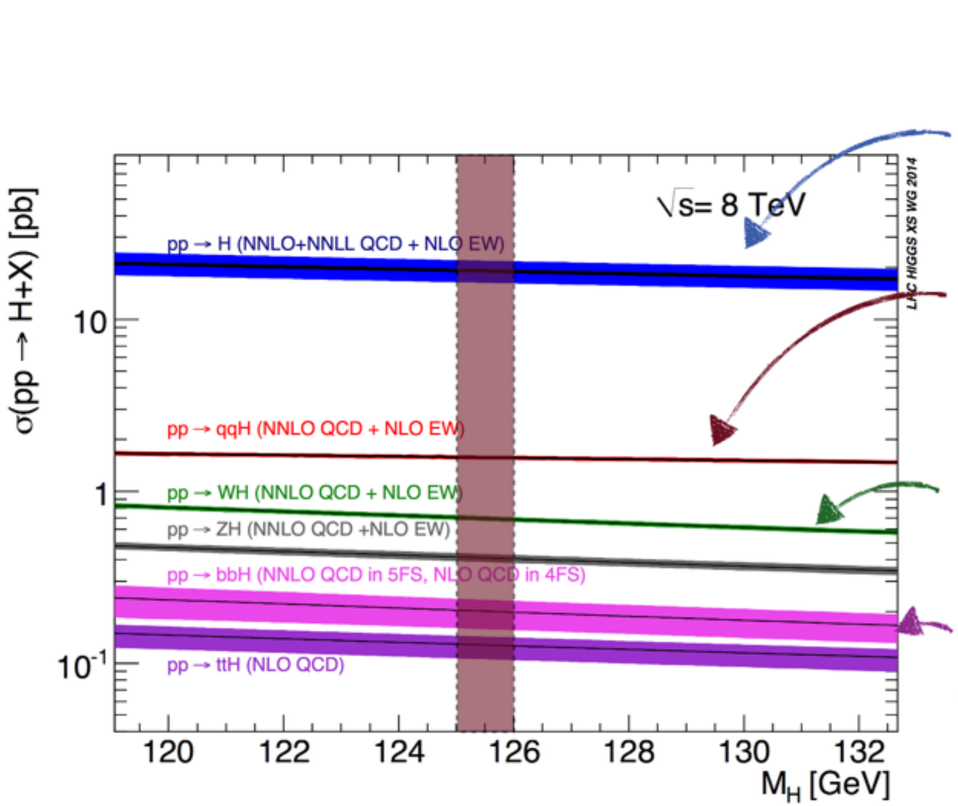

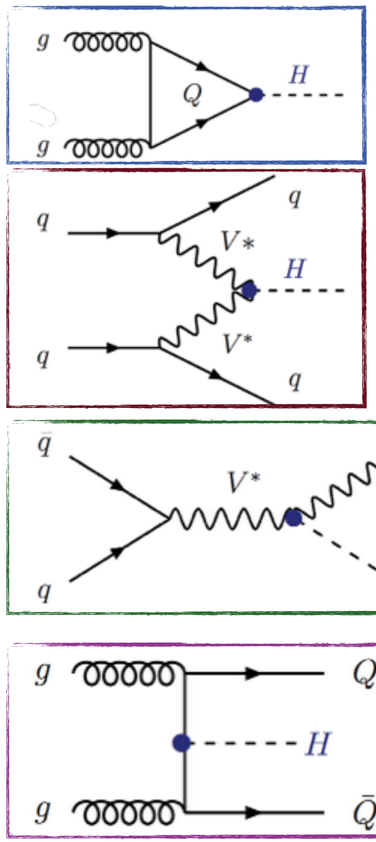

87%

7%

5%

~1%

for
m_H=125GeV

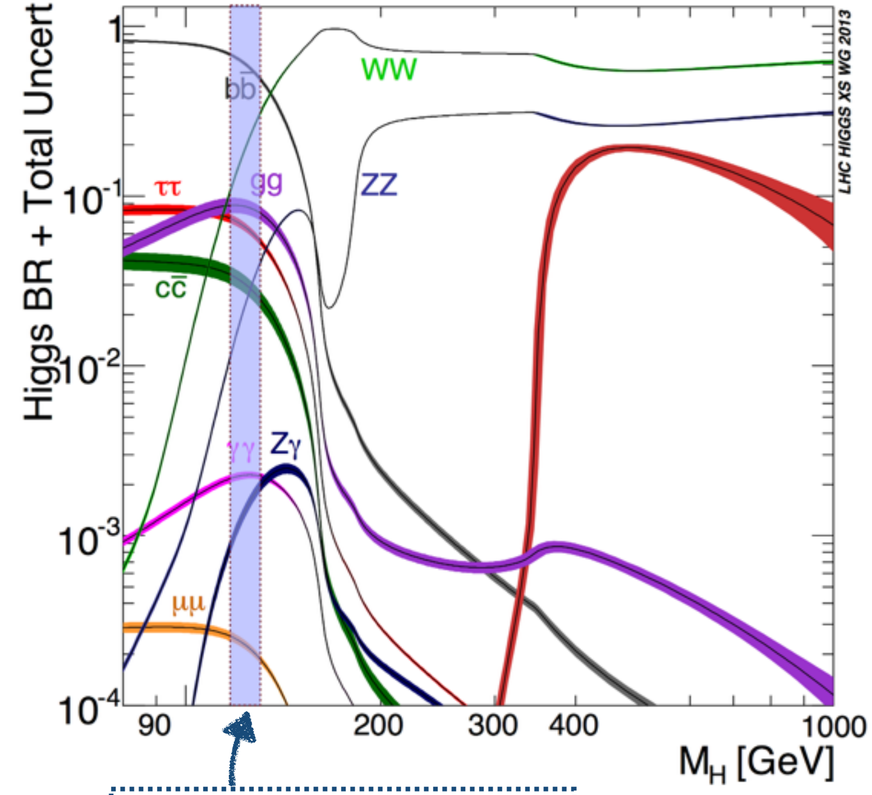

m_H~125GeV gives access to several decay modes

The production cross-section for m_H=125GeV

17.5pb @ 7 TeV → 57.4pb @ 14 TeV

start of Run I — Run II

Gauge bosons: γγ, ZZ*, WW*, Zγ

Fermions: ττ, bb, μμ

Phys. Rev. D 90, 052004

ATLAS-HIGG-2013-08

Mass: H→γγ

- Narrow peak in $m_{\gamma\gamma}$, clean signature, inclusive S/B ~ 3-4%
- Backgrounds:
  - ~80% di-photon → $m_{\gamma\gamma}$ resolution [~1.7GeV]
  - ~20% γj & jj → photon ID
- Signature: 2 isolated ($|\eta|<2.47$) high-E_T (>0.35 (0.25)*$m_{\gamma\gamma}$) photons
- Categories: (un)converted, central/transition, high-low p_{Tt}
- Discriminant: $m_{\gamma\gamma}$ distribution

Improved

- Optimization
  - new e/γ calibration (~10% improved resolution)
  - photon quality due to event categorization

$p_{T\gamma\gamma}$ perpendicular to γγ thrust axis

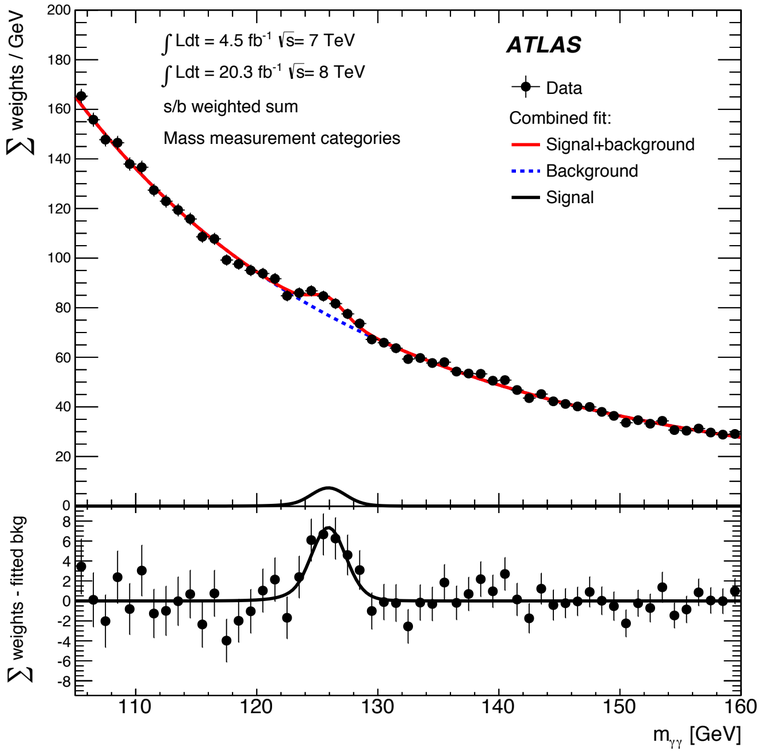

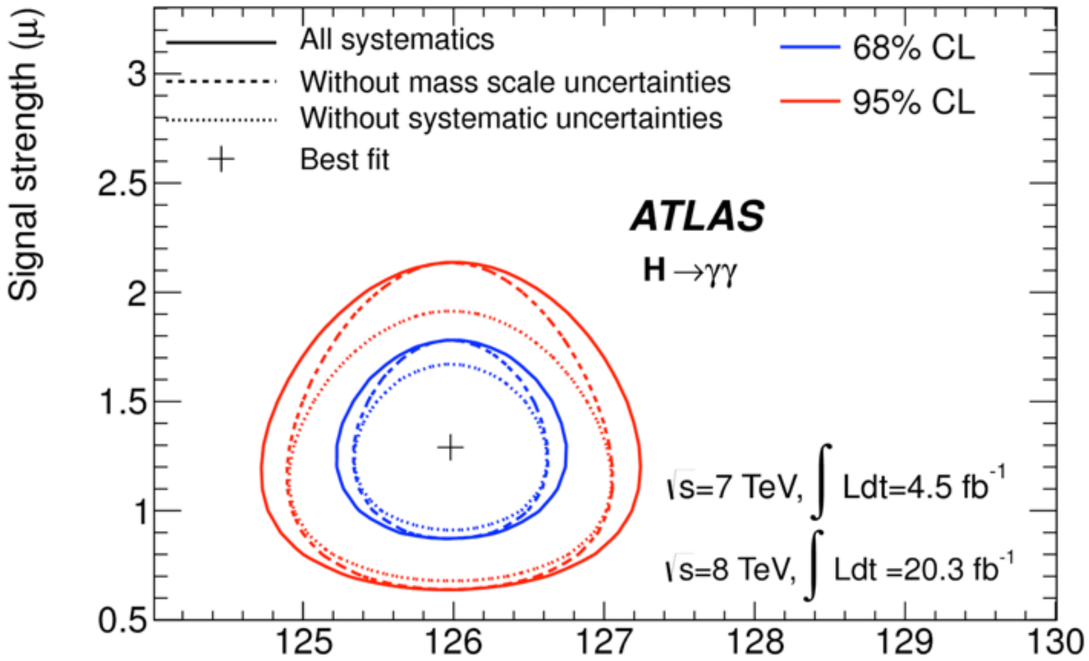

Maximum local significance $7.4\sigma(4.1\sigma)$
at $m_H = 125.98 \pm 0.50\ GeV$
with $\mu = 1.29 \pm 0.30$
Direct limit $\Gamma_H < 5.0\ (6.2)\ GeV$
at $95\%\ CL$

Updated couplings analysis

Nicolas' talk

Phys. Rev. D 90, 052004

Mass: H→ZZ*→4l

- High S/B~2 for 120-130GeV, excellent m_{res} (~1.6-2.2 GeV)
- Signature: SF , OS, isolated di-leptons (req. p_T, vertexing and m_{ll})
- Backgrounds: ZZ→4l, Z+jets, $t\bar{t}$
- Discriminant: 2D information from m_{4l} & O_{BDTzz}
- Optimization
  - electron identification → Likelihood method
  - Updated EM calibration
  - Combined fit of track momentum and cluster energy
  - O_{BDTzz} :MVA to separate signal and ZZ* background

Improved

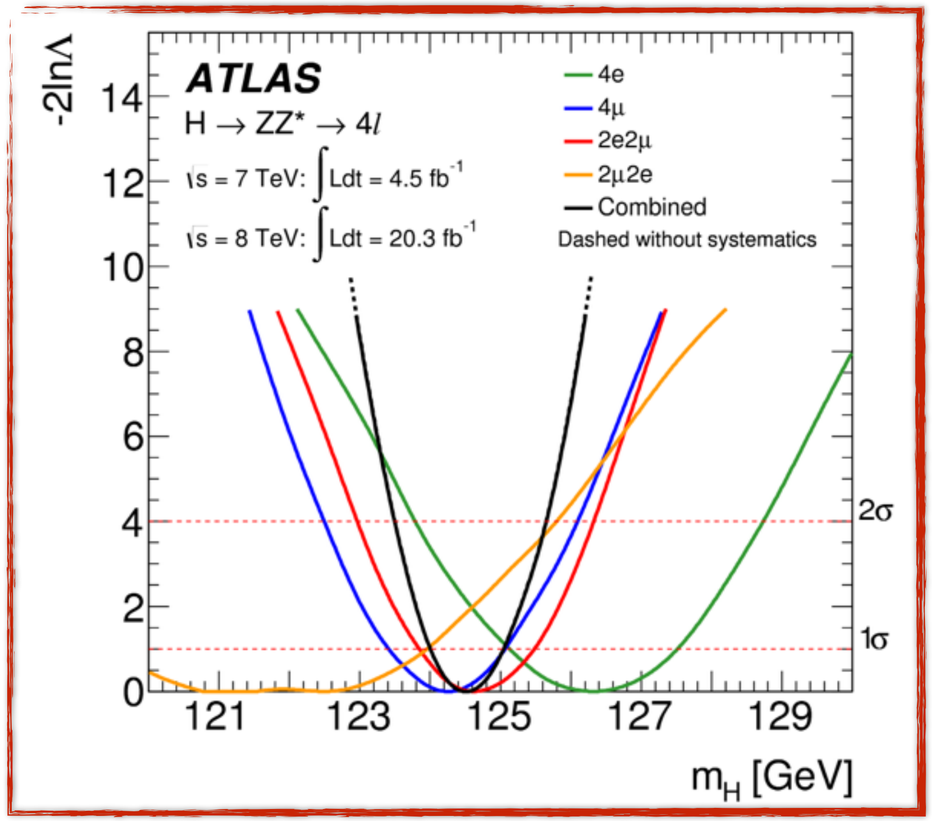

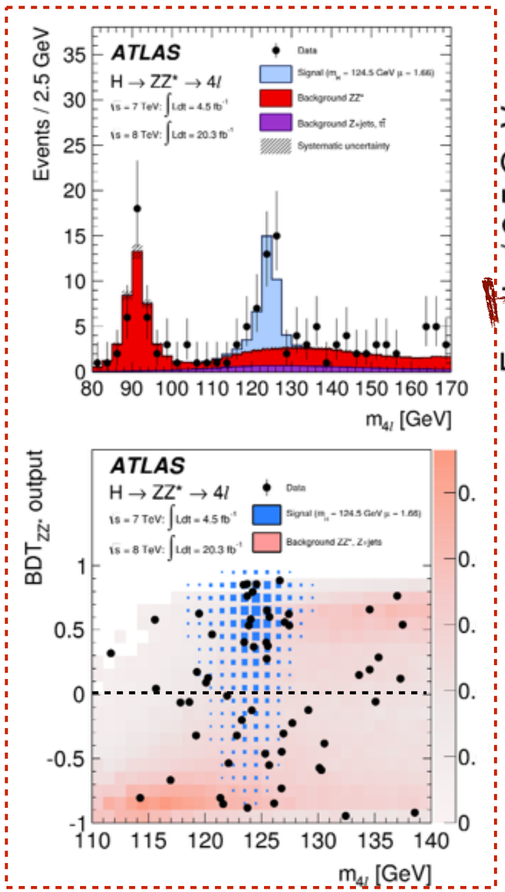

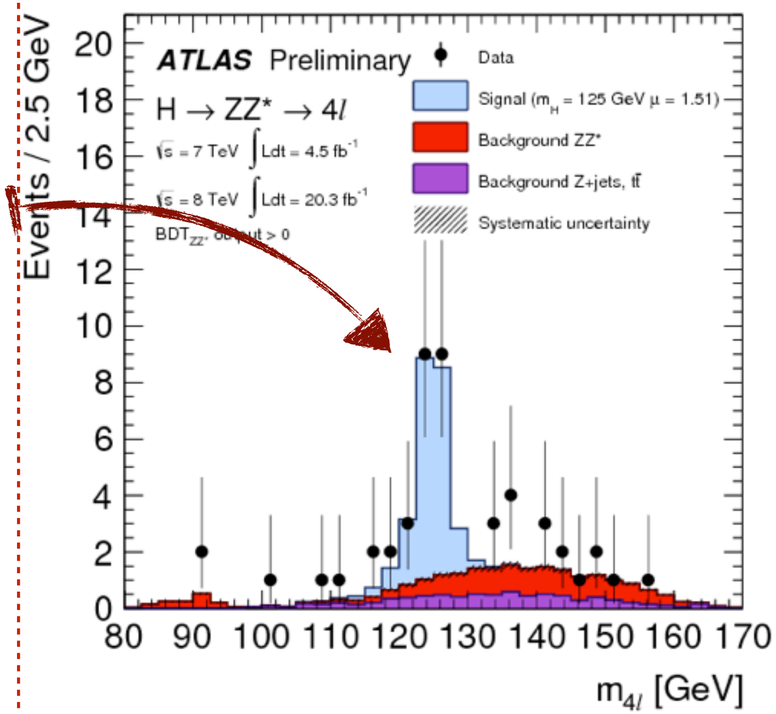

Updated couplings analysis

Nicolas' talk

Maximum local significance 8.2σ (5.8σ)

at $m_H = 124.51 \pm 0.52 GeV$

with $\mu = 1.66^{+0.45}_{-0.38}$

Direct limit $\Gamma_H < 2.6$ $(6.2) GeV$ at 95% CL

Phys. Rev. D 90, 052004

Mass: H→γγ & H→ZZ*

ATLAS higgs combined mass result:

$$m_H = 125.36 \pm 0.41\ GeV$$

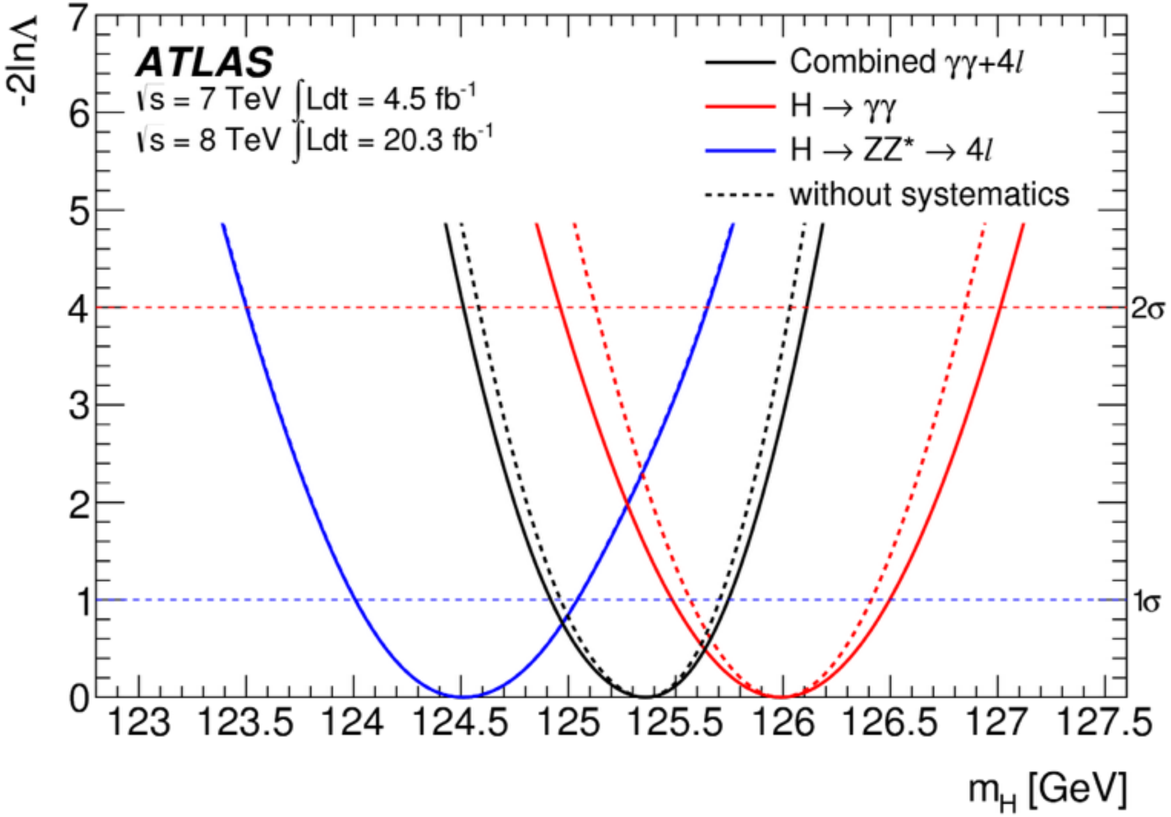

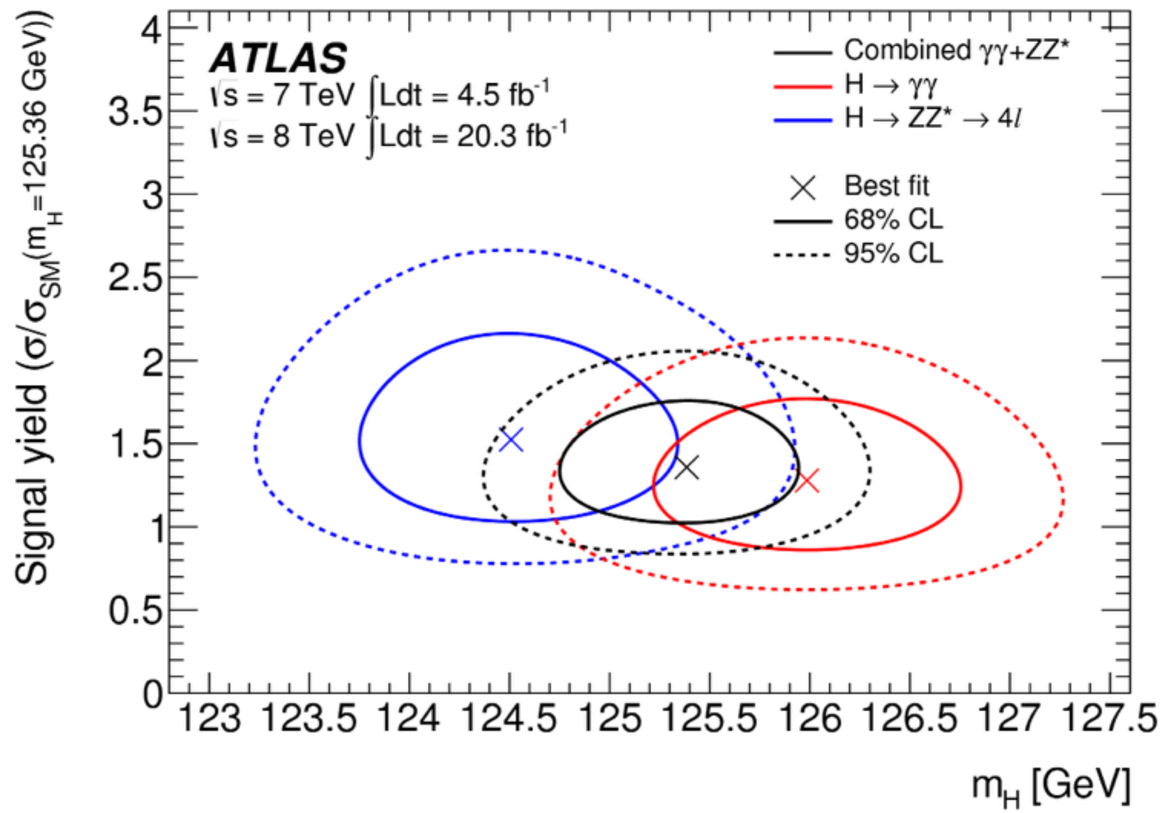

ATLAS-CONF-2014-042

$\mu_{\text{off-shell}}$ & Γ_H

- Direct $H \to ZZ \to 4l$: $\Gamma_H < 2.6$ (6.2@SM rate) GeV at 95% CLs
- Direct $H \to \gamma\gamma$: $\Gamma_H < 5.0$ (6.2@SM rate) GeV at 95% CLs

- Provide an upper limit on $\mu_{\text{off-shell}}$
  - combined with $\mu_{\text{on-shell}}$ also provides a limit on the Γ_H

$$\mu_{\text{on-shell}} = \frac{\kappa^2_{g,\text{on-shell}} \cdot \kappa^2_{V,\text{on-shell}}}{\Gamma_H/\Gamma^{\text{SM}}_H}$$

$$\mu_{\text{off-shell}} = \kappa^2_{g,\text{off-shell}} \cdot \kappa^2_{V,\text{off-shell}}$$

Implemented with $H \to ZZ$ with the assumptions

- Background insensitive to new physics modifying off-shell couplings
- $\kappa_{i,\text{on-shell}} = \kappa_{i,\text{off-shell}}$ (*)
- use inclusive selections
- $gg \to ZZ$ background K-factors in the off-shell region unknown

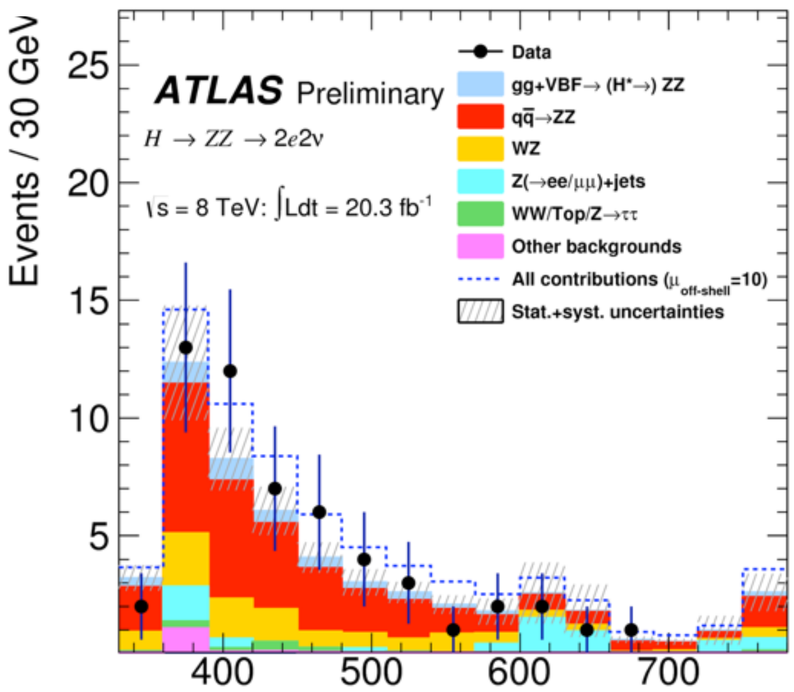

ZZ→llνν : Similar to ZH analysis
- Limit on off-shell rate based on event counting.

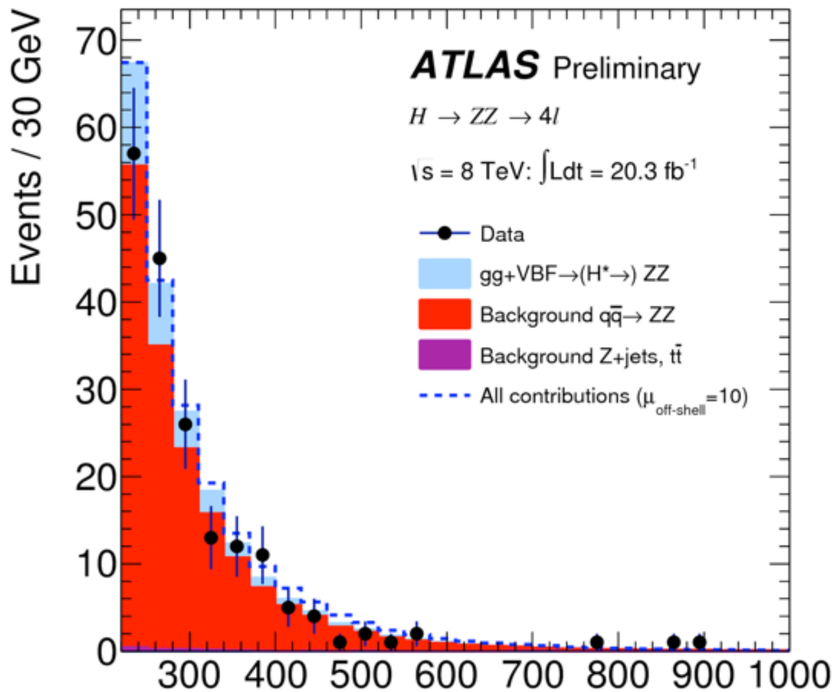

ZZ→4l : Similar to 4l analysis
- Limit on off-shell rate based on fit on matrix element kinematic discriminant shape.

ATLAS-CONF-2014-042

$\mu_{\text{off-shell}}$ & Γ_H

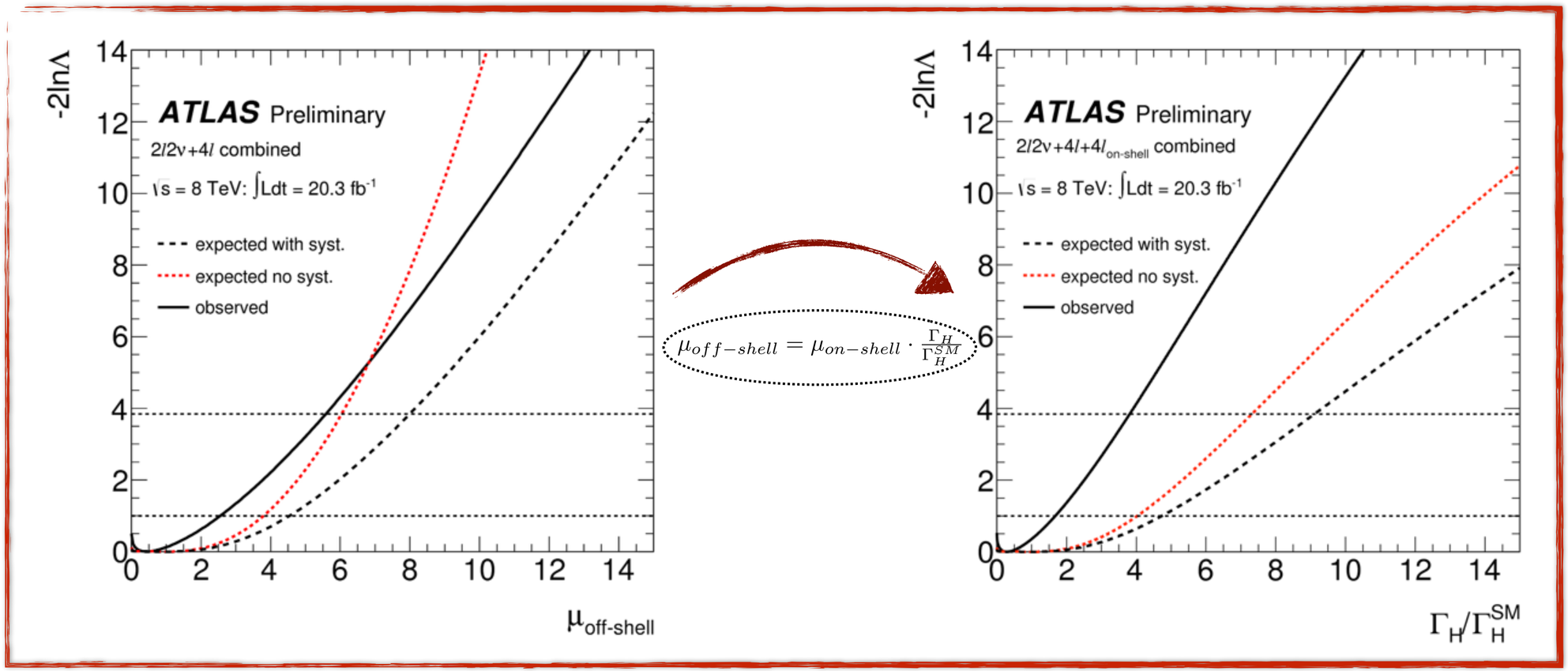

$$\mu_{off-shell} = \mu_{on-shell} \cdot \frac{\Gamma_H}{\Gamma_H^{SM}}$$

$$\mu_{on-shell} = 1.54^{+0.40}_{-0.34}$$

$$\mu_{off-shell} = 0.4^{+2.1}_{-0.4}$$

$$\frac{\Gamma_H}{\Gamma_H^{SM}} = 0.3^{+1.4}_{-0.3}$$

1σ compatibility

Assuming background K-factors same as for signal:

- $\Gamma_H/\Gamma_{SM}<4.8(5.8)$ at 95% CLs with alt. $R_{B,H^*}=1$, $\Gamma_H/\Gamma_{SM}=1$ and $\mu_{on\text{-}shell}=1.51$
- $\Gamma_H/\Gamma_{SM}<5.7(8.5)$ at 95% CLs with alt. $R_{B,H^*}=1$, $\Gamma_H/\Gamma_{SM}=1$ and $\mu_{on\text{-}shell}=1.00$

ATLAS-CONF-2013-075

Phys. Lett. B 726(2013), pp.99-119

H→WW*→lνlν

- Large S/B but low mass resolution
- Signature: Two high-pT, OS, isolated leptons + large MET
- Backgrounds: WW, st, W+jets, $t\bar{t}$
- Categorization: (S/D)F with ggF signal in 0/1-jet VBF with ≥2jet
- Discriminant: m_T distribution

$$m_T = \sqrt{(E_T^{\ell\ell} + E_T^{\nu\nu})^2 + |\vec{p}_T^{\,\ell\ell} + \vec{E}_T^{\nu\nu}|^2}$$

- Analysis designed to select VH(→ WW)
  - 3l final state: WH→WWW→lνlνlν
  - 4l final state: ZH→ZWW→lllνlν

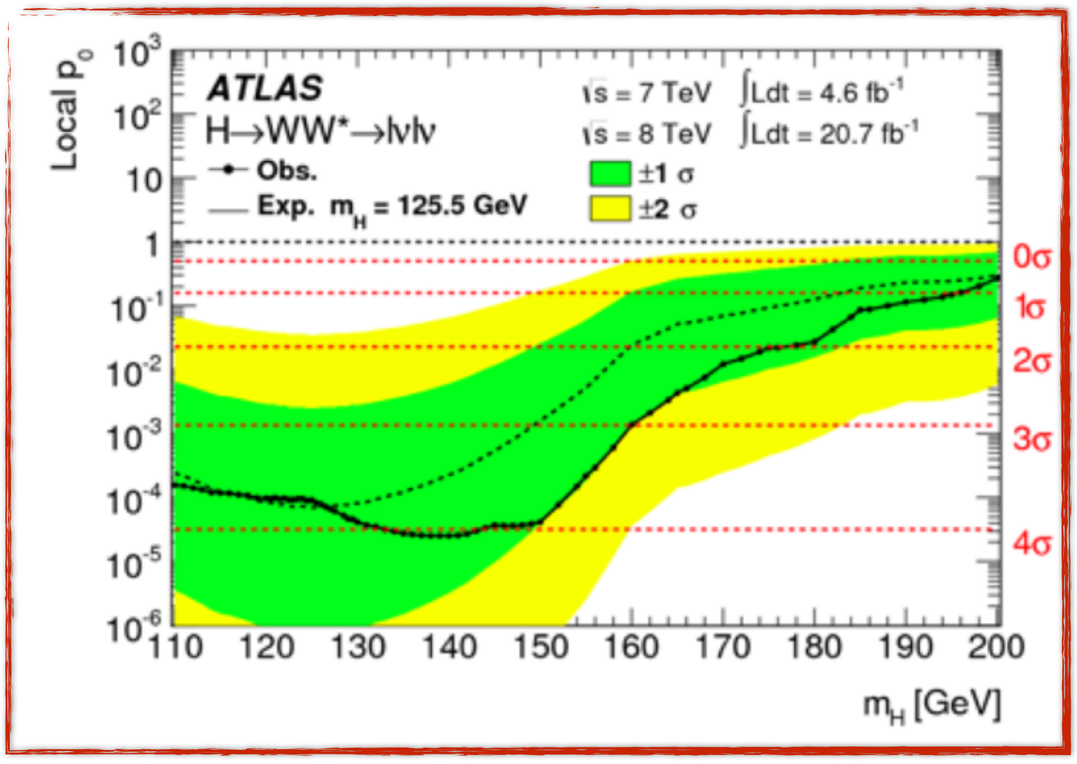

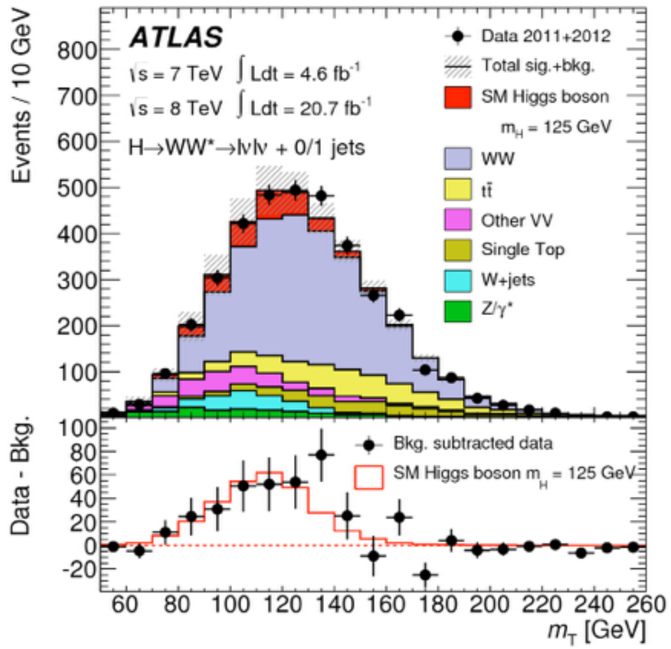

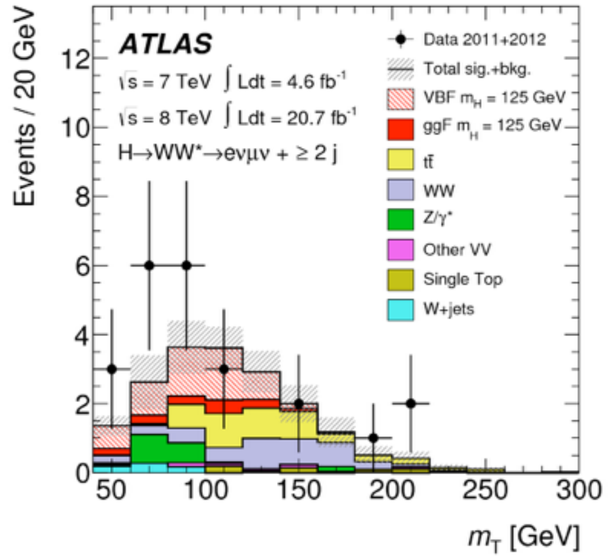

For mH=125GeV

Local significance $3.8\sigma\ (3.7\sigma)$

with

$\mu = 1.01 \pm 0.31$

Updated couplings analysis to appear

Nicolas' talk

ATLAS-CONF-2013-108

H→ττ

- BR~6.3% @ m_H=125GeV
- Signature: 3 channels: H→$\tau_{lep}\tau_{lep}$,$\tau_{had}\tau_{had}$ $\tau_{lep}\tau_{had}$ in 2 categories:VBF & Boosted
  - $\tau_{lep}\tau_{lep}$: 2 isolated O.S. leptons, with a τ_{had} veto, satisfying E_T, $m_{\tau\tau,vis}$ and $x_{\tau1,\tau2}$ requirements
  - $\tau_{lep}\tau_{had}$: 1 lepton and one τ_{had} candidate, m_T
  - $\tau_{had}\tau_{had}$: 2 τhad candidates with O.S., e/μ veto, p_T, η, $E_{T,miss}$
- Backgrounds: Z→ττ, W+jets, (DD), semileptonic $t\bar{t}$ (DD), multijet
- Discriminant: BDT score for each SR

For m_H=125 GeV

Nicolas' talk

local significance 4.1σ (3.2σ)

with

$\mu = 1.43\ ^{+0.31}_{-0.29}(stat)\ ^{+0.41}_{-0.30}(sys)$

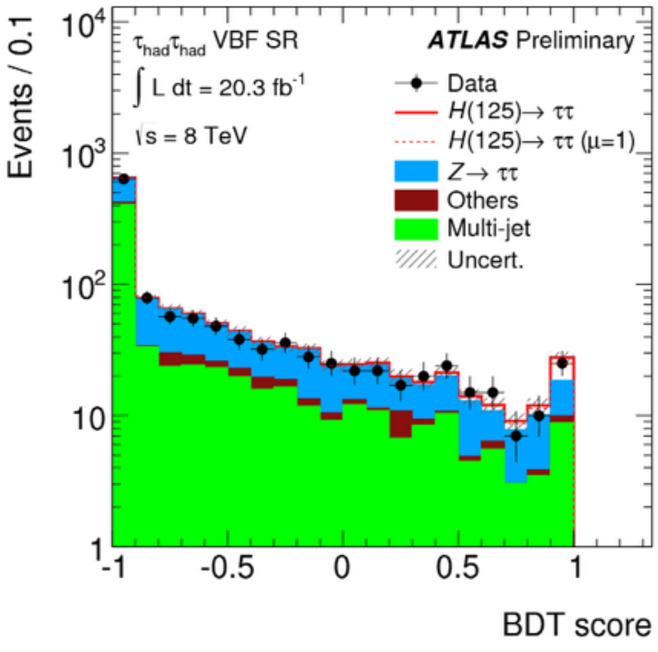

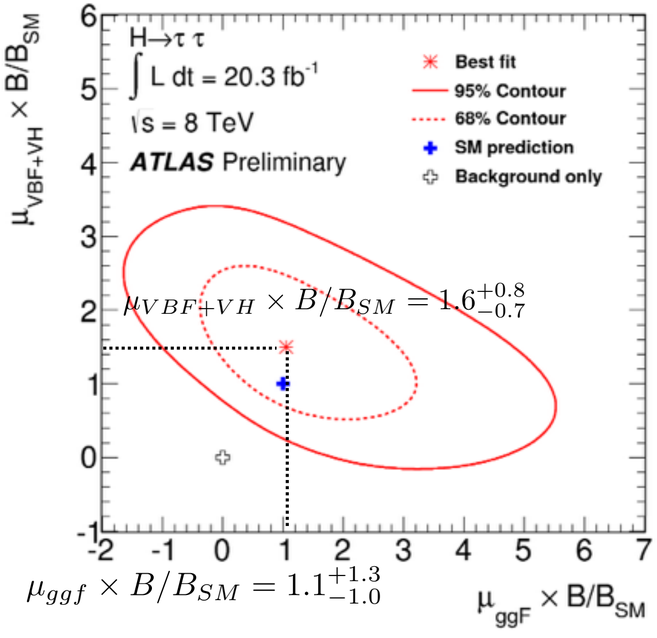

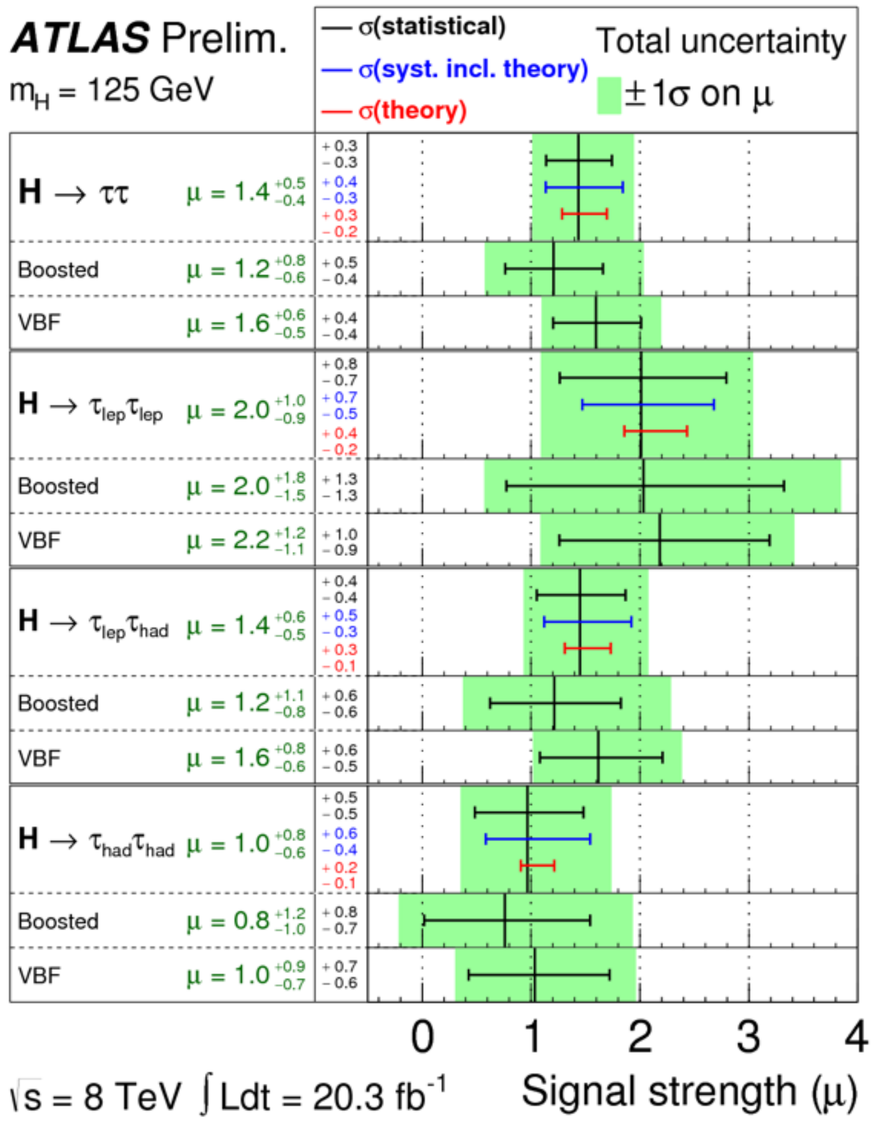

ATLAS-CONF-2013-079

arXiv:1409.6212

VH→bb

- BR~58% for m_H=125GeV
- Signature: 2 high-p_T isolated jets (p_T>20, |η|<2.5) [eff(b-tag)~70%]
  and 0,1,2 leptons from (W/Z) H→bb, W→lν, Z→ll, Z→νν
- Topological selection to suppress multijet and $t\bar{t}$, depending on $p_{T,V}$ intervals
- Categories: in terms of channel (0/1/2 lep), $p_{T,V}$ & jet multiplicity (2/3 jets)
- Backgrounds: $Wb\bar{b}$, $t\bar{t}$, multijet
- Discriminant: m_{bb} distribution

New analysis: MVA for 8TeV data

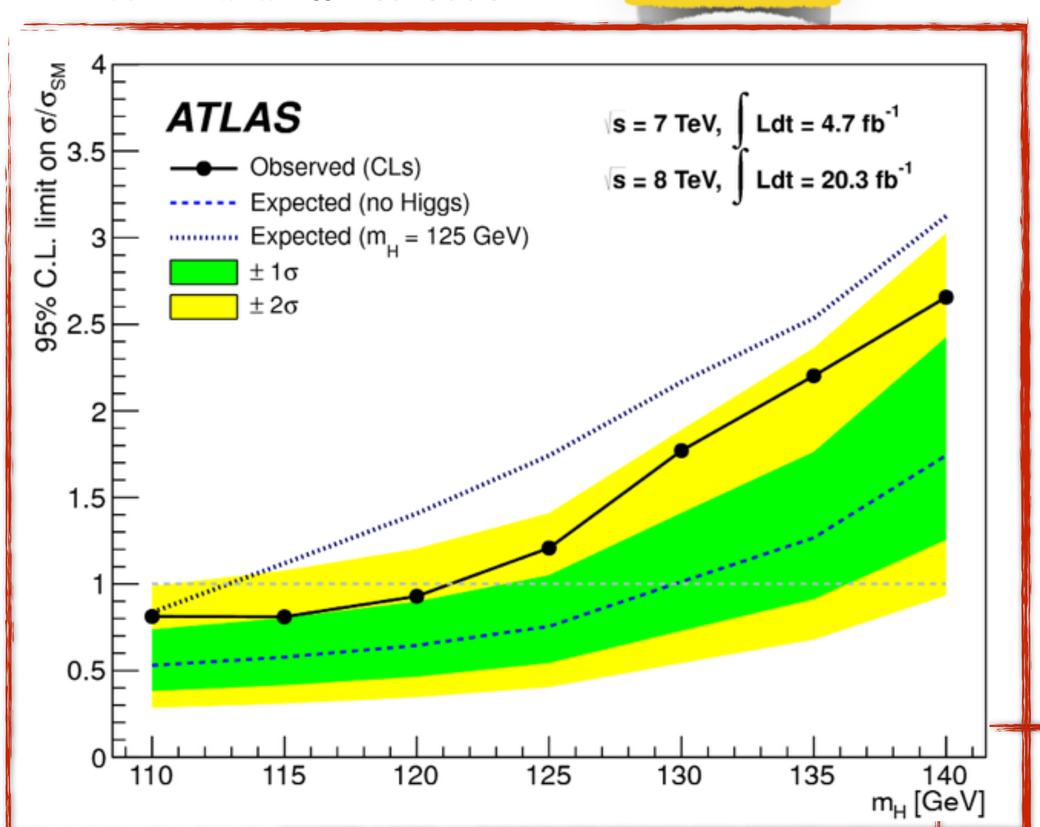

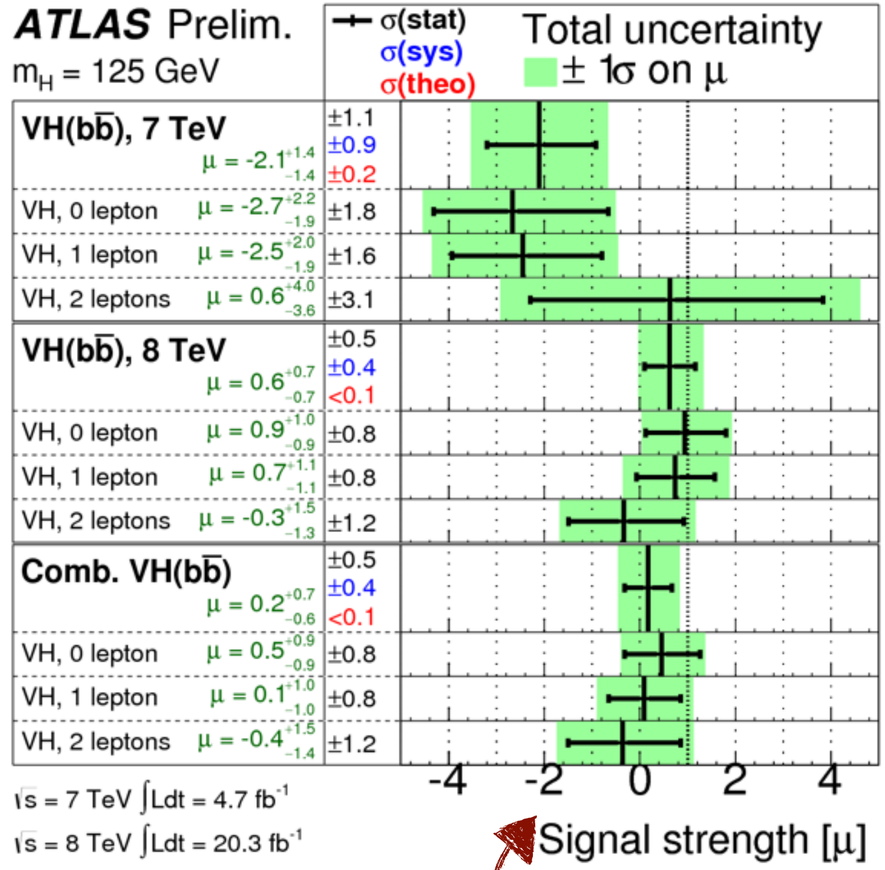

For m_H=125.36GeV

$1.4\sigma(2.6\sigma)$ significance with

$\mu = 0.52 \pm 0.32(stat) \pm 0.24(sys)$

NEW

Nicolas' talk

Analysis for couplings

For m_H=125GeV

1.4σ (1.3σ) significance with

$\mu = 0.2 \pm 0.5(stat) \pm 0.4(sys)$

Couplings: Signal Strength

ATLAS-CONF-2014-009

- 7+8 TeV: H→γγ, H→ZZ*, H→WW*, H→bb
- 8 TeV : H→ττ
- Hypothesis testing and CL based on the *profile likelihood ratio*
- Main theoretical uncertainty: cross-sections and BR

$$\mu^{H\to\gamma\gamma,ZZ^*,WW^*} = 1.35 \pm 0.14(stat)\ ^{+0.16}_{-0.14}(sys)$$

$$\mu^{H\to b\bar{b},\tau\tau} = 1.09 \pm 0.24(stat)\ ^{+0.27}_{-0.21}(sys)$$

3.7σ evidence for fermionic decay

for m_H=125.5GeV

$$\mu^{combined} = 1.30 \pm 0.12(stat)\ ^{+0.14}_{-0.11}(sys)$$

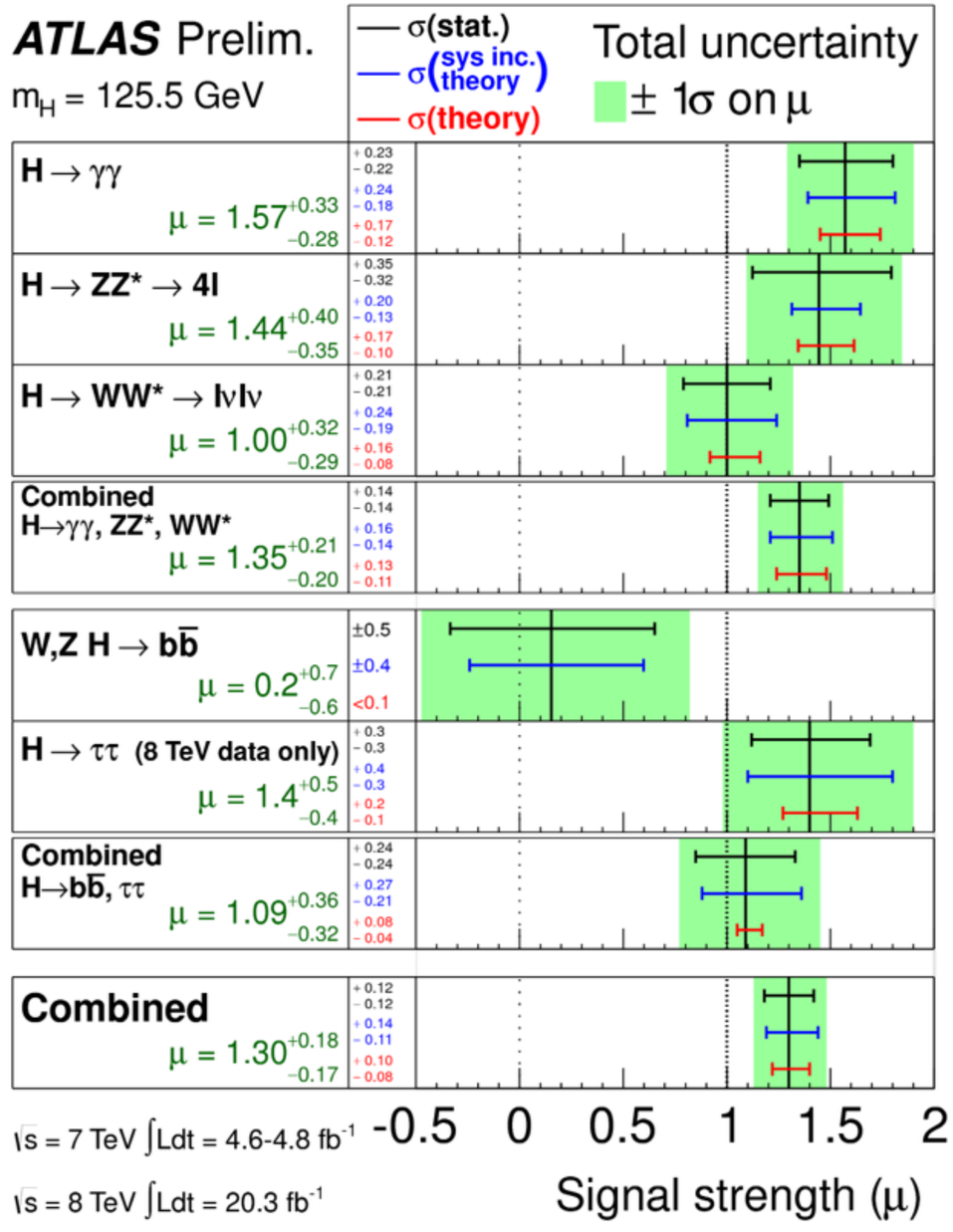

Couplings: Production modes

ATLAS-CONF-2014-009

- H → bb is not included (analysis only sensitive to VH as up to now)
- Assumption:

$$\mu_{VBF+VH} = \mu_{VBF} = \mu_{VH} \qquad \mu_{ggf+t\bar{t}H} = \mu_{ggf} = \mu_{t\bar{t}}$$

$$\frac{\mu_{VBF+VH}}{\mu_{ggf+t\bar{t}H}} = 1.4\ ^{+0.5}_{-0.4}(stat)\ ^{+0.4}_{-0.2}(sys)$$

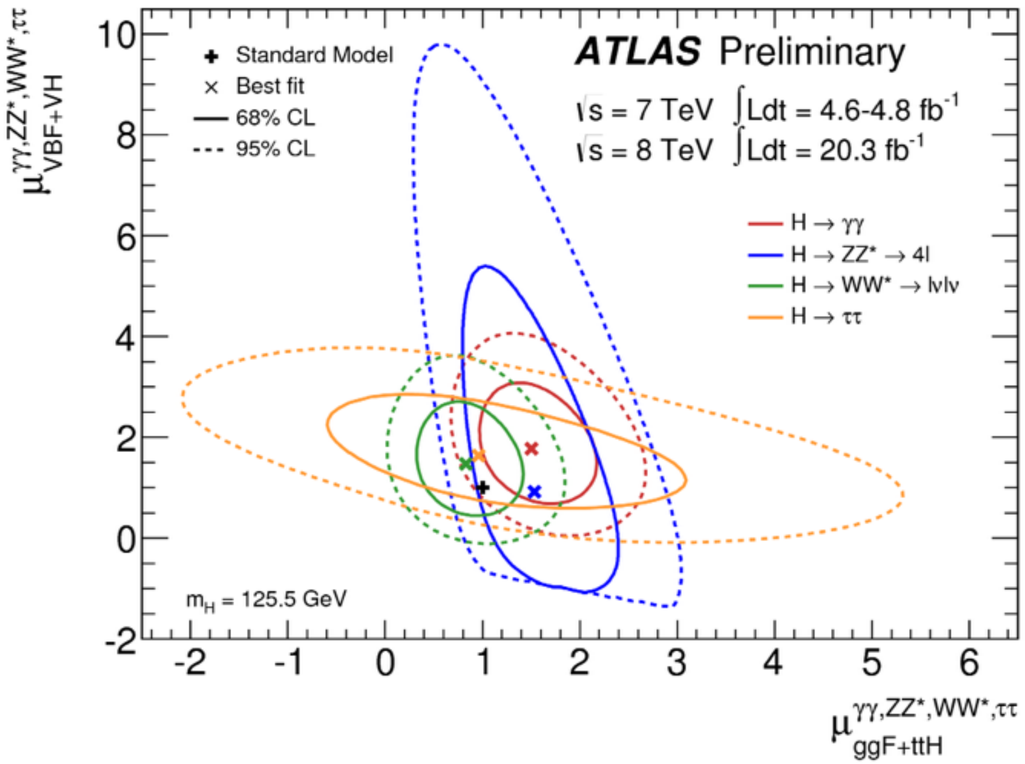

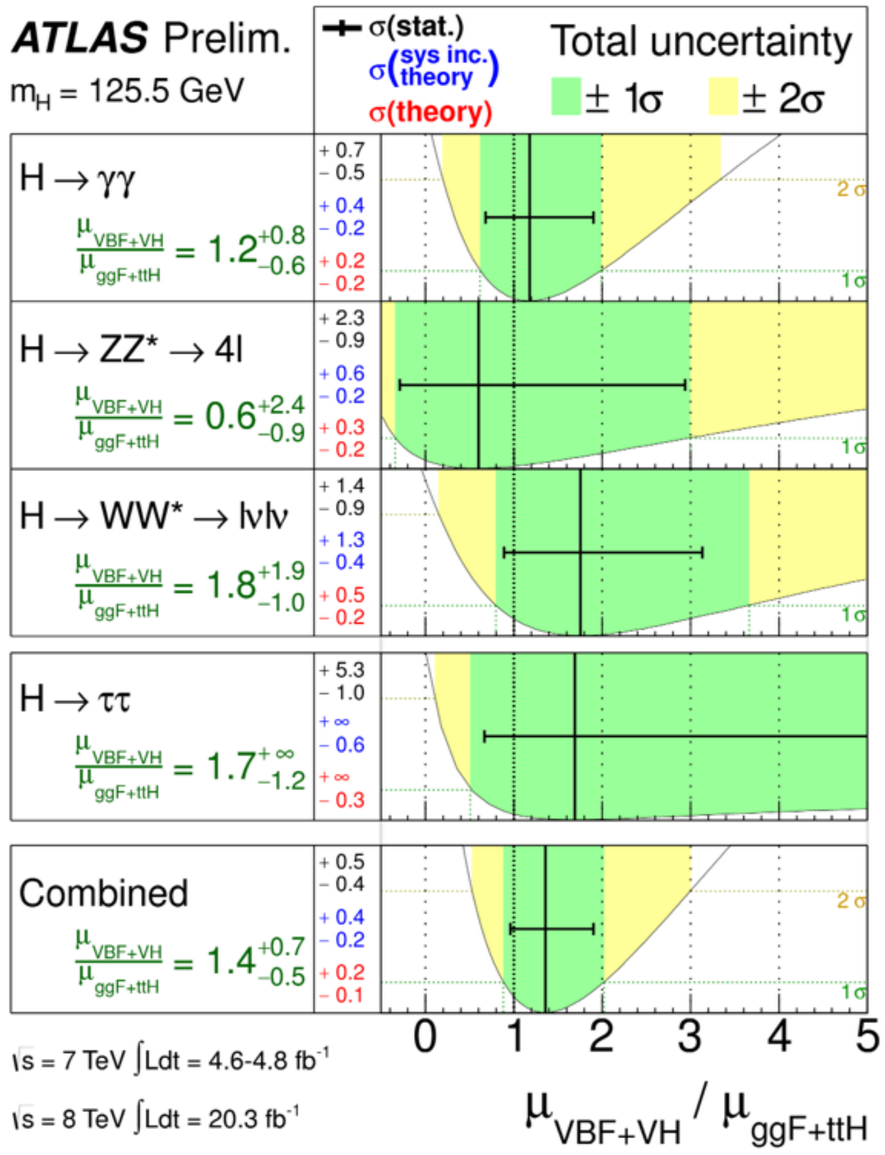

Releasing the assumption:

$$\frac{\mu_{VBF}}{\mu_{ggf+t\bar{t}H}} = 1.4\ ^{+0.5}_{-0.4}(stat)\ ^{+0.4}_{-0.3}(sys)$$

→ 4.1σ evidence of VBF production

ATLAS-CONF-2014-009

Couplings: Strengths

- Framework Assumptions
  - observed signal comes from a single narrow resonance with peak ~125.5GeV
  - zero-width approximation
  - SM tensor structure kept intact

Assumption: Γ_H given by the sum of SM decay modes

$$\kappa_V = \kappa_W = \kappa_Z = 1.15 \pm 0.08$$
$$\kappa_F = \kappa_t = \kappa_b = \kappa_\tau = \kappa_g = 0.99 \pm 0.17$$

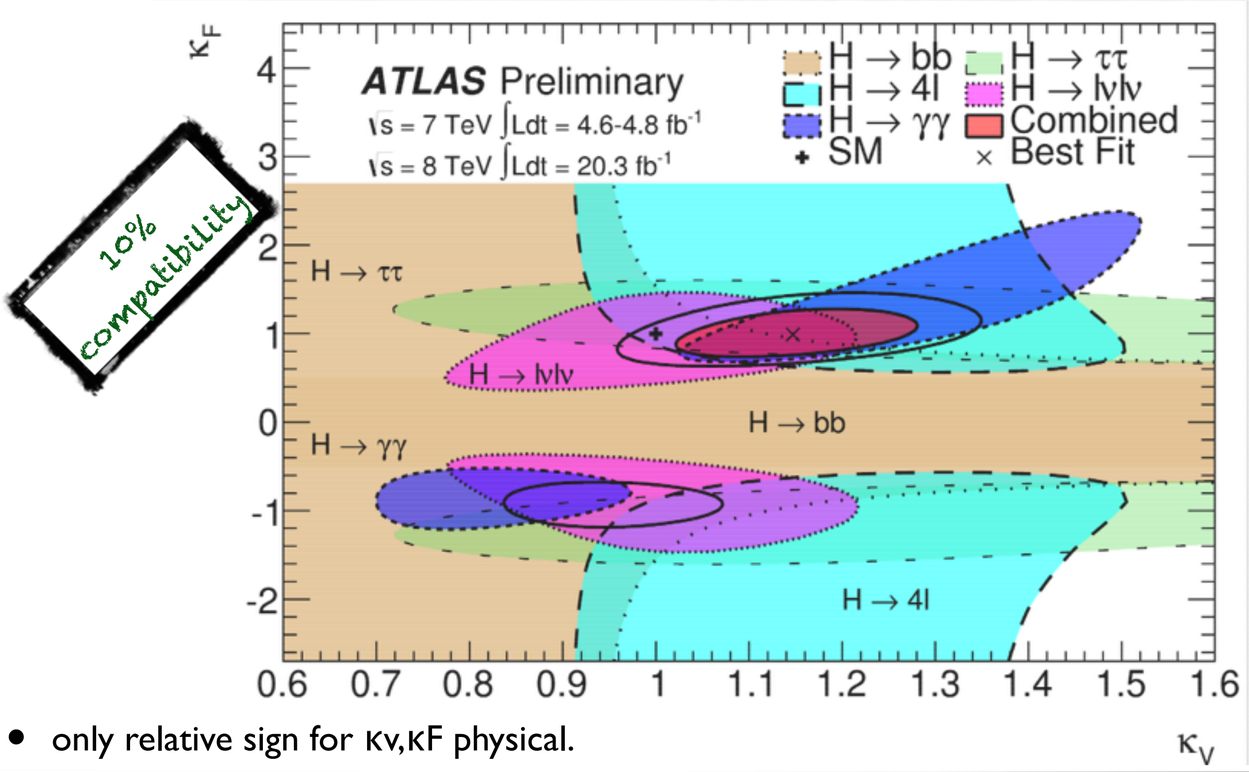

- only relative sign for κv,κF physical.

No Γ_H Assumption

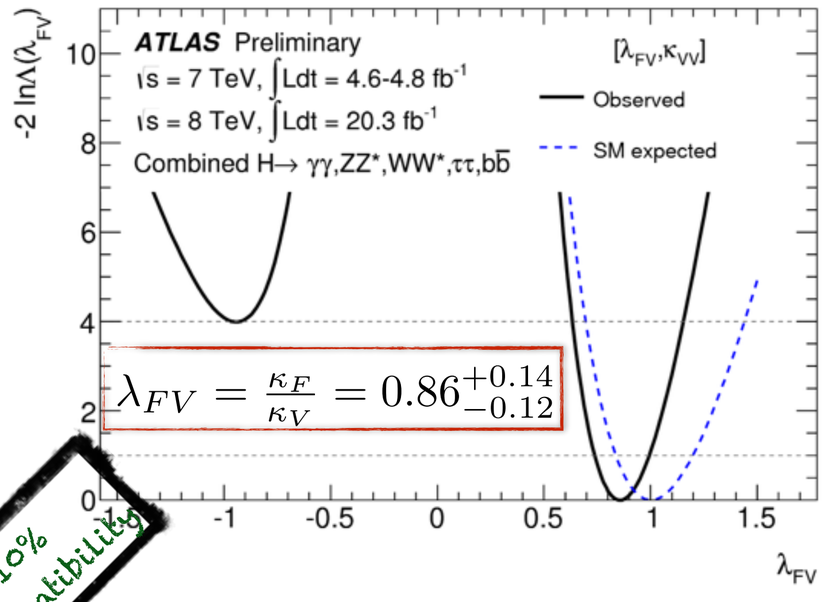

$$\lambda_{FV} = \frac{\kappa_F}{\kappa_V} = 0.86^{+0.14}_{-0.12}$$

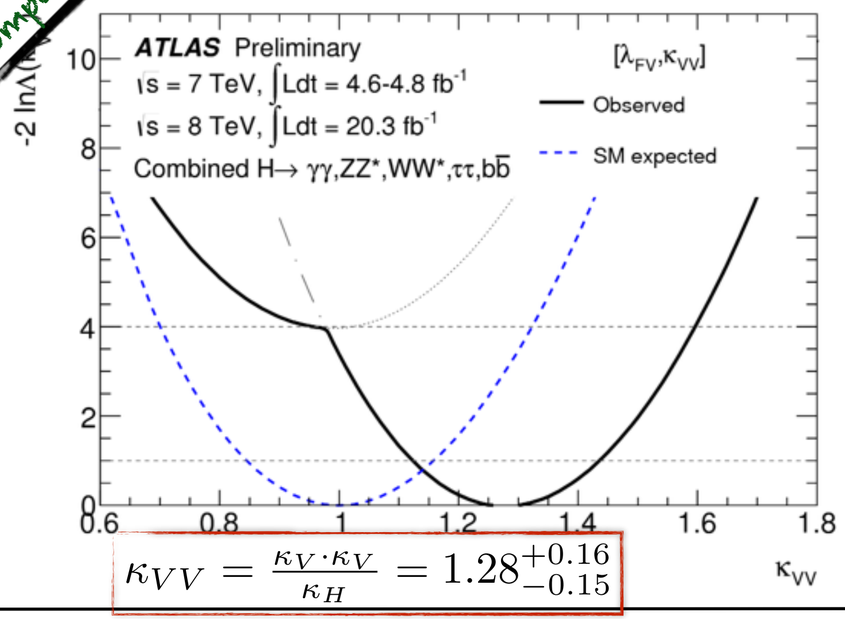

$$\kappa_{VV} = \frac{\kappa_V \cdot \kappa_V}{\kappa_H} = 1.28^{+0.16}_{-0.15}$$

ATLAS-CONF-2014-009

Couplings: Custodial

- Testing the constraint on the scale factors of W,Z bosons
- λ_{wz} is constrained
  - partly by the decays in H→WW and H→ZZ and the (W/Z)H
  - indirectly via VBF production (74% W fusion, 26% Z fusion)
- ambiguity of relative sign → cannot be probed at LHC → chosen positive, without loss of generality

19% compatibility

$$\lambda_{WZ} = \frac{\kappa_W}{\kappa_Z} = 0.94^{+0.14}_{-0.29}$$

$$\lambda_{FZ} = \frac{\kappa_F}{\kappa_Z} \in [-0.91, -0.63] \cup [0.65, 1.00]$$

$$\kappa_{ZZ} = \frac{\kappa_Z \cdot \kappa_Z}{\kappa_H} = 1.41^{+0.49}_{-0.34}$$

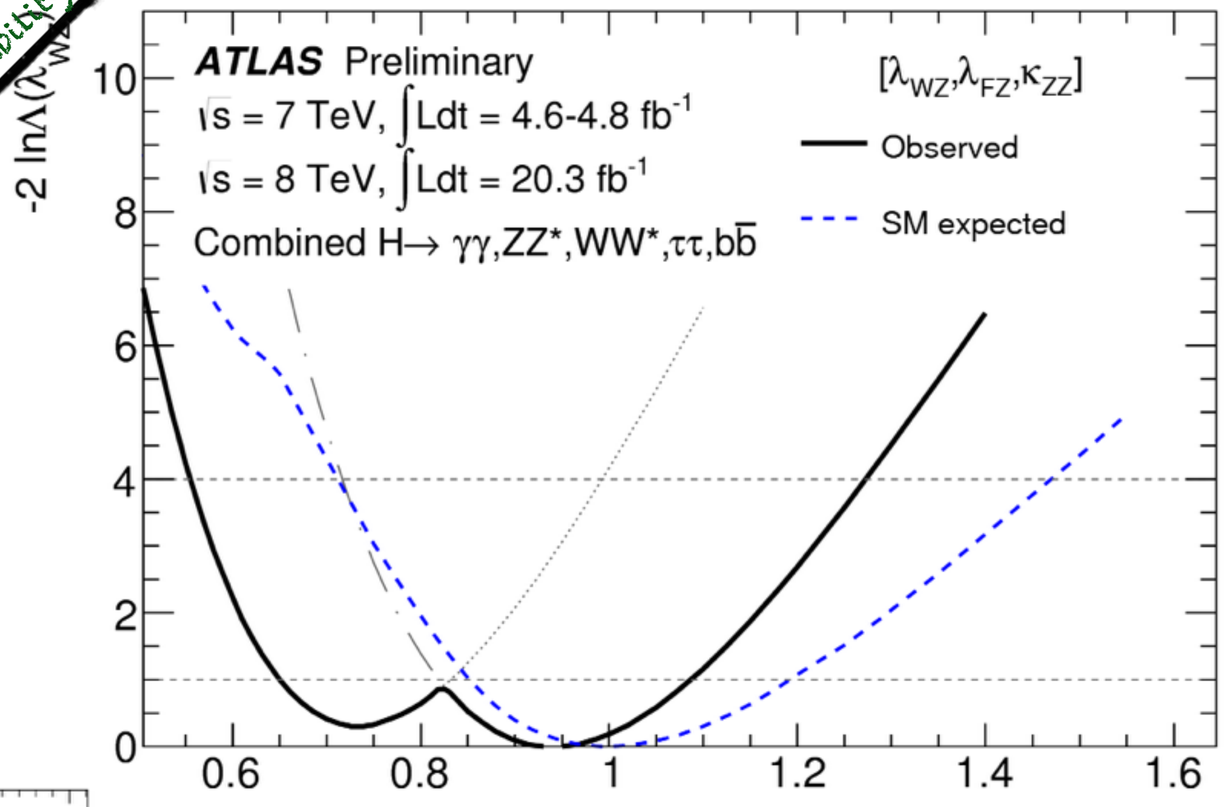

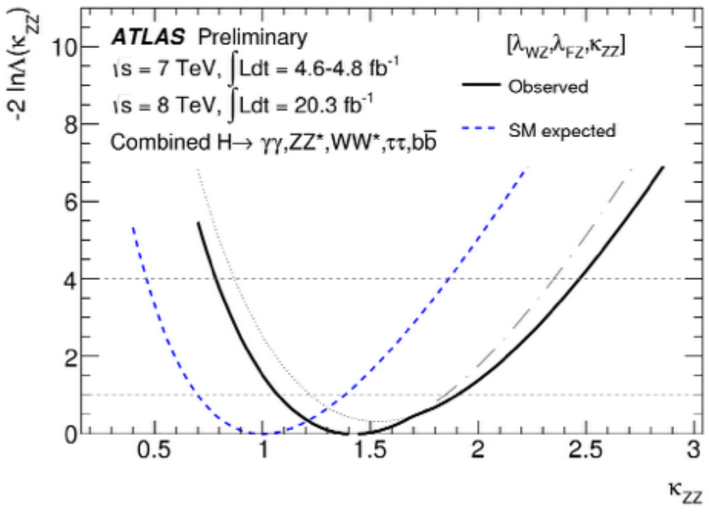

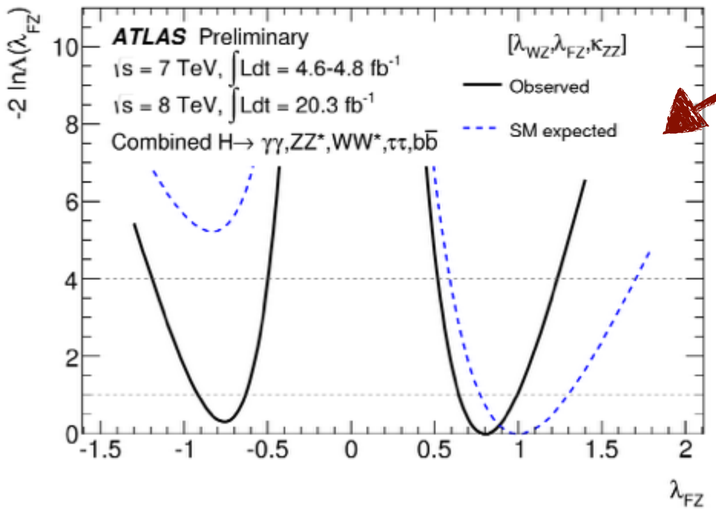

Fit prefers SM-like local min with positive sign
→ negative within 1σ
Agreement with custodial symmetry of $\lambda_{wz,SM}$=1

ATLAS-CONF-2014-009

Couplings: Up-(down-)type

- 2HDM models (e.g. MSSM) predict different u/d couplings
- κ_u indirectly constrained from the gg→H production
- κ_d is constrained from H→bb and H→ττ decays

$$\lambda_{du} = \frac{\kappa_d}{\kappa_u} \in [-1.24, 0.81] \cup [0.78, 1.15]$$

$$\lambda_{Vu} = \frac{\kappa_V}{\kappa_u} = 1.21^{+0.24}_{-0.26}$$

$$\kappa_{uu} = \frac{\kappa_u \cdot \kappa_u}{\kappa_H} = 0.86^{+0.41}_{-0.21}$$

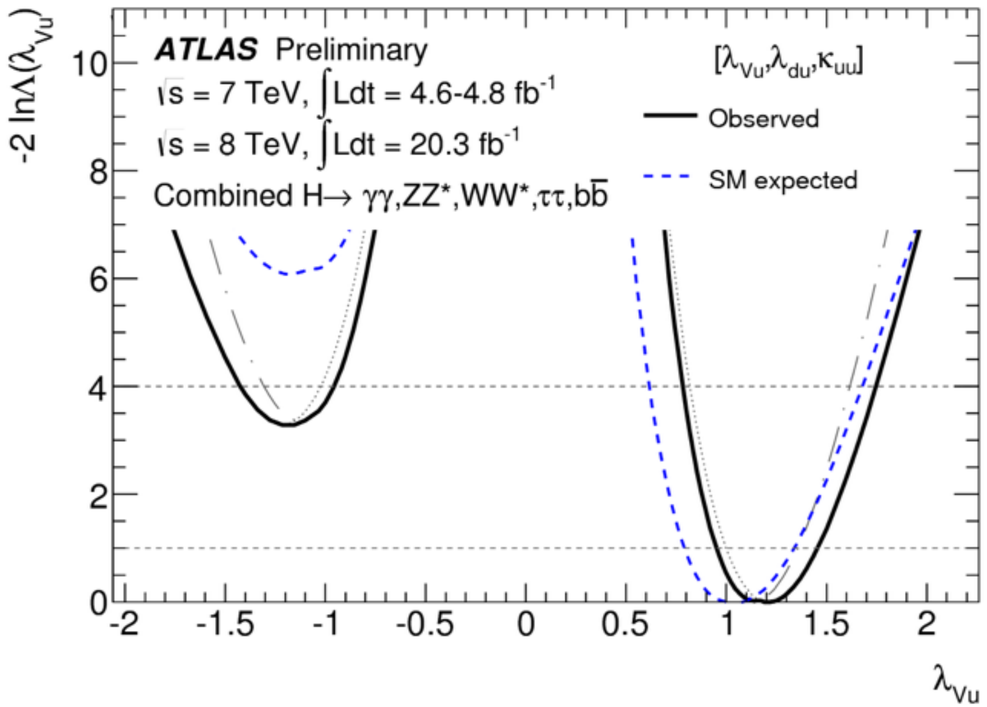

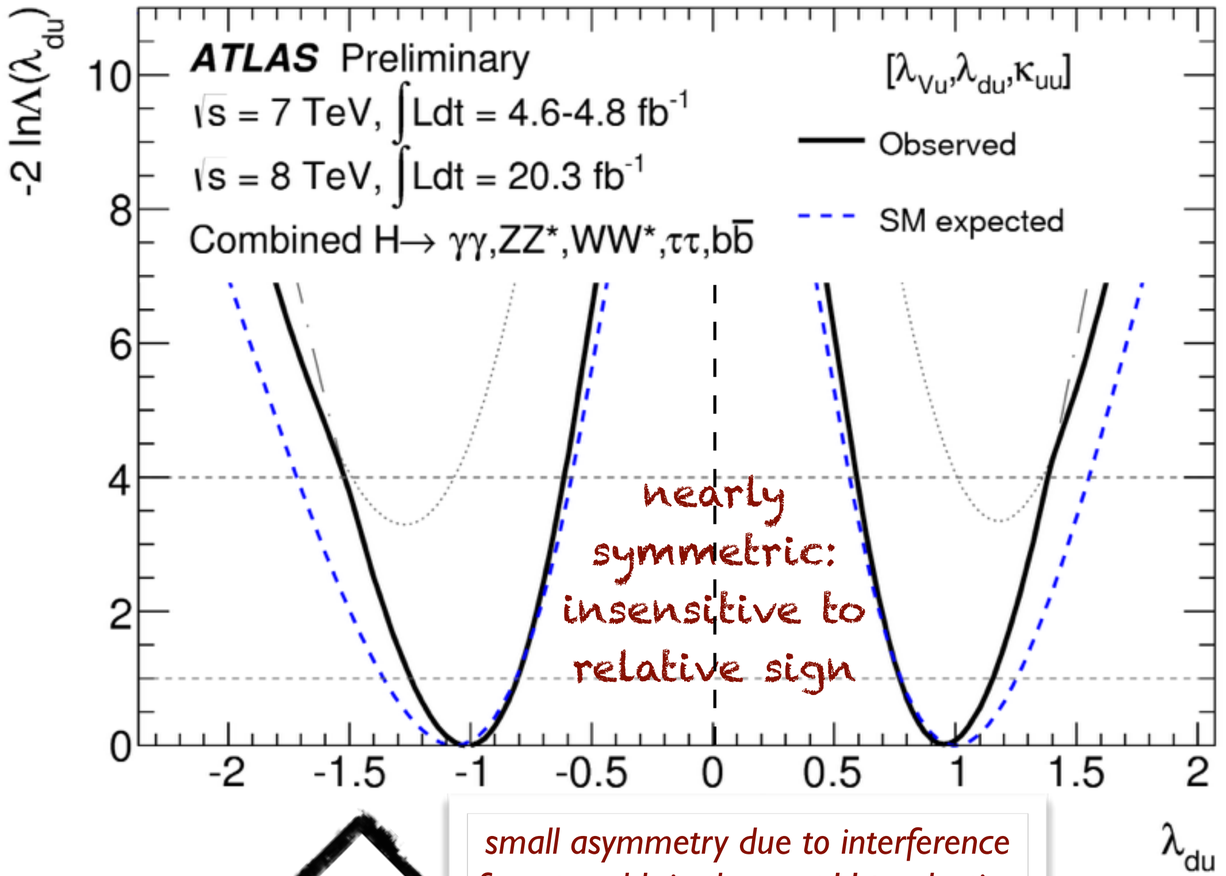

small asymmetry due to interference from t and b in the gg→H production

20% compatibility

Value of λ_{du}=1 (SM) is

$$\lambda_{du} = 0.95^{+0.20}_{-0.18}$$

3.6σ evidence of Higgs coupling to down-type fermions.

ATLAS-CONF-2014-009

Couplings: Quark-Lepton

- Lepton coupling strength currently constrained from H→ττ

$$\lambda_{\ell q} = \frac{\kappa_\ell}{\kappa_q} \in [-1.48, 0.99] \cup [0.99, 1.50]$$

$$\lambda_{Vq} = \frac{\kappa_V}{\kappa_q} = 1.27^{+0.23}_{-0.20}$$

$$\kappa_{qq} = \frac{\kappa_q \cdot \kappa_q}{\kappa_H} = 0.82^{+0.23}_{-0.19}$$

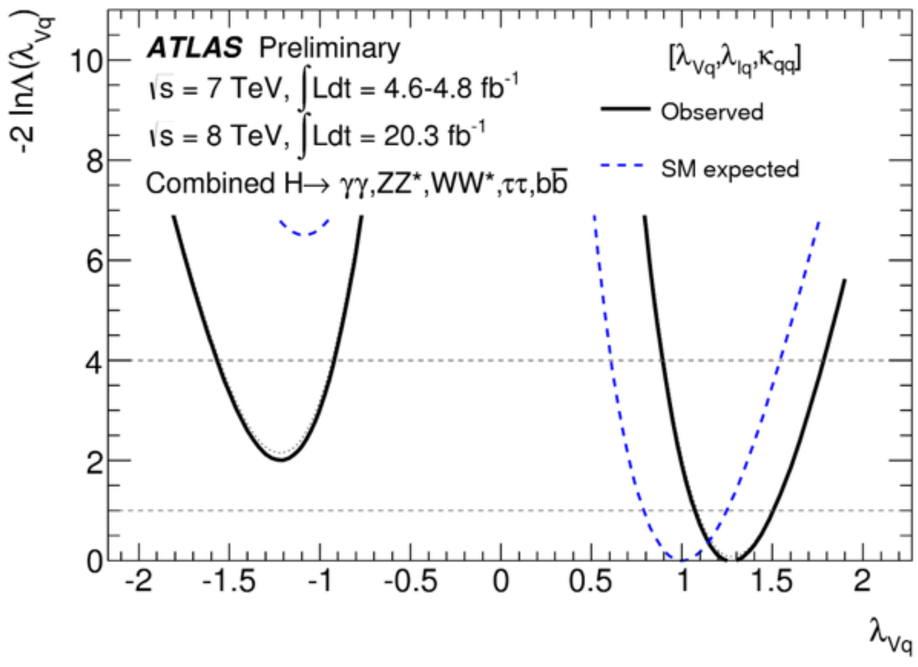

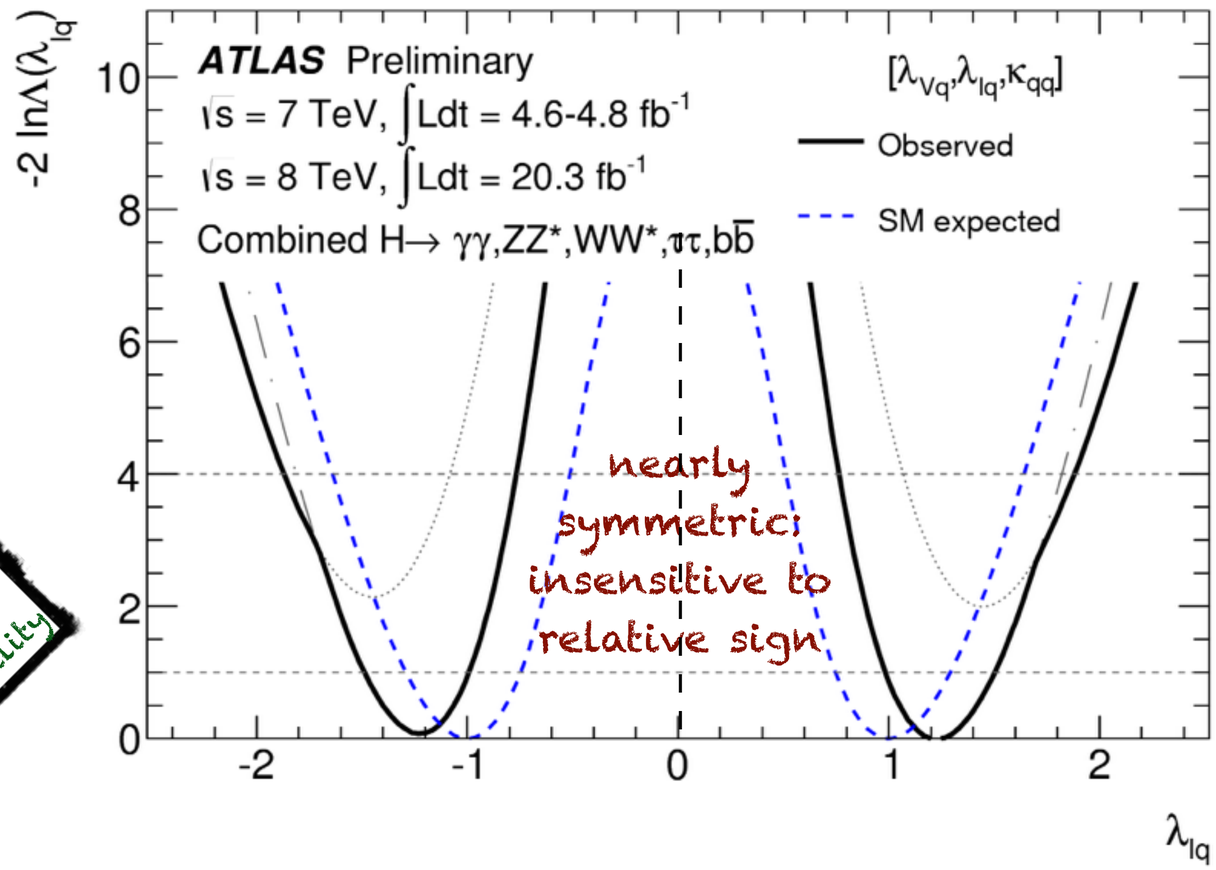

15% compatibility

value of λlq=1 (SM) is

$$\lambda_{\ell q} = 1.22^{+0.28}_{-0.24}$$

vanishing coupling of Higgs to leptons excluded at 4.0σ due to H→ττ

Couplings: New Analyses

ATLAS-HIGG-2013-08

H→γγ

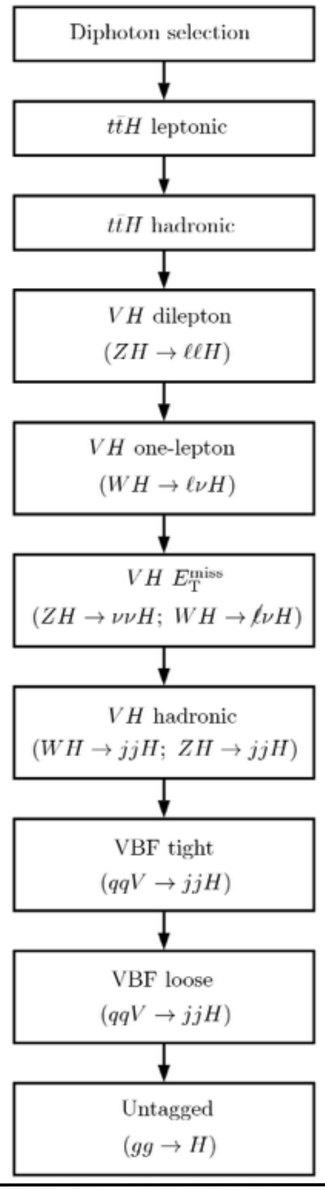

ATLAS-HIGG-2013-21

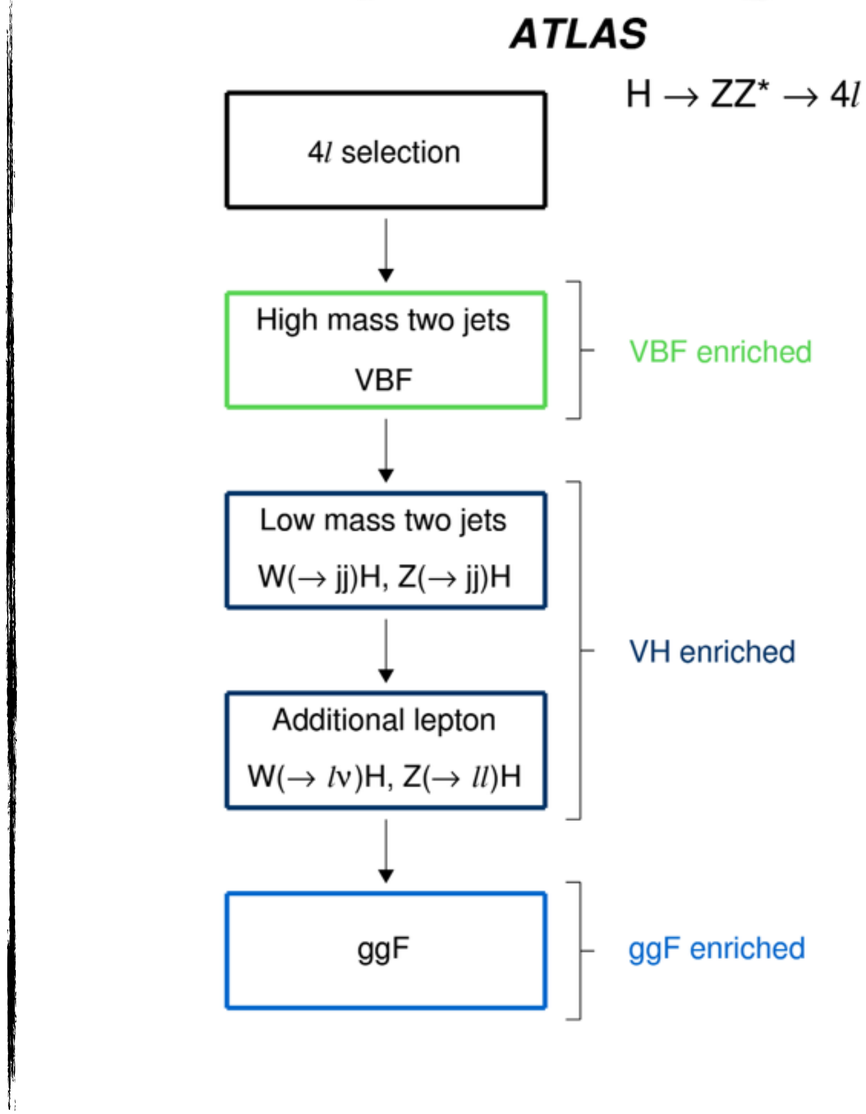

updated H→WW* couplings soon to appear

new results from VH→bb

For more info: look at Nicolas' talk

Phys. Lett. B 726(2013), pp.120-144

Spin/CP: H→γγ spin

- H→γγ contributes in the spin-2 exclusion, spin-1 → Landau-Yang
- Main background: non-resonant γγ → between spin-0 & spin-2
- Discriminant: |cosθ*| in the Collins-Soper frame and $m_{\gamma\gamma}$ (min. ISR)

$$|cos\theta^*| = \frac{|sinh(\Delta\eta^{\gamma\gamma})|}{\sqrt{1+(\frac{p_T^{\gamma\gamma}}{m_{\gamma\gamma}})^2}} \cdot \frac{2p_T^{\gamma 1}p_T^{\gamma 2}}{m_{\gamma\gamma}^2}$$

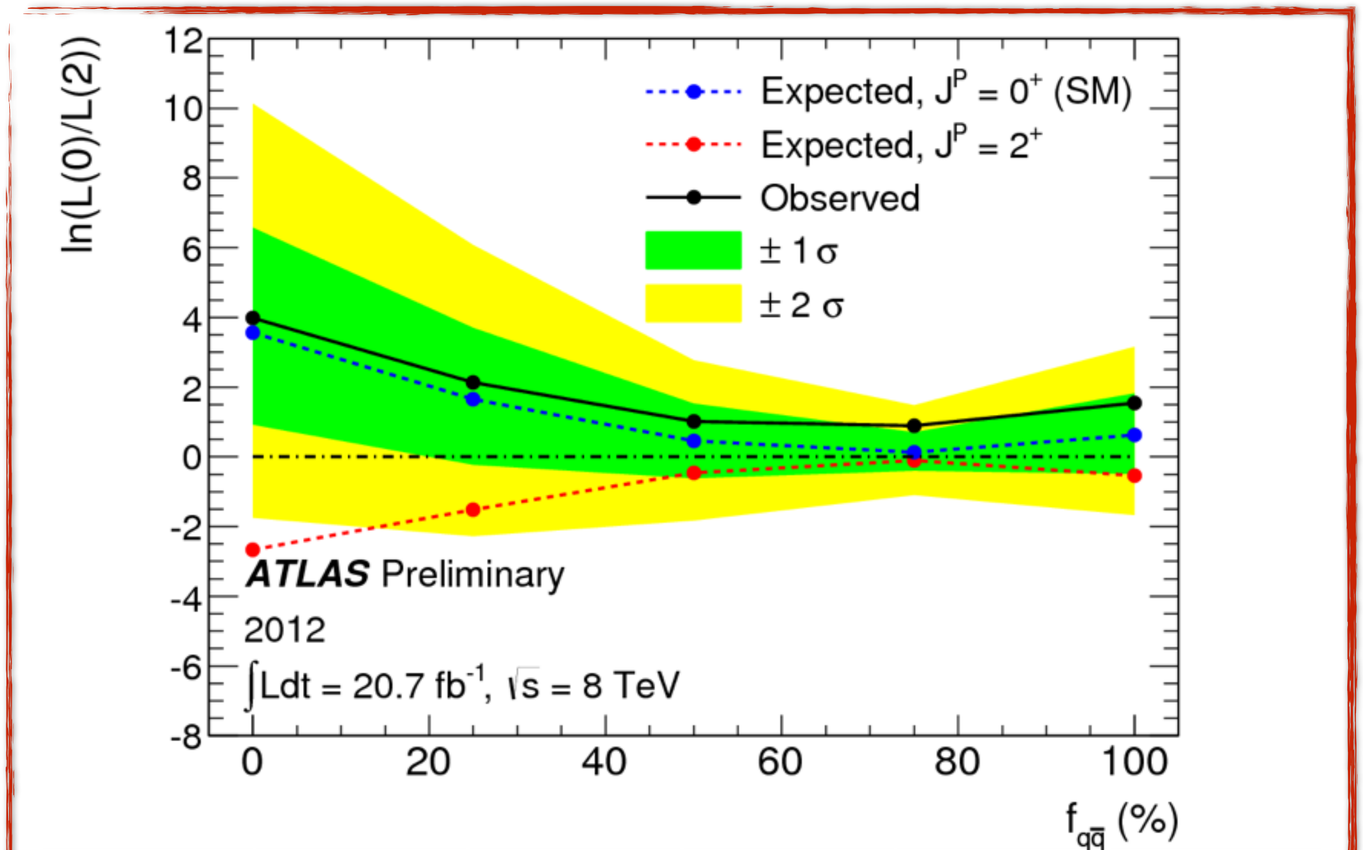

$f_{q\bar{q}} = \frac{q\bar{q}\to X2}{gg\to X2}$	$2^+(100\%)$	$2^+(75\%)$	$2^+(50\%)$	$2^+(25\%)$	$2^+(0\%)$
$CL(J^P = 2^+)$	0.124	0.337	0.260	0.054	0.007

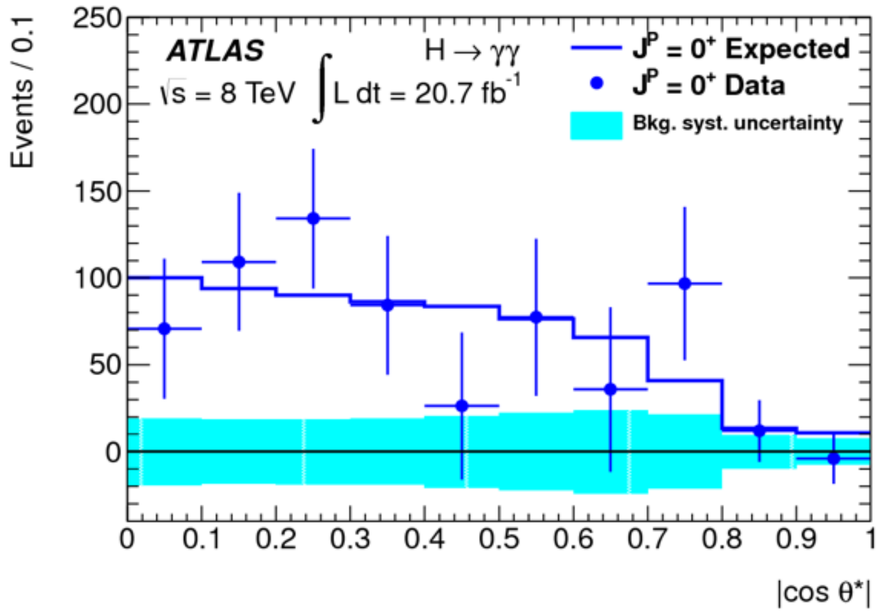

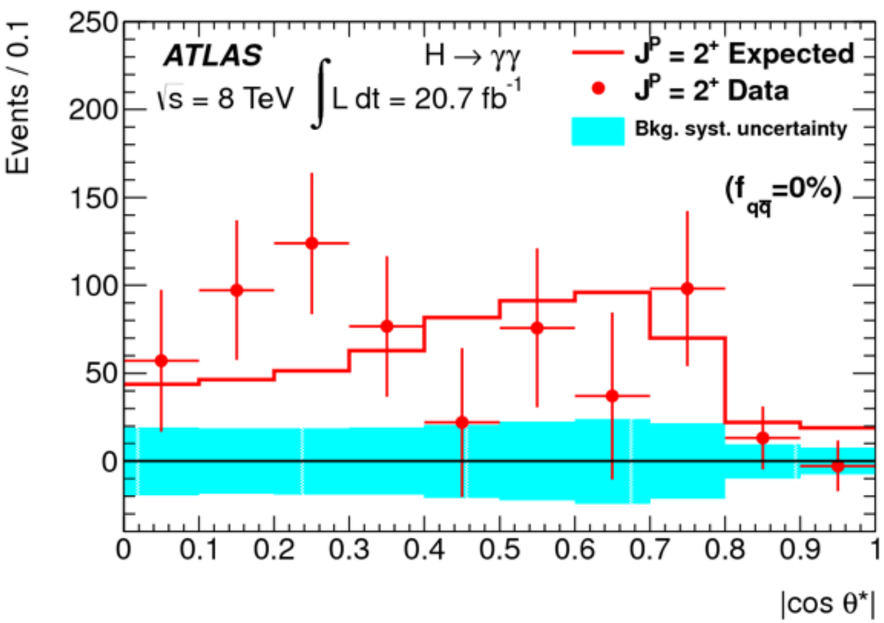

Phys. Lett. B 726(2013), pp.120-144
ATLAS-CONF-2013-013

Spin/CP: H→ZZ*

- Full reconstruction of the final state allows for rest frame boosting.
- Discriminant: BDT trained with the Cabibbo-Maksymowicz variables
  - studied in two regions:
    - high S/B : 121<m_{4l}<127 GeV
    - low S/B : [115,121]U[127-130] GeV

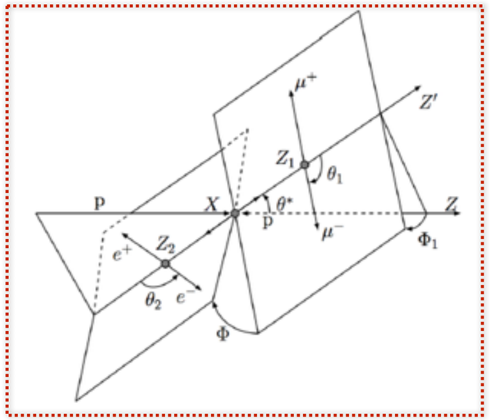

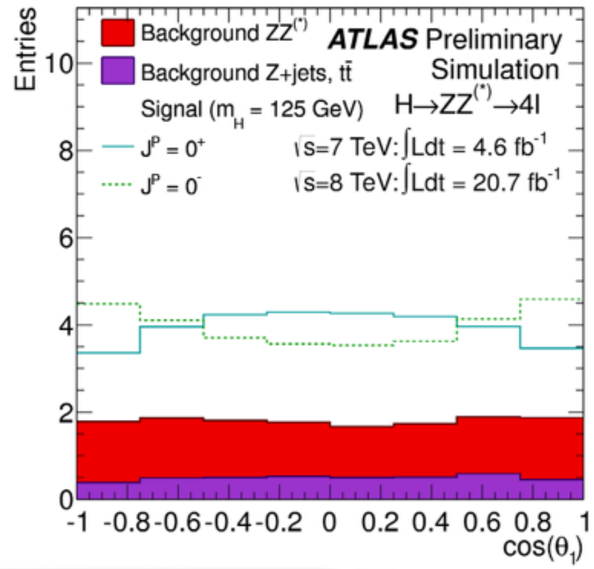

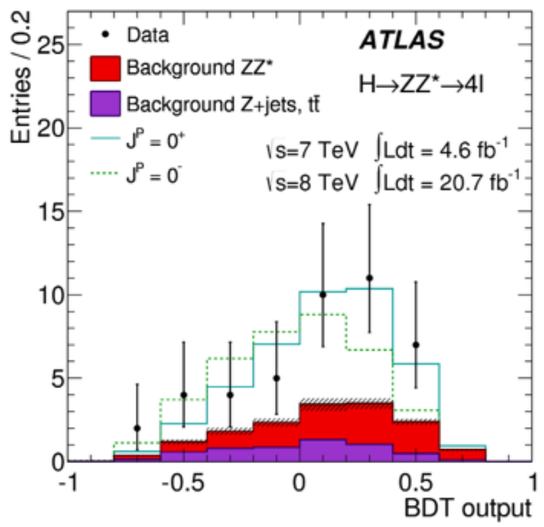

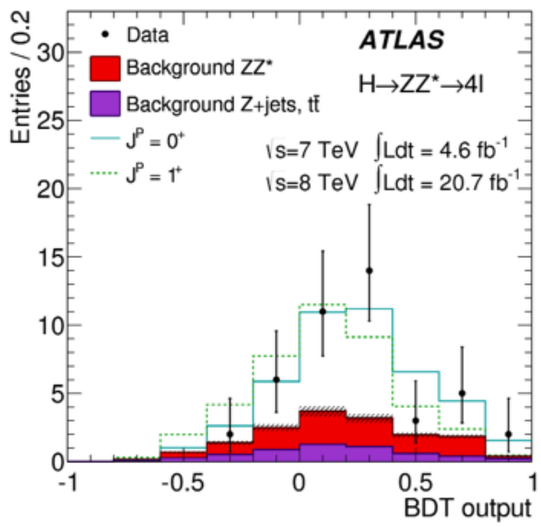

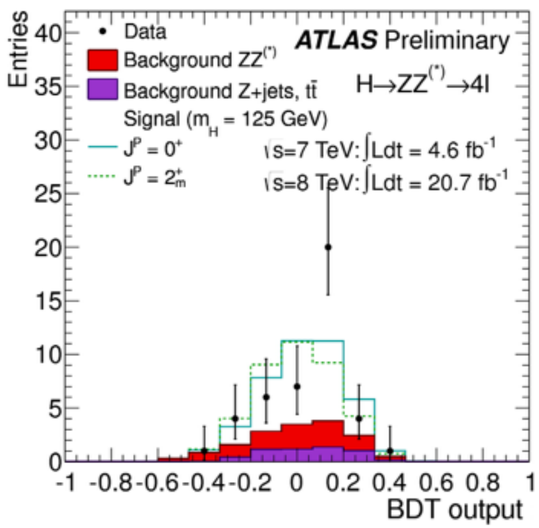

Test	0^-	1^+	1^-	$2^+(100\%)$	$2^+(75\%)$	$2^+(50\%)$	$2^+(25\%)$	$2^+(0\%)$
CL	0.022	0.002	0.060	0.026	0.039	0.035	0.036	0.169

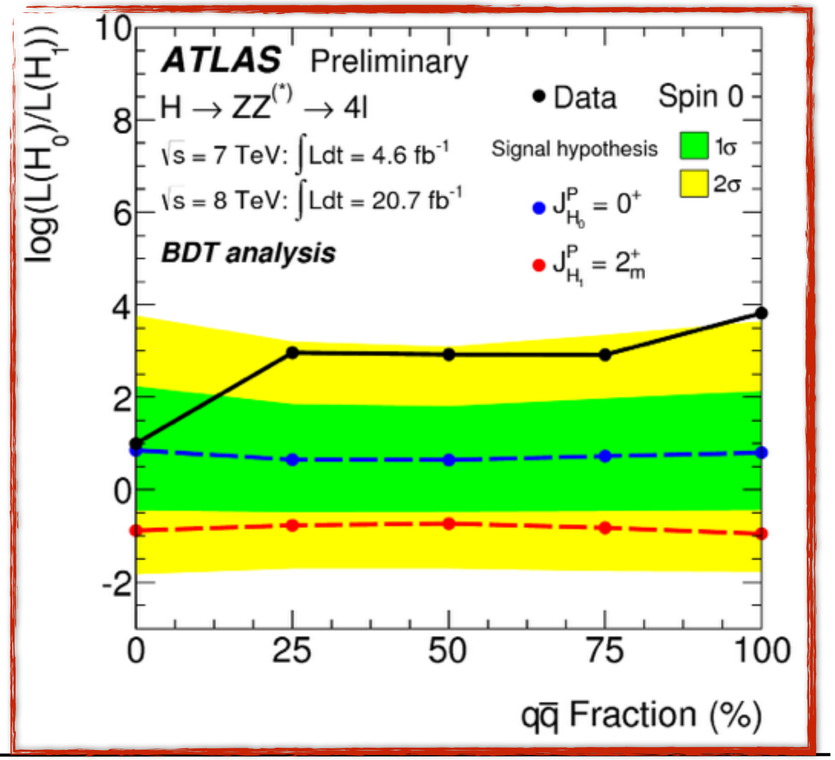

Phys. Lett. B 726(2013), pp.120-144

ATLAS-CONF-2013-031

Spin/CP: H→WW*

- Same selection as the mass search with looser selection criteria to allow for spin2 enriched phase-space
- Discriminant: Unrolled 2D BDT

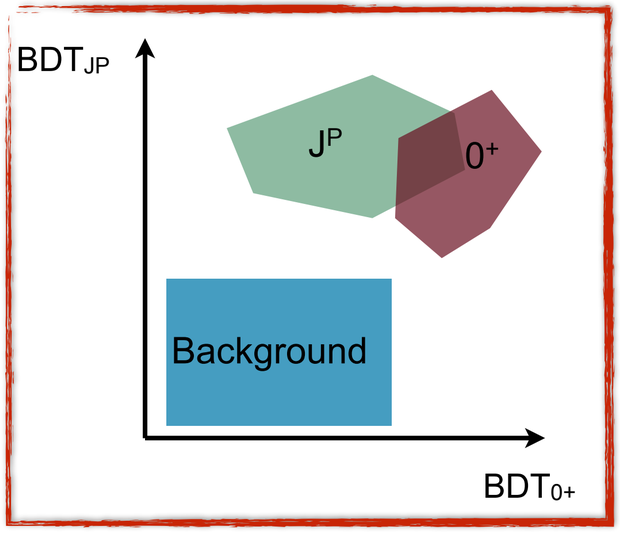

Test	CLs
1^+	0.080
1^-	0.017
$2^+(100\%)$	0.124
$2^+(75\%)$	0.337
$2^+(50\%)$	0.260
$2^+(25\%)$	0.054
$2^+(0\%)$	0.007

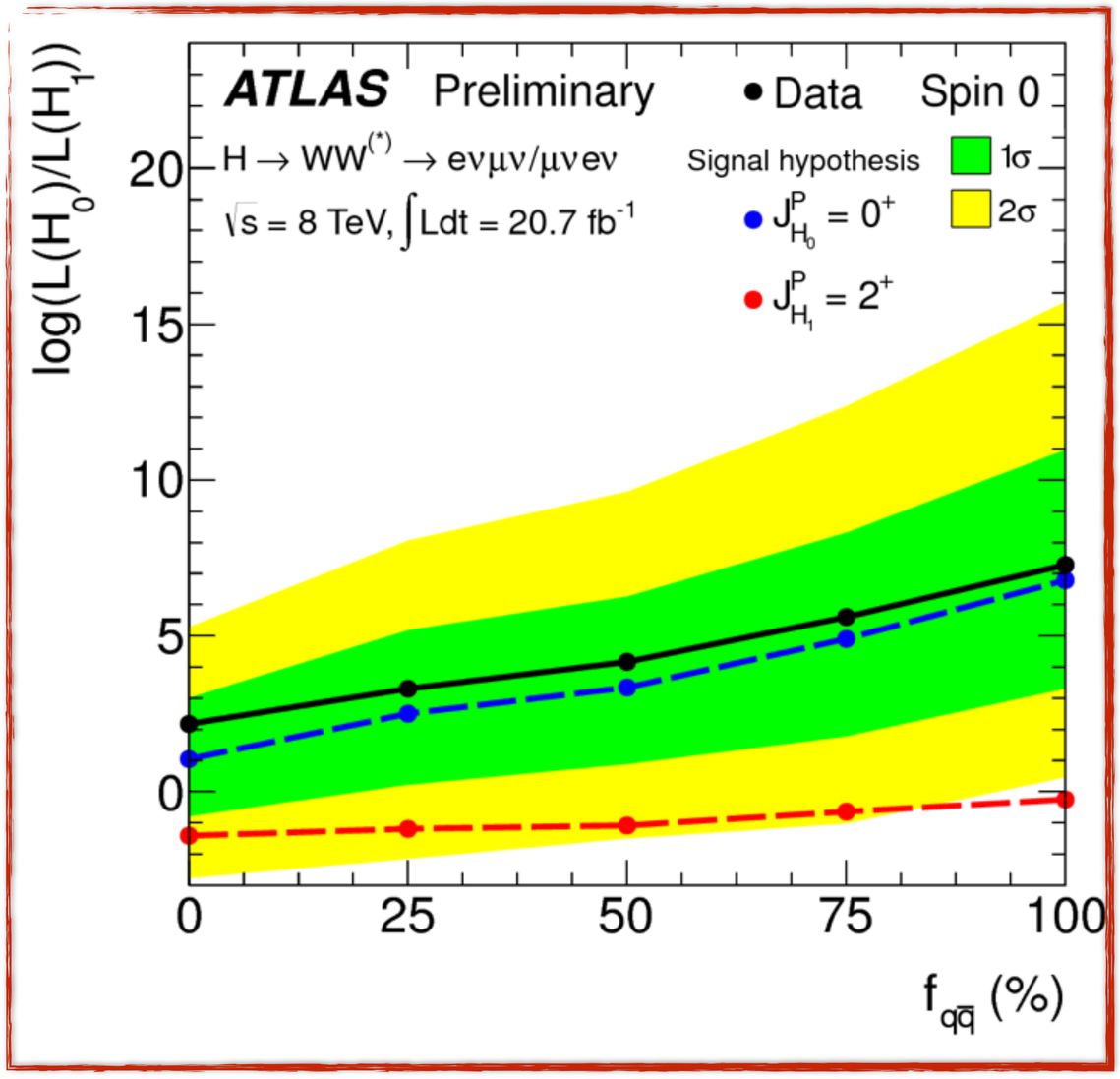

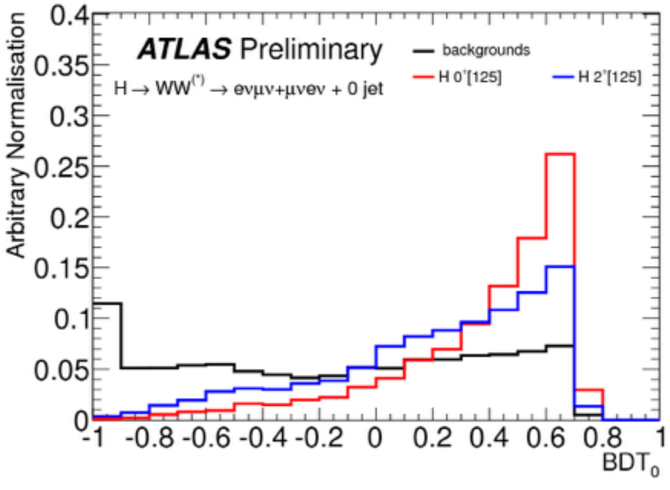

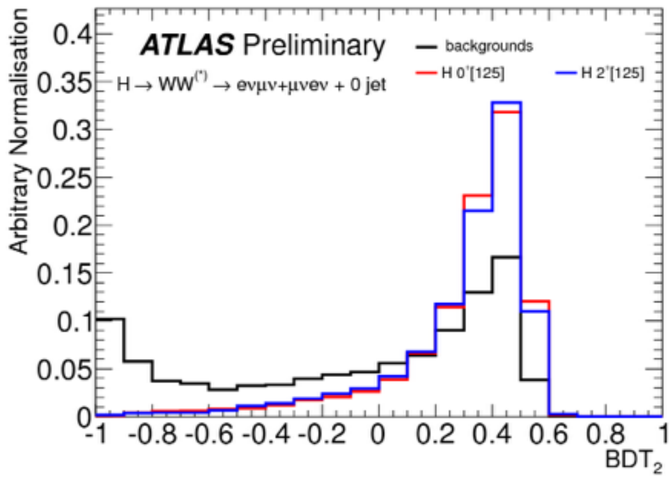

Phys. Lett. B 726(2013), pp.120-144

Combination of Spin/CP

	$H \to ZZ^{(*)} \to 4\ell$	$H \to WW^{(*)} \to \ell\nu\ell\nu$	$H \to \gamma\gamma$
0^-	✓	-	-
1^+	✓	✓	-
1^-	✓	✓	-
2^+	✓	✓	✓

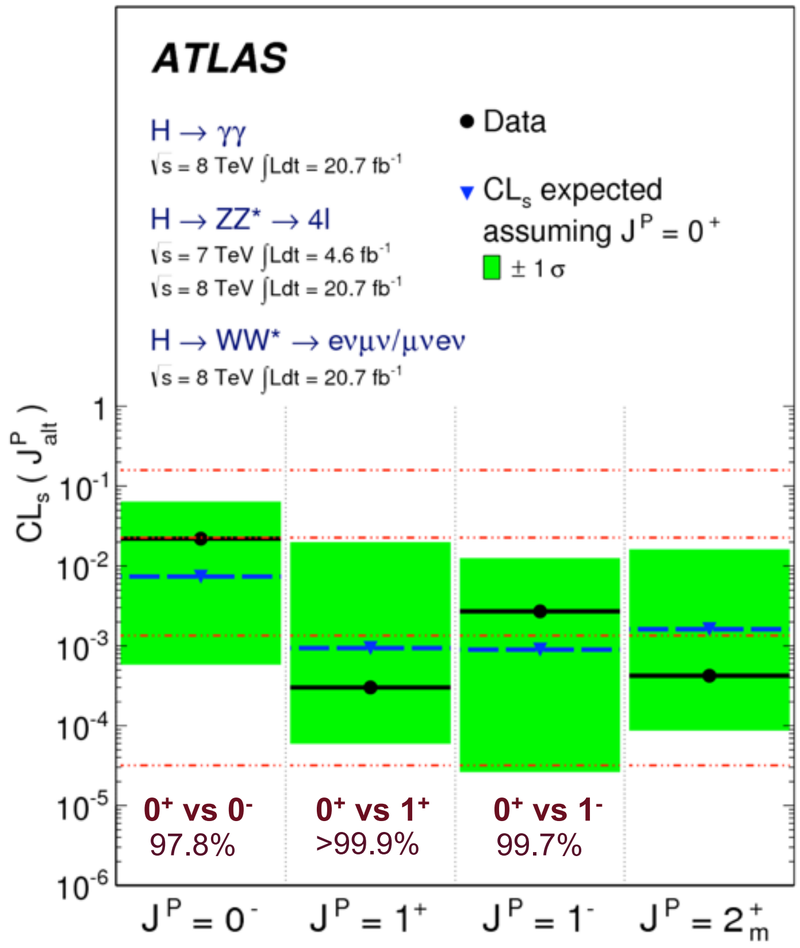

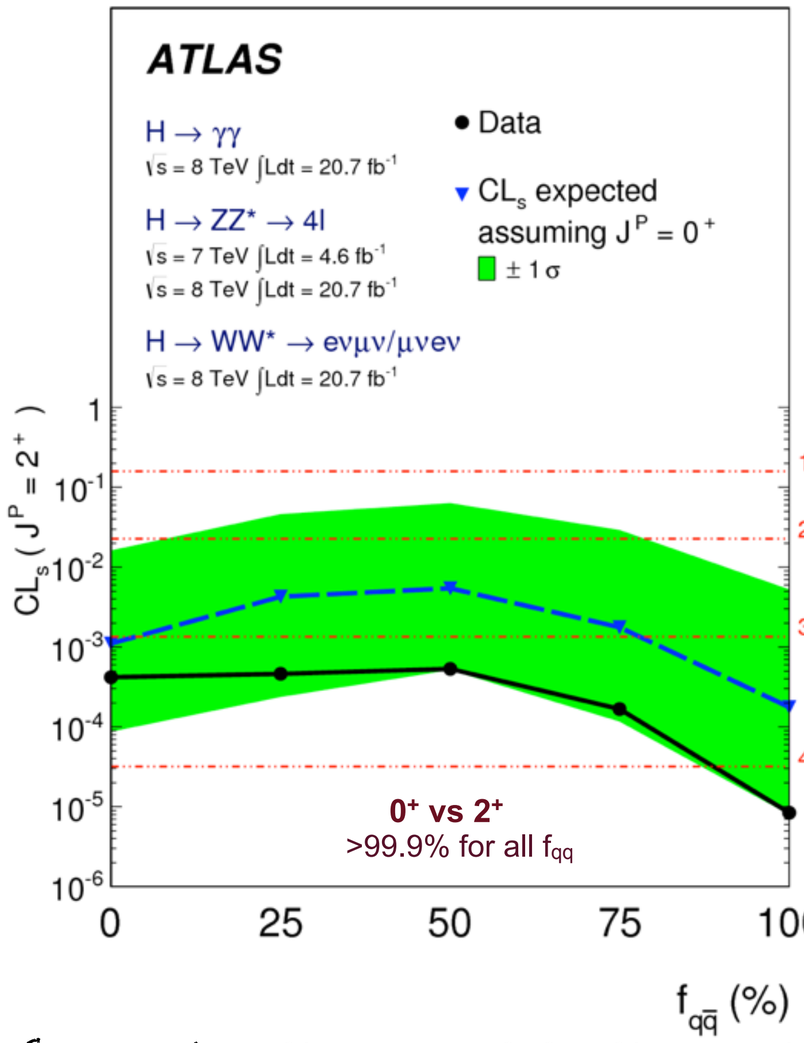

All studied alternative hypotheses are strongly disfavored with respect to the 0+ hypothesis!

Summary

Two years after the observation of the Higgs-like boson, data indicate that it is a SM-like Higgs boson!

m_H=125.36 ± 0.37 (stat) ± 0.18 (sys) GeV

Production rates and coupling strengths are in agreement with SM expectations, data compatible with 0+ hypothesis, physics reach of LHC extended in the Γ_H front following the fruitful dialogue with theory community!

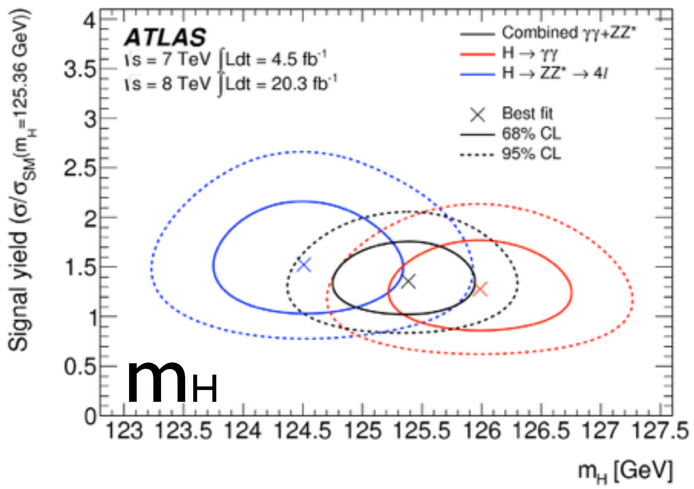

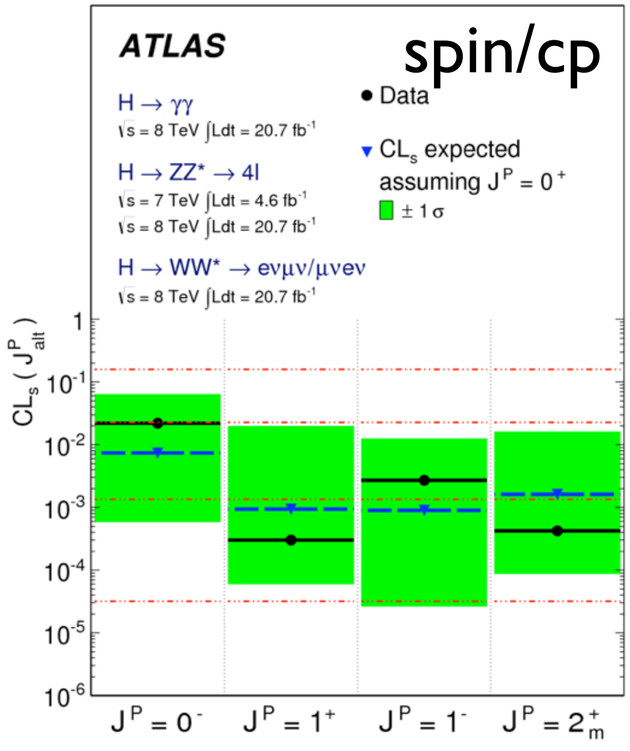

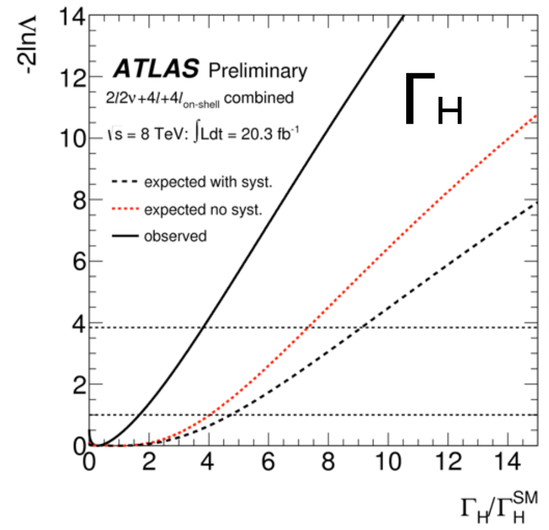

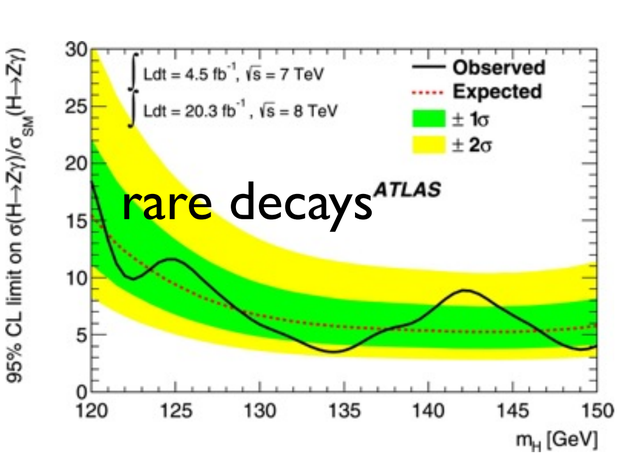

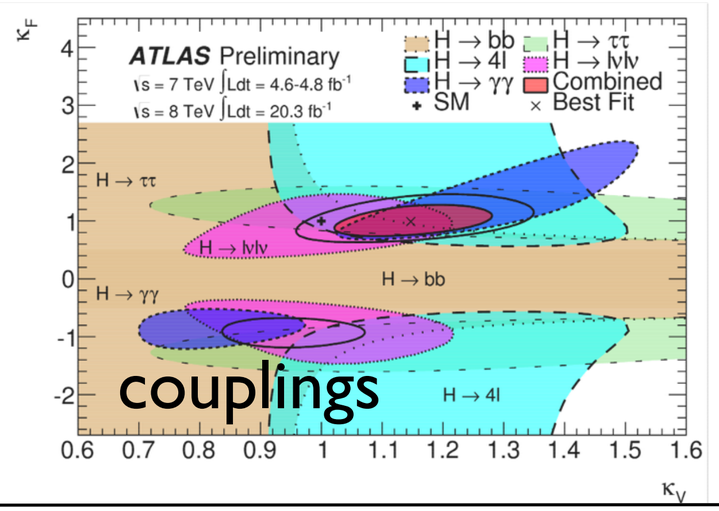

Final Run I results already out for most of the analyses.
More to come in the very near future!
Looking forward to 10 times more Higgs bosons in Run II!!

Backup

A Toroidal LHC Apparatus

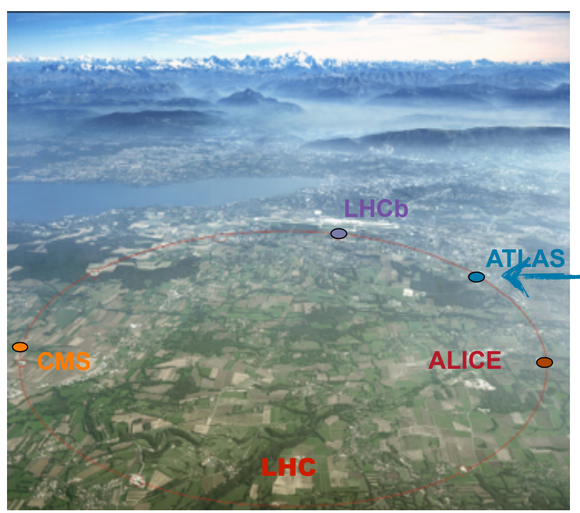

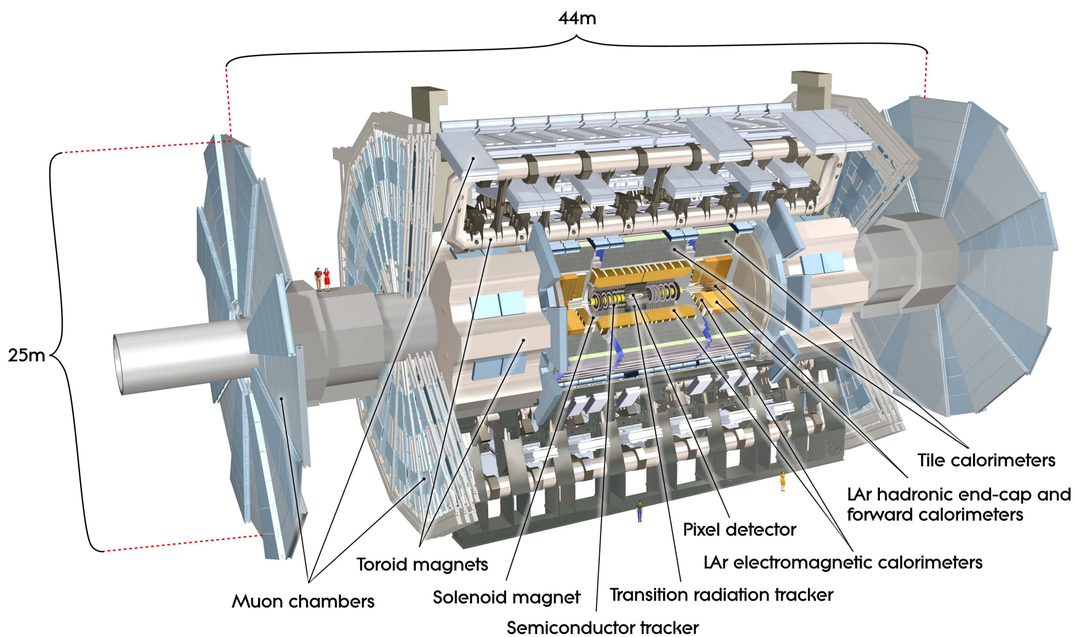

→ Multi-purpose detector designed for the harsh LHC environment

→ High data-taking efficiency and very good data-quality

ATLAS p-p run: April-December 2012										
Inner Tracker			Calorimeters		Muon Spectrometer				Magnets	
Pixel	SCT	TRT	LAr	Tile	MDT	RPC	CSC	TGC	Solenoid	Toroid
99.9	99.4	99.8	99.1	99.6	99.6	99.8	100.	99.6	99.8	99.5
All good for physics: 95.8%										

Luminosity weighted relative detector uptime and good quality data delivery during 2012 stable beams in pp collisions at $\sqrt{s}$=8 TeV between April 4th and December 6th (in %) – corresponding to 21.6 fb^{-1} of recorded data.

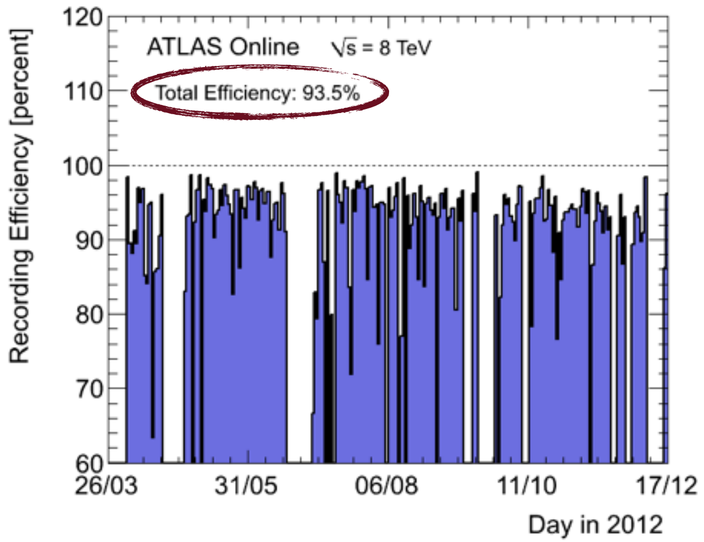

Performance: γ E_scale

- Uncertainties in the calibration are significantly reduced:
  - data-driven measurements for the inter calibration of the calorimeter layers
  - estimate of the material in fron of the calorimeter
  - improving the accuracy of the in situ calibration with Z->ee events

- **Intercalibration of calorimeter layers**
- The relative calib. for the first 2 layers performed with Z->mumu muons & comparing the measured energy loss data/simulation
- Uncertainty of calib. ~1-2% [domin.by amount of LAr transversed by muons and simulation accuracy]

- **Material in front of EM**
- Verified from data studying the EM shower longitudinal development in the first 2 layers.
- Material between pre sampler and the first layer measured using unconverted photons (low energy deposit @ presampler) -> well described w. 0.03-0.05 X0 lengths
- Integral material in front of pre sampler : difference between e & unconv. γ longitudinal shower profiles. Accuracy (0.02-0.10)X0 depending on η -> 5% uncertainty

- **Cell energy calib. & stability**
- Signal is converted in deposited energy using the electronics calibration of EM.
- Calibration coefficients determined periodically and stable better than 0.1%
- Relative calibration for different gains studying Z->e+e- sample (used for the global energy scale) as function of electron energy
- Stability of calo response for data is monitored from W/Z decays ->better than 0.05%

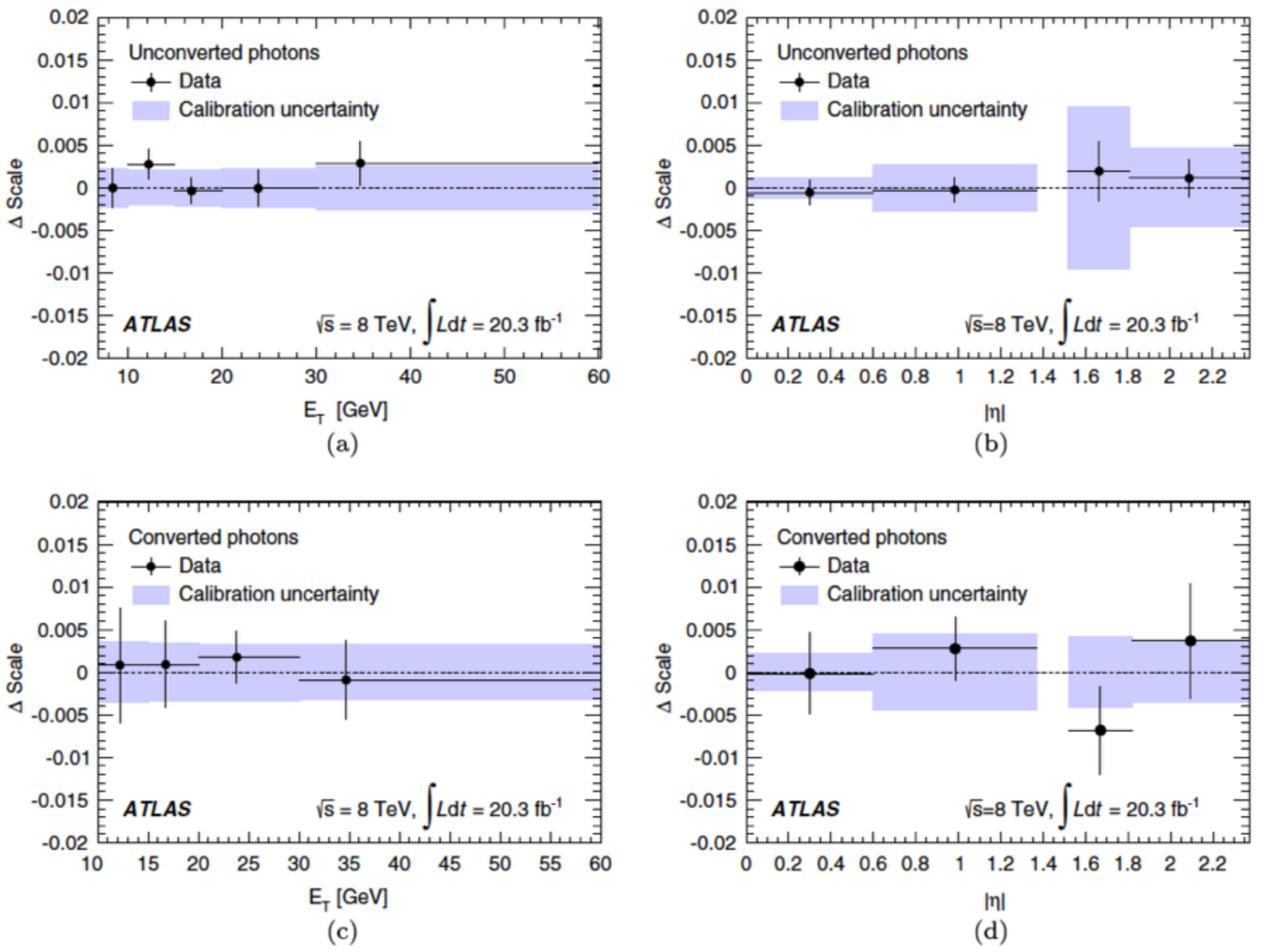

FIG. 2 (color online). Relative scale difference, Δ Scale, between the measured photon energy scale using $Z \to \ell\ell\gamma$ events and the nominal energy scale: (a) as a function of E_T for unconverted photons, (b) as a function of η for unconverted photons, (c) as a function of E_T for converted photons and (d) as a function of η for converted photons. Photons reconstructed in the transition region between the barrel and end-cap calorimeters are not considered. The $Z \to \ell\ell\gamma$ measurements are the points with error bars. The uncertainty on the nominal energy scale for photons is shown as the shaded area. The error bars include the systematic uncertainties specific to the $Z \to \ell\ell\gamma$ measurement.

Performance: Muon Reco, Momentum Scale/Reso

- ID + MS Systems
- Most muon candidates identified by : reconstructed ID track and complete (partial) track in MS
  - if complete -> combined
  - else momentum measured @ ID and identified with MS
- Extended identification coverage by forward region (2.5<|η|<2.7 of MS)
- Track parameters for tracks reconstructed in MS are expressed at I.P. by extrapolating back to the point of closest approach to the beam line (energy loses considered)
- Center of barrel (no MS) ID tracks with pT>15GeV identified as muons if their Calo energy deposits are consistent with MIP
- Muon reco in sim is corrected to match the momentum scale/reso from collision data (J/ψ->μμ & Z->μμ)
- For ID corrections: template fits to the J/ψ->μμ & Z->μμ invariant mass distributions and the difference between momentum measured in ID and MS.
- MS corrections derived in pT and η bins

- Major improvement: the use of J/ψ->μμ in addition to Z->μμ —> Significant reduction of momentum scale uncertainty in the low momentum range (relevant to HZZ)
- ID momentum scale corrections <0.1%
- Systematic uncertainty on ID scale (increases with η) : 0.02% (at 0) to 0.2% (at η>2)
- MS scale corrections : -0.4% to +0.3% depending on η, φ regions
- Systematic uncertainty on MS momentum scale : 0.1%-0.2%
- Systematic uncertianty on momentum scale for CB muons 0.04% (barrel) to 0.2% (|η|>2)

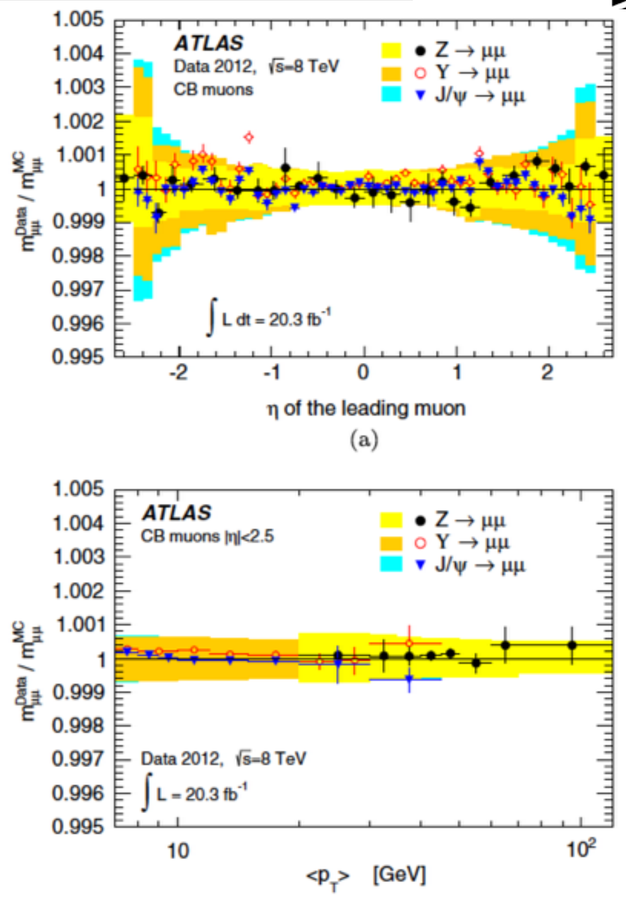

FIG. 3 (color online). Ratio of the reconstructed dimuon invariant mass for data to the corrected mass in simulation for J/ψ, Υ and Z events: (a) as a function of η of the higher-p_T muon and (b) as a function of $\langle p_T \rangle$ of the two muons, as defined in the text. The shaded areas show the systematic uncertainty on the simulation corrections for each of the three samples. The error bars on the points show the combined statistical and systematic uncertainties as explained in the text. In (a), the two large $|\eta|$ bins have measurements only from Z events due to trigger limitations above $|\eta| = 2.4$.

Performance - Escale/reso

- **e/γ objects**
- Unconverted (converted) : clusters of energy in EM without (with) matching track (originating from γ conversion) or reconstructed conversion vertex in the ID
- Energy collected in cels : $\Delta\eta \times \Delta\varphi$ = 0.075x0.175 (e, conv γ @ barrel) , 0.075x0.125 (unvonv. γ @ barrel), 0.125x0.125 (e/γ @ endcaps) [different selection due to deflection of charged particles in the magnetic field & bremsstrahlung in upstream material]
- MVA regression to calibrate the energy measurements: +10% in energy expected H->γγ mass measurement
  - Inputs: measured energy per call layer (including presampler), η of cluster, local position of shower within the second-layer cell corresponding to the cluster centroid.
    - for converted γ: track pT and conversion radius to improve energy reso.
- Corrections : for the energy deposited in front and outside of the cluster
  - for the variation of the energy response as a function of the impact point on the calo
- For e/γ candidates : associated tracks fitted with Gausisian-Sum Filter to account for bremsstrahlung energy losses
  - For H->ZZ candidates : resulting momentum measurement combined with energy measured in the calo to improve electron energy measurement (especially @low energy OR in barrel-endcap transition area)

- **Cell energy calib. & stability**
- Signal is converted in deposited energy using the electronics calibration of EM.
- Calibration coefficients determined periodically and stable better than 0.1%
- Relative calibration for different gains studying Z->e+e- sample (used for the global energy scale) as function of electron energy
- Stability of calo response for data is monitored from W/Z decays ->better than 0.05%

- **Global Energy scale adjustment**
- Determined by Z->ee decays comparing reconstructed mass in data/sim done per η bins of electrons.
- Energy scale correction factors 1-3% (uncertainty on this measurement ~0.1% up to 0.3% for the transition area) —> significantly reduced due to the improved detector description, simulation and inter calibration corrections and also larger Z decay sample
- Effective constant term for calo energy reso: adjusting the Z width from sim/data -> 0.7% for $|\eta|<0.6$, 0.7-1.5% for the rest (3.5% in the transition, 2.5% @ end of end cap acceptance)

- **Intercalibration of calorimeter layers**
- The relative calib. for the first 2 layers performed with Z->mumu muons & comparing the measured energy loss data/ simulation
- Uncertainty of calib. ~1-2% [domin.by amount of LAr transversed by muons and simulation accuracy]

- **Systematic unc. on energy scale**
  - Uncertainty on non-linearity of energy measurement at cell level: relative calibration -> 0.1% on the energy scale of photons
  - Uncertainty on relative calibration on different layers: 0.10 - 0.15% on energy scale of photons
  - Uncertainty on amount of material in front of calo: 0.1-0.3 for unconverted γ (half for converted)
  - Uncertainty on modelling of lateral shower type: 0.05-0.3%

- **Material in front of EM**
- Verified from data studying the EM shower longitudinal development in the first 2 layers.
- Material between pre sampler and the first layer measured using unconverted photons (low energy deposit @ presampler) -> well described w. 0.03-0.05 X0 lengths
- Integral material in front of pre sampler : difference between e & unconv. γ longitudinal shower profiles. Accuracy (0.02-0.10)X0 depending on η -> 5% uncertainty

- **Systematic unc. on energy reso**
- arise from : modeling of sampling term , measurement of the constant term in Z decays
  - ~10% for γ from H decays
  - 10% - 5% for e in ET 10-45 GeV

Mass: H→γγ categories

Table 1: Summary of the expected number of signal events in the 105–160 GeV mass range n_{sig}, the FWHM of mass resolution, σ_{eff} (half of the smallest range containing 68% of the signal events), number of background events b in the smallest mass window containing 90% of the signal (σ_{eff90}), and the ratio s/b and $s/\sqrt{b}$ with s the expected number of signal events in the window containing 90% of signal events, for the $H \to \gamma\gamma$ channel. b is derived from the fit of the data in the 105–160 GeV mass range. The value of m_H is taken to be 126 GeV and the signal yield is assumed to be the expected Standard Model value. The estimates are shown separately for the 7 TeV and 8 TeV datasets and for the inclusive sample as well as for each of the categories used in the analysis.

Category	n_{sig}	FWHM [GeV]	σ_{eff} [GeV]	b in $\pm\sigma_{eff90}$	s/b [%]	$s/\sqrt{b}$
$\sqrt{s}$=8 TeV						
Inclusive	402.	3.69	1.67	10670	3.39	3.50
Unconv. central low p_{Tt}	59.3	3.13	1.35	801	6.66	1.88
Unconv. central high p_{Tt}	7.1	2.81	1.21	26.0	24.6	1.26
Unconv. rest low p_{Tt}	96.2	3.49	1.53	2624	3.30	1.69
Unconv. rest high p_{Tt}	10.4	3.11	1.36	93.9	9.95	0.96
Unconv. transition	26.0	4.24	1.86	910	2.57	0.78
Conv. central low p_{Tt}	37.2	3.47	1.52	589	5.69	1.38
Conv. central high p_{Tt}	4.5	3.07	1.35	20.9	19.4	0.88
Conv. rest low p_{Tt}	107.2	4.23	1.88	3834	2.52	1.56
Conv. rest high p_{Tt}	11.9	3.71	1.64	144.2	7.44	0.89
Conv. transition	42.1	5.31	2.41	1977	1.92	0.85
$\sqrt{s}$=7 TeV						
Inclusive	73.9	3.38	1.54	1752	3.80	1.59
Unconv. central low p_{Tt}	10.8	2.89	1.24	128	7.55	0.85
Unconv. central high p_{Tt}	1.2	2.59	1.11	3.7	30.0	0.58
Unconv. rest low p_{Tt}	16.5	3.09	1.35	363	4.08	0.78
Unconv. rest high p_{Tt}	1.8	2.78	1.21	13.6	11.6	0.43
Unconv. transition	4.5	3.65	1.61	125	3.21	0.36
Conv. central low p_{Tt}	7.1	3.28	1.44	105	6.06	0.62
Conv. central high p_{Tt}	0.8	2.87	1.25	3.5	21.6	0.40
Conv. rest low p_{Tt}	21.0	3.93	1.75	695	2.72	0.72
Conv. rest high p_{Tt}	2.2	3.43	1.51	24.7	7.98	0.40
Conv. transition	8.1	4.81	2.23	365	2.00	0.38

Signal Model: Crystal-Ball + wide Gaussian
Background Model: exponential (high pTt), second order polynomial (others)
m_H resolution differences: estimate of effective constant term from Z→ee events and from lower pile-up in 7 TeV

Mass:H→γγ Systematics

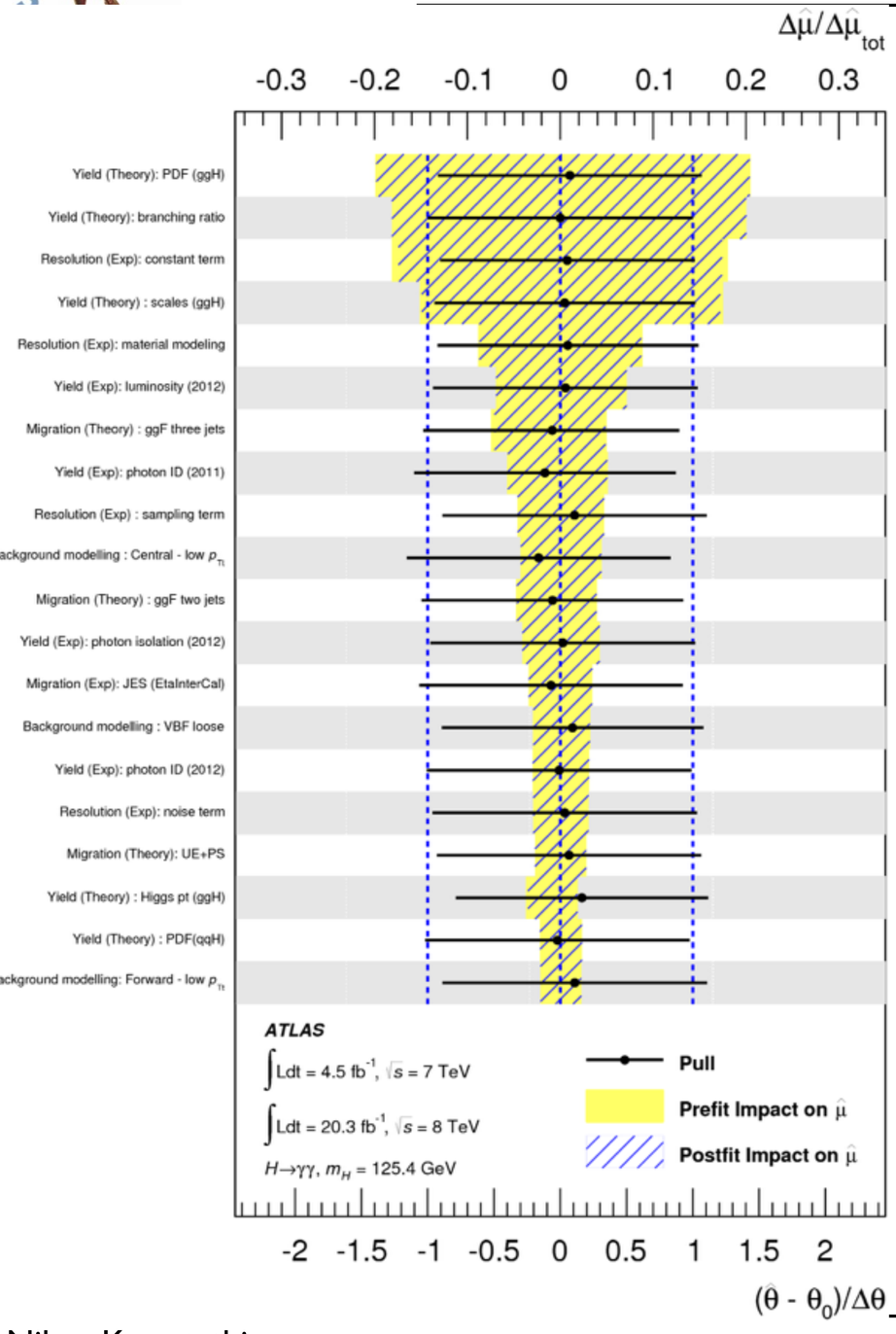

Table 2: Summary of the relative systematic uncertainties (in %) on the $H \to \gamma\gamma$ mass measurement for the different categories described in the text. The first seven rows give the impact of the photon energy scale systematic uncertainties, grouped into seven classes.

	Unconverted					Converted				
	Central		Rest		Trans.	Central		Rest		Trans.
Class	low p_{Tt}	high p_{Tt}	low p_{Tt}	high p_{Tt}		low p_{Tt}	high p_{Tt}	low p_{Tt}	high p_{Tt}	
$Z\to e^+e^-$ calibration	0.02	0.03	0.04	0.04	0.11	0.02	0.02	0.05	0.05	0.11
LAr cell non-linearity	0.12	0.19	0.09	0.16	0.39	0.09	0.19	0.06	0.14	0.29
Layer calibration	0.13	0.16	0.11	0.13	0.13	0.07	0.10	0.05	0.07	0.07
ID material	0.06	0.06	0.08	0.08	0.10	0.05	0.05	0.06	0.06	0.06
Other material	0.07	0.08	0.14	0.15	0.35	0.04	0.04	0.07	0.08	0.20
Conversion reconstruction	0.02	0.02	0.03	0.03	0.05	0.03	0.02	0.05	0.04	0.06
Lateral shower shape	0.04	0.04	0.07	0.07	0.06	0.09	0.09	0.18	0.19	0.16
Background modeling	0.10	0.06	0.05	0.11	0.16	0.13	0.06	0.14	0.18	0.20
Vertex measurement	0.03									
Total	0.23	0.28	0.24	0.30	0.59	0.21	0.25	0.27	0.33	0.47

Finally, uncertainties on the predicted overall signal yield are estimated as follows [17]. The uncertainty on the predicted cross-section for Higgs boson production is about 10% for the dominant gluon fusion process. The uncertainty on the predicted branching ratio to two photons is 5%. The uncertainty from the photon identification efficiency is derived from studies using several control samples: a sample of radiative Z decays, a sample of $Z\to e^+e^-$ events, where the shower shapes of electrons are corrected to resemble the shower shapes of photons, and a sample of high E_T isolated prompt photons. The estimated photon identification uncertainty amounts to 1.0% for the 8 TeV dataset, after correcting for small residual differences between simulation and data, and 8.4% for the 7 TeV dataset. The uncertainty is larger for the 7 TeV dataset because of the stronger correlation of the neural network photon identification with the photon isolation, and because the neural network identification relies more strongly on the correlations between the individual shower shape variables, complicating the measurement and introducing larger uncertainties on the estimate of its performance in data. The uncertainty on the integrated luminosity is 2.8% for the 8 TeV dataset and 1.8% for the 7 TeV dataset [31]. The uncertainties on the isolation cut efficiency and on the trigger efficiency are less than 1% for both the 7 TeV and 8 TeV datasets. These uncertainties on the overall signal yield also have a negligible effect on the mass measurement.

TABLE IX. Relative systematic uncertainties on the inclusive yields [%] for the 7 TeV and 8 TeV data. The numbers in parentheses refer to the uncertainties applied to events in the categories that are sensitive to $t\bar{t}H$ and VH production modes. The ranges of the category-dependent uncertainties due to the isolation efficiency are reported.

Uncertainty source	$\sqrt{s} = 7$ TeV	$\sqrt{s} = 8$ TeV
Luminosity	1.8	2.8
Trigger	0.2	0.2
Photon Id.	8.4(9.3)	1.0(4.1)
Isolation	1.3–2.3(3.8)	1.3–2.3(3.8)

Finally, uncertainties on the signal yields due to the photon energy scale and primary vertex selection are found to be negligible relative to the ones discussed above.

Mass: Hγγ mass consistency

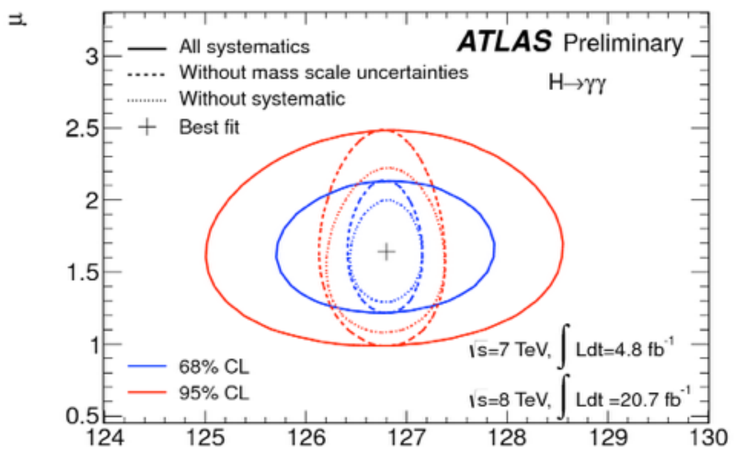

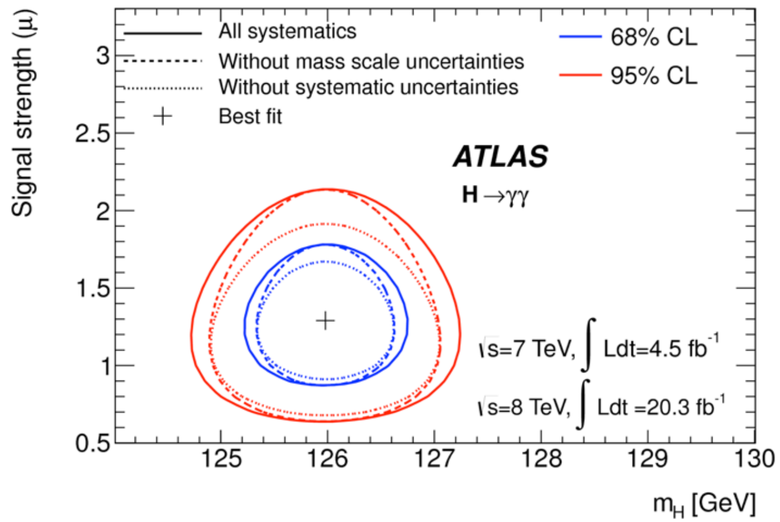

Higgs boson mass measurement using H→γγ:

- OLD : **126.8 ± 0.2 (stat) ± 0.7 (syst) GeV**
- NEW: **125.98 ± 0.42(stat) ± 0.28(syst) GeV**
- consistent with expected change from **updated photon energy scale calibration with smaller uncertainty**
  - average shift of -0.45 GeV with stat spread ~0.35 GeV expected
  - estimated from the distribution of the mass difference of the common events in the mass sidebands
- statistical uncertainty compatible with expected for given signal level (p-value 16%)
  - larger than in the past: a) lower signal strength (uncertainty inversely proportional to μ) , and b) larger resolution (in the past the observed resolution was better than expected for ideal detector)

Mass: HZZ Yields Inclusive

TABLE III. The number of events expected and observed for a $m_H = 125$ GeV hypothesis for the four-lepton final states. The second column shows the number of expected signal events for the full mass range. The other columns show the number of expected signal events, the number of ZZ^* and reducible background events, and the signal-to-background ratio (s/b), together with the numbers of observed events, in a window of $120 < m_{4\ell} < 130$ GeV for 4.5 fb^{-1} at $\sqrt{s} = 7$ TeV and 20.3 fb^{-1} at $\sqrt{s} = 8$ TeV as well as for the combined sample.

Final state	Signal Full mass range	Signal	ZZ^*	$Z+$jets, $t\bar{t}$	s/b	Expected	Observed
$\sqrt{s} = 7$ TeV							
4μ	1.00 ± 0.10	0.91 ± 0.09	0.46 ± 0.02	0.10 ± 0.04	1.7	1.47 ± 0.10	2
$2e2\mu$	0.66 ± 0.06	0.58 ± 0.06	0.32 ± 0.02	0.09 ± 0.03	1.5	0.99 ± 0.07	2
$2\mu 2e$	0.50 ± 0.05	0.44 ± 0.04	0.21 ± 0.01	0.36 ± 0.08	0.8	1.01 ± 0.09	1
$4e$	0.46 ± 0.05	0.39 ± 0.04	0.19 ± 0.01	0.40 ± 0.09	0.7	0.98 ± 0.10	1
Total	2.62 ± 0.26	2.32 ± 0.23	1.17 ± 0.06	0.96 ± 0.18	1.1	4.45 ± 0.30	6
$\sqrt{s} = 8$ TeV							
4μ	5.80 ± 0.57	5.28 ± 0.52	2.36 ± 0.12	0.69 ± 0.13	1.7	8.33 ± 0.6	12
$2e2\mu$	3.92 ± 0.39	3.45 ± 0.34	1.67 ± 0.08	0.60 ± 0.10	1.5	5.72 ± 0.37	7
$2\mu 2e$	3.06 ± 0.31	2.71 ± 0.28	1.17 ± 0.07	0.36 ± 0.08	1.8	4.23 ± 0.30	5
$4e$	2.79 ± 0.29	2.38 ± 0.25	1.03 ± 0.07	0.35 ± 0.07	1.7	3.77 ± 0.27	7
Total	15.6 ± 1.6	13.8 ± 1.4	6.24 ± 0.34	2.00 ± 0.28	1.7	22.1 ± 1.5	31
$\sqrt{s} = 7$ TeV and $\sqrt{s} = 8$ TeV							
4μ	6.80 ± 0.67	6.20 ± 0.61	2.82 ± 0.14	0.79 ± 0.13	1.7	9.81 ± 0.64	14
$2e2\mu$	4.58 ± 0.45	4.04 ± 0.40	1.99 ± 0.10	0.69 ± 0.11	1.5	6.72 ± 0.42	9
$2\mu 2e$	3.56 ± 0.36	3.15 ± 0.32	1.38 ± 0.08	0.72 ± 0.12	1.5	5.24 ± 0.35	6
$4e$	3.25 ± 0.34	2.77 ± 0.29	1.22 ± 0.08	0.76 ± 0.11	1.4	4.75 ± 0.32	8
Total	18.2 ± 1.8	16.2 ± 1.6	7.41 ± 0.40	2.95 ± 0.33	1.6	26.5 ± 1.7	37

Mass: HZZ Systematics

Table 9: The expected impact of the systematic uncertainties on the signal yield, derived from simulation, for $m_H = 125$ GeV, are summarized for each of the four final states for the combined 4.5 fb^{-1} at $\sqrt{s} = 7$ TeV and 20.3 fb^{-1} at $\sqrt{s} = 8$ TeV. The symbol "–" signifies that the systematic uncertainty does not contribute to a particular final state. The last three systematic uncertainties apply equally to all final states. All uncertainties have been symmetrized.

Source of uncertainty	4μ	$2e2\mu$	$2\mu2e$	$4e$	combined
Electron reconstruction and identification efficiencies	–	1.7%	3.3%	4.4%	1.6%
Electron isolation and impact parameter selection	–	0.07%	1.1%	1.2%	0.5%
Electron trigger efficiency	–	0.21%	0.05%	0.21%	<0.2%
$\ell\ell + ee$ backgrounds	–	–	3.4%	3.4%	1.3%
Muon reconstruction and identification efficiencies	1.9%	1.1%	0.8%	–	1.5%
Muon trigger efficiency	0.6%	0.03%	0.6%	–	0.2%
$\ell\ell + \mu\mu$ backgrounds	1.6%	1.6%	–	–	1.2%
QCD scale uncertainty					6.5%
PDF, α_s uncertainty					6.0%
$H \to ZZ^*$ branching ratio uncertainty					4.0%

Phys. Rev. D 90, 052004

Mass: H→ZZ*→4l

- High S/B~2 for 120-130GeV, excellent mass reso. (~1.6-2.2 GeV)
- Signature:
  - Same flavor, opposite sign, isolated di-leptons(e/μ)
  - Requirements on lepton p_T, vertexing and m_{ll}
- Backgrounds: ZZ→4l, Z+jets, ttbar
- Discriminant: 2D information from m_{4l} & O_{BDTzz}

Improved

- e-Identification→Likelihood method→ x2 better rejection of light jets and photon conversions for same signal efficiency
- Updated EM calibration (MVA) used for e and FSR photons
- Combined fit of track momentum and cluster energy → 4% improved m_{4l} resolution for H→ZZ*→4e/2e2μ
- O_{BDTzz} :MVA to separate signal and ZZ* background

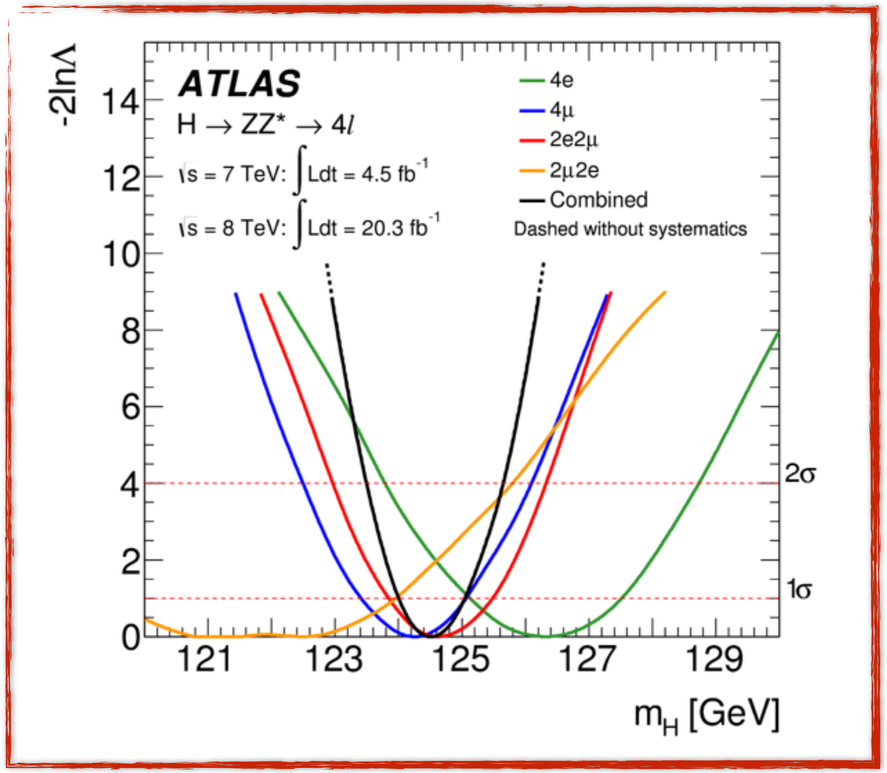

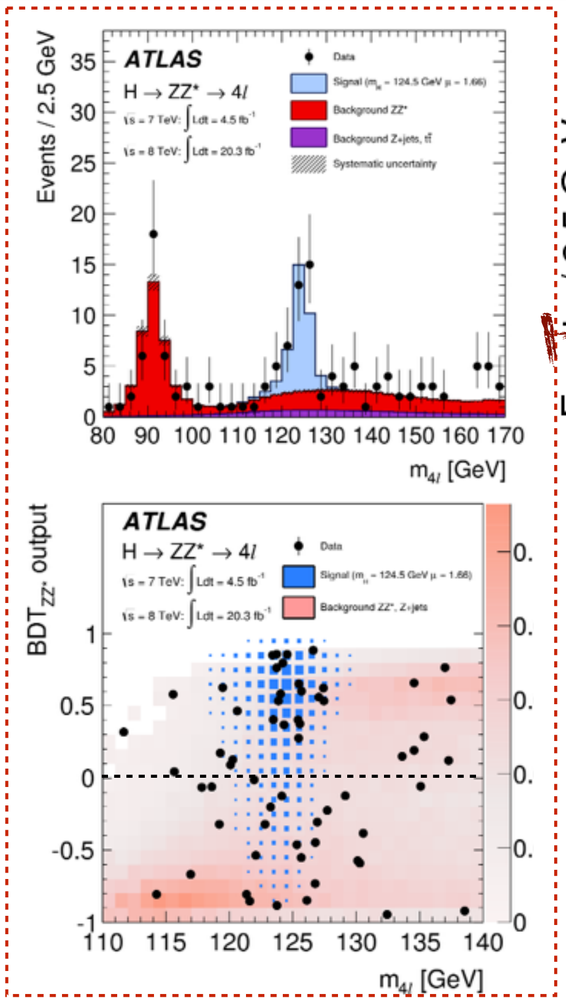

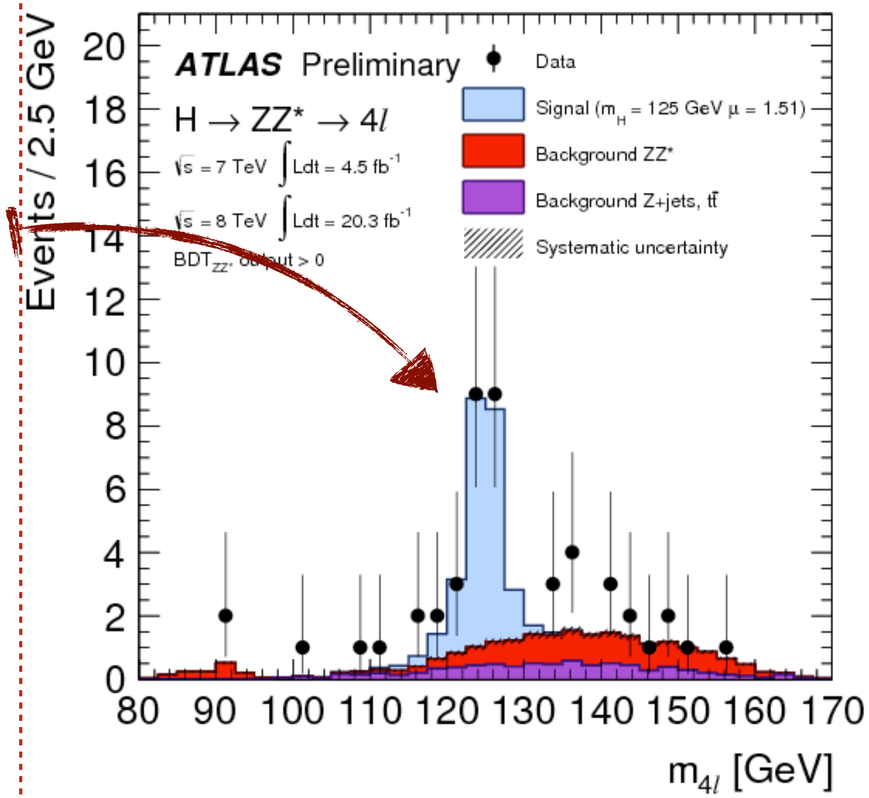

Maximum local significance 8.2σ (5.8σ)

at $m_H = 124.51 \pm 0.52 GeV$

with $\mu = 1.66^{+0.45}_{-0.38}$

Direct limit $\Gamma_H < 2.6\ (6.2) GeV$ at $95\%\ CL$

For more info: look at Nicolas' talk

Mass: HZZ

BDTs

BDT discriminant introduced to suppress ZZ* contribution
- Inputs: Matrix Element-based Kinematic Discriminant, p_{T4l}, η_{4l}

BDT discriminant introduced to discriminate between VBF signal and other (mainly ggF) contributions
- Inputs: m_{jj}, $\Delta\eta_{jj}$, Leading and Sub-leading jet pT, leading jet η

BDT discriminant introduced to discriminate between VH hadronic signal and other (mainly ggF) signals
- Inputs: m_{jj}, $\Delta\eta_{jj}$, Leading and Sub-leading jet pT, leading jet η

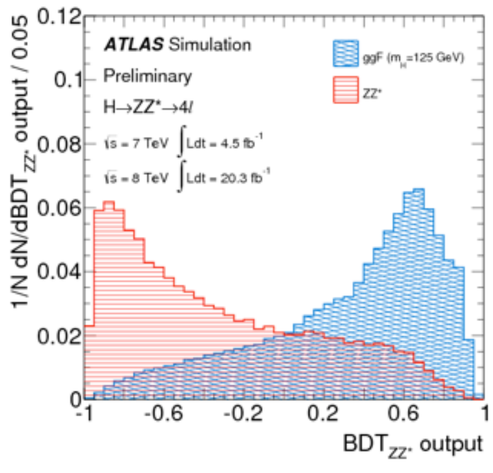

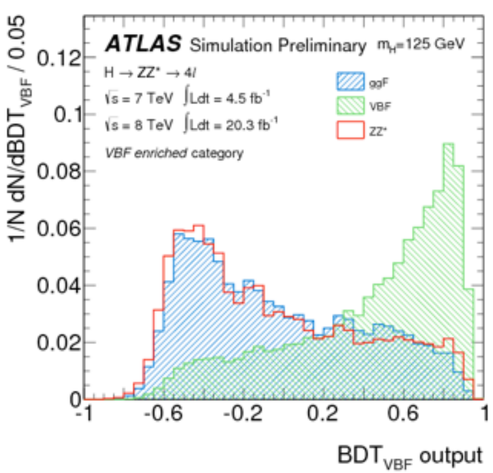

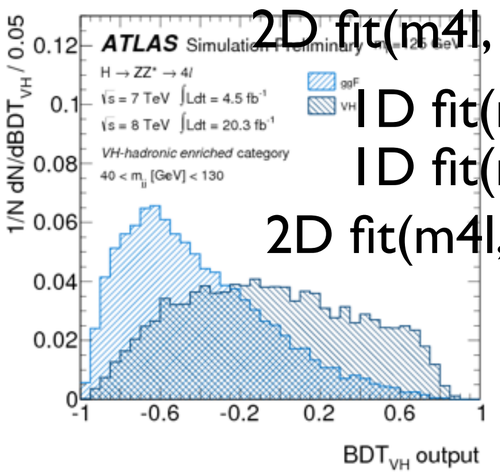

2D fit(m4l, BDTvbf)

1D fit(m4l)

1D fit(m4l)

2D fit(m4l,BDTzz)

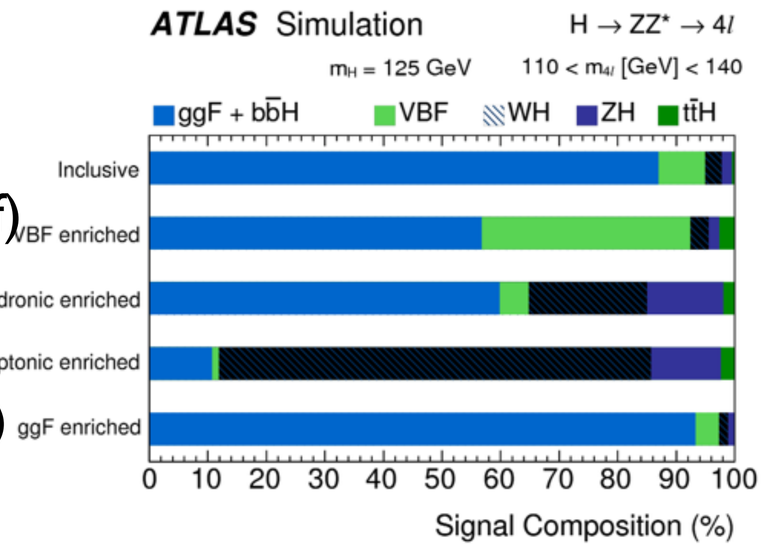

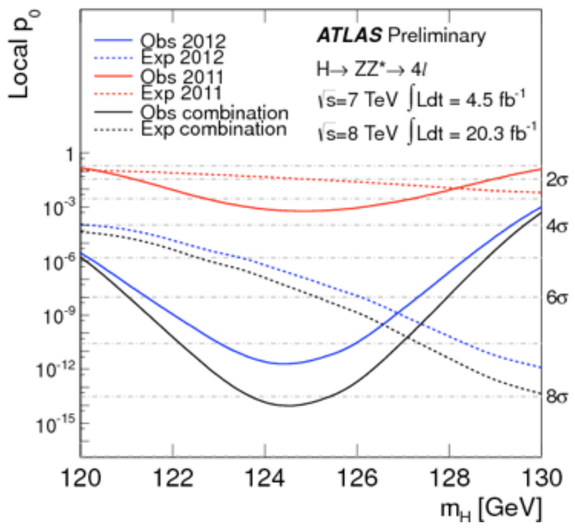

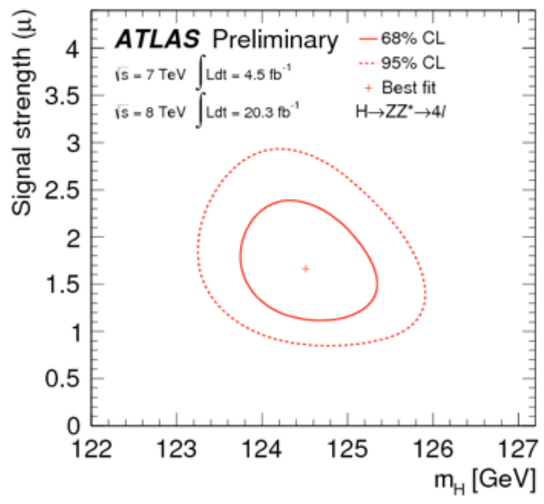

Inclusive Analysis

	Signal	ZZ	Other BKG	Observed	S/B
4μ	6.20±0.61	2.82±0.14	0.79±0.13	14	~1.7
2μ2e	3.15±0.32	1.38±0.08	0.72±0.12	6	~1.5
2e2μ	4.04±0.40	1.99±0.10	0.69±0.11	9	~1.5
4e	2.77±0.29	1.22±0.08	0.76±0.11	8	~1.4

Mass Combination Syst.

TABLE IV. Principal systematic uncertainties on the combined mass. Each uncertainty is determined from the change in the 68% CL range for m_H when the corresponding nuisance parameter is removed (fixed to its best-fit value), and it is calculated by subtracting this reduced uncertainty from the original uncertainty in quadrature.

Systematic	Uncertainty on m_H [MeV]
LAr syst on material before presampler (barrel)	70
LAr syst on material after presampler (barrel)	20
LAr cell nonlinearity (layer 2)	60
LAr cell nonlinearity (layer 1)	30
LAr layer calibration (barrel)	50
Lateral shower shape (conv)	50
Lateral shower shape (unconv)	40
Presampler energy scale (barrel)	20
ID material model ($\|\eta\| < 1.1$)	50
$H \to \gamma\gamma$ background model (unconv rest low p_{Tt})	40
$Z \to ee$ calibration	50
Primary vertex effect on mass scale	20
Muon momentum scale	10
Remaining systematic uncertainties	70
Total	180

Indirect Γ_H

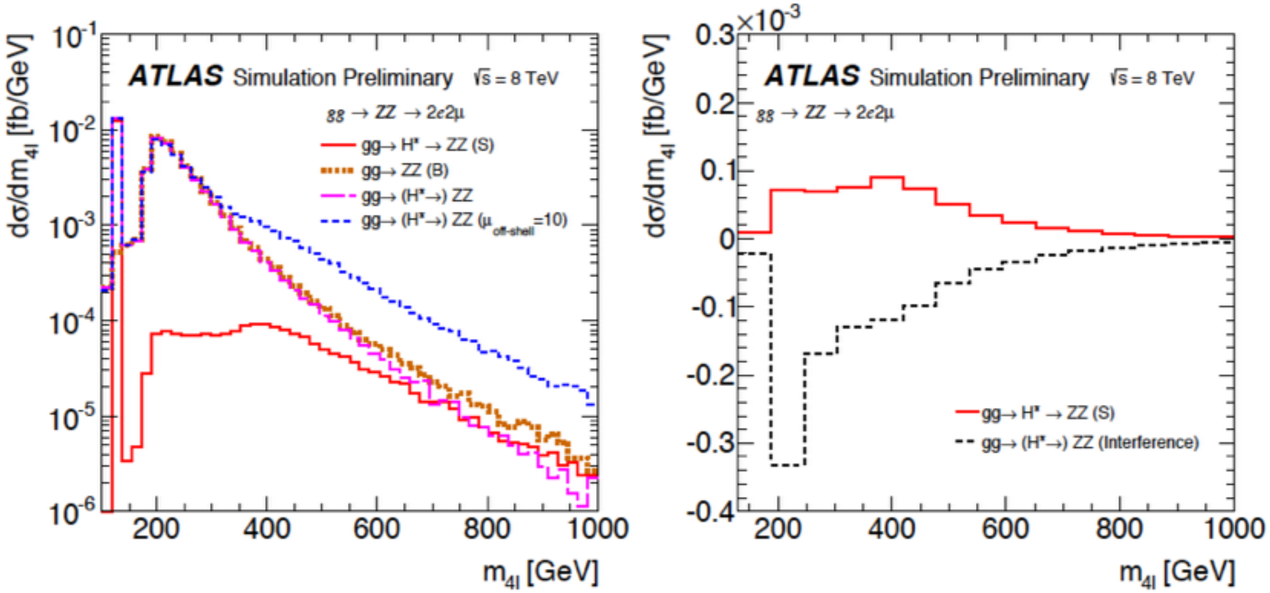

(a) (b)

Figure 1: (a) Differential cross-sections for the $gg \to (H^* \to)ZZ \to 2e2\mu$ channel at the parton level, for the $gg \to H^* \to ZZ$ signal (red solid line), $gg \to ZZ$ continuum background (thick brown dotted line), $gg \to (H^* \to)ZZ$ with SM Higgs coupling (magenta long dashed line) and $gg \to (H^* \to)ZZ$ with $\mu_{\text{off-shell}} = 10$ (blue long dashed line). (b) Differential cross-section as a function of m_{4l} for the $gg \to H^* \to ZZ \to 2e2\mu$ signal (solid red line) and its interference with the $gg \to ZZ \to 2e2\mu$ continuum background (black dashed line).

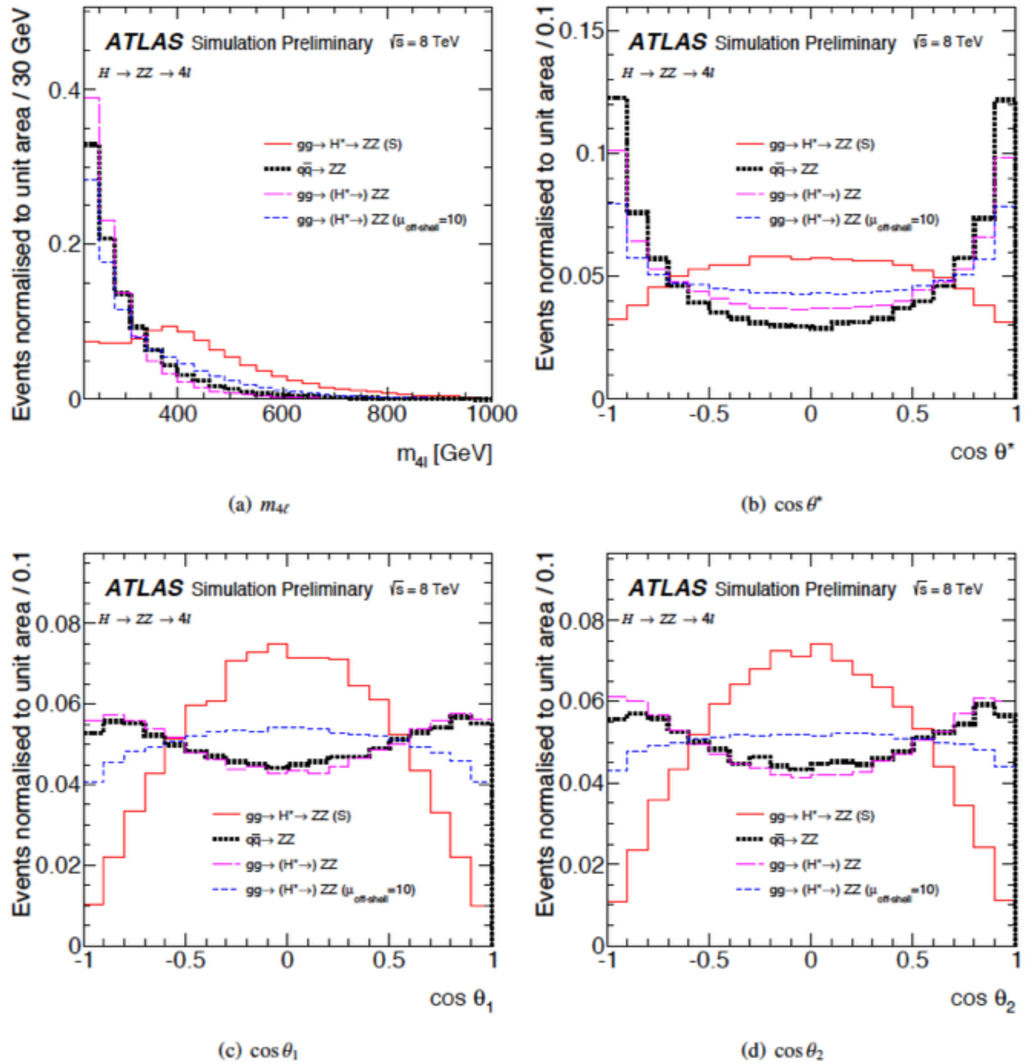

(a) $m_{4\ell}$ (b) $\cos\theta^*$

(c) $\cos\theta_1$ (d) $\cos\theta_2$

Figure 2: Distributions of the key input variables to the ME-based discriminant, for all lepton final states combined, normalised to unit area for shape comparisons, for the full off-peak region (220 GeV < $m_{4\ell}$ < 1000 GeV). The thick black dotted line represents the $q\bar{q} \to ZZ$ background, the red solid line the $gg \to H^* \to ZZ$ signal with SM couplings, the magenta long-dashed line the $gg \to (H^* \to)ZZ$ with SM $\mu_{\text{off-shell}}$, and the blue dashed line is for $gg \to (H^* \to)ZZ$ with $\mu_{\text{off-shell}} = 10$.

Indirect Γ_H

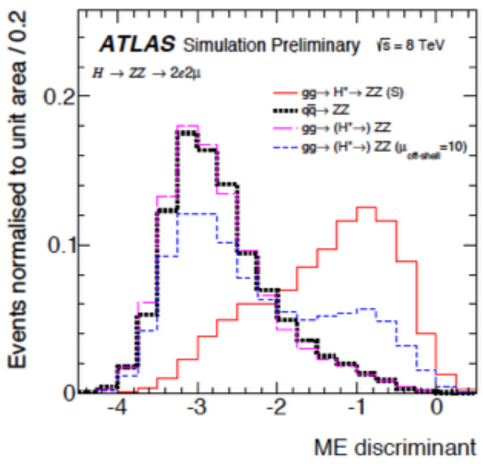

(a) $2e2\mu$

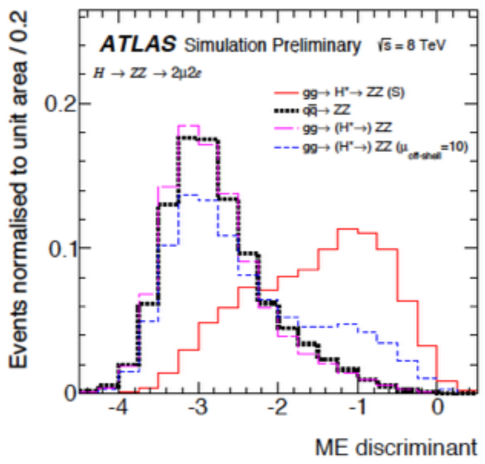

(b) $2\mu2e$

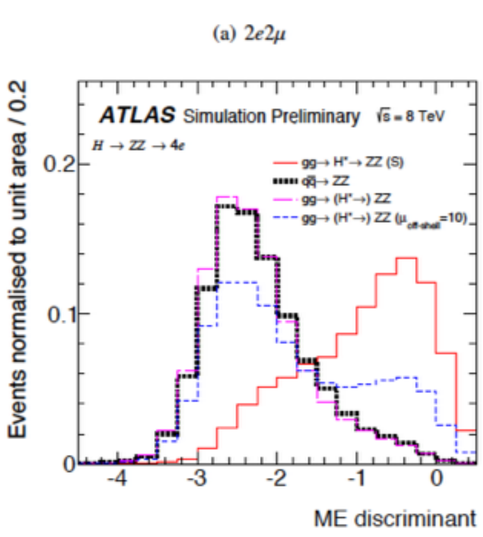

(c) $4e$

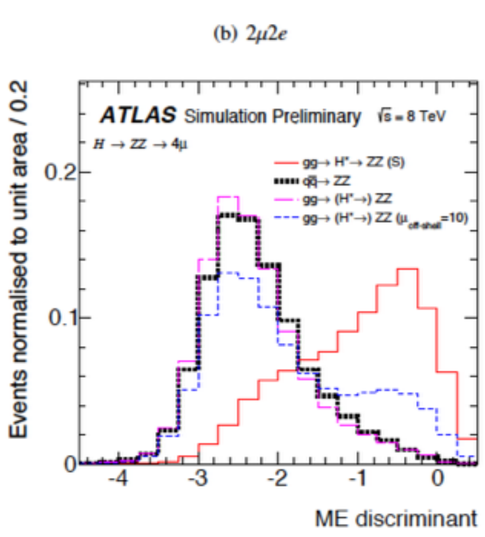

(d) 4μ

Figure 3: Distributions of the ME-based discriminant in the four lepton final states normalised to unit area to show the shape comparisons, for the full off-peak region (220 GeV < $m_{4\ell}$ < 1000 GeV). The thick black dotted line represents the $q\bar{q} \to ZZ$ background, the red solid line the $gg \to H^* \to ZZ$ signal with SM couplings, the magenta long-dashed line the $gg \to (H^* \to)ZZ$ with SM $\mu_{\text{off-shell}}$, and the blue dashed line is for $gg \to (H^* \to)ZZ$ with $\mu_{\text{off-shell}} = 10$.

Indirect Γ_H for the 2 analyses

ZZ→4l
- Off-peak region [220 GeV, 1TeV]
- Matrix Element Kinematic Discriminant to separate gg→H*→ZZ→4l from qq→ZZ→4l/ gg→(H*)→ZZ→4l
- Limit on off-shell rate based on fit on MEKD shape

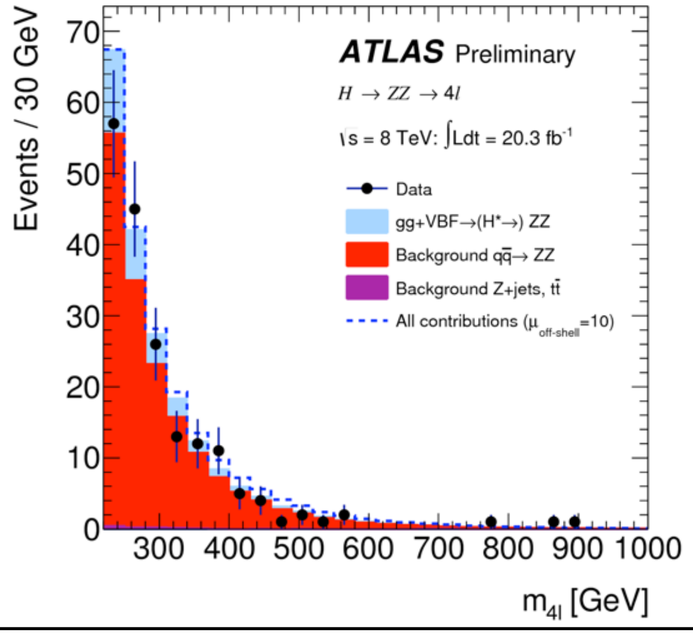

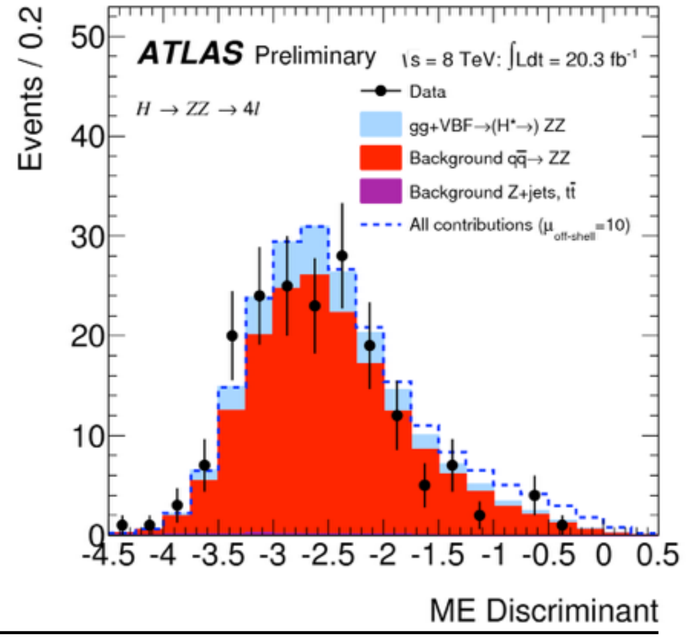

- H→ZZ→4l :
  - Event-by-event (det. response)⊗(H line-shape)
- H→γγ : Non relativistic Breight-Wigner ⊗ (det. resolution)

ZZ→llνν
- ETmiss>150 GeV and 76 GeV<m_{ll}<106
- Main backgrounds: qq→ZZ and WZ/WW, Z+jets and top
- Off-peak region m_{TZZ}>350 GeV
- Limit on off-shell rate based on event counting

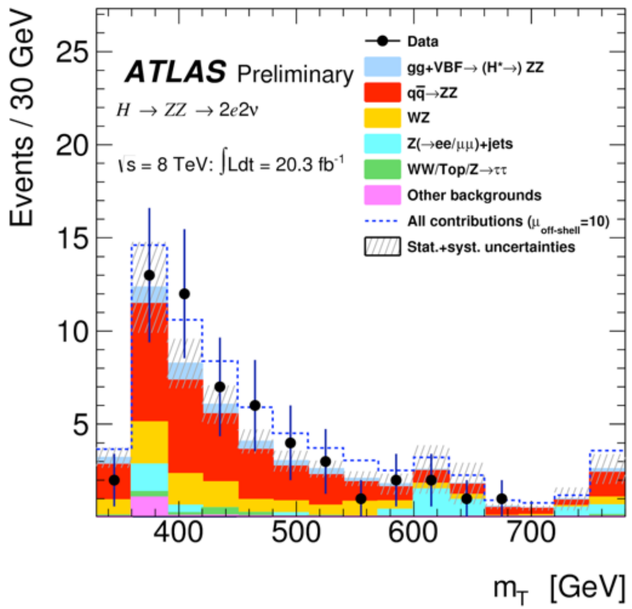

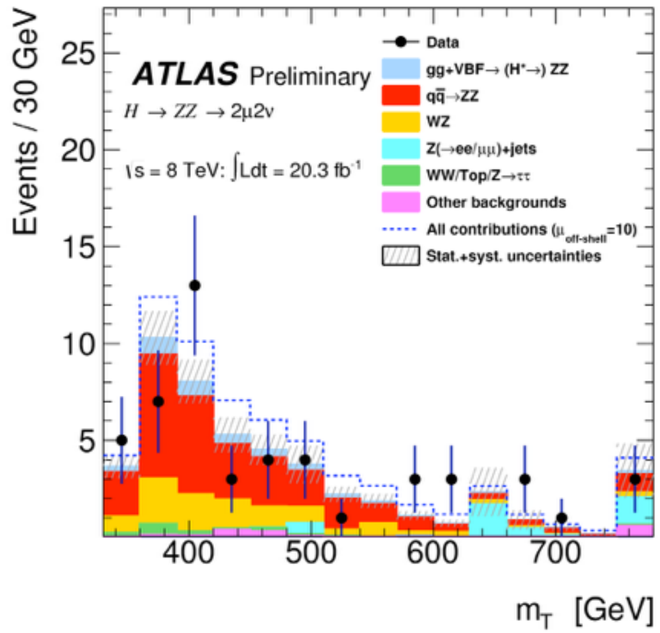

ΓH: Systematics

	Observed			Median expected		
$R^B_{H^*}$	0.5	**1.0**	2.0	0.5	**1.0**	2.0
$2\ell 2\nu$ cut-based	10.4	**11.3**	12.8	8.6	**9.9**	12.9

Table 5: The observed and expected 95% CL upper limit on $\mu_{\text{off-shell}}$ in the $2\ell 2\nu$ channel, within the range of $0.5 < R^B_{H^*} < 2$. The bold numbers correspond to the limit assuming $R^B_{H^*} = 1$. The upper limits are evaluated using the CL_s method, with the alternative hypothesis $R^B_{H^*} = 1$ and $\mu_{\text{off-shell}} = 1$.

	Observed			Median expected		
$R^B_{H^*}$	0.5	**1.0**	2.0	0.5	**1.0**	2.0
cut-based	10.8	**12.2**	14.9	13.6	**15.6**	19.9
ME-based discriminant analysis	6.1	**7.2**	9.9	8.7	**10.2**	14.0

Table 3: The observed and expected 95% CL upper limits on $\mu_{\text{off-shell}}$ in the cut-based and the ME-based discriminant analyses in the 4ℓ channel, within the range of $0.5 < R^B_{H^*} < 2$. The bold numbers correspond to the limit assuming $R^B_{H^*} = 1$. The upper limits are evaluated using the CL_s method, with the alternative hypothesis $R^B_{H^*} = 1$ and $\mu_{\text{off-shell}} = 1$.

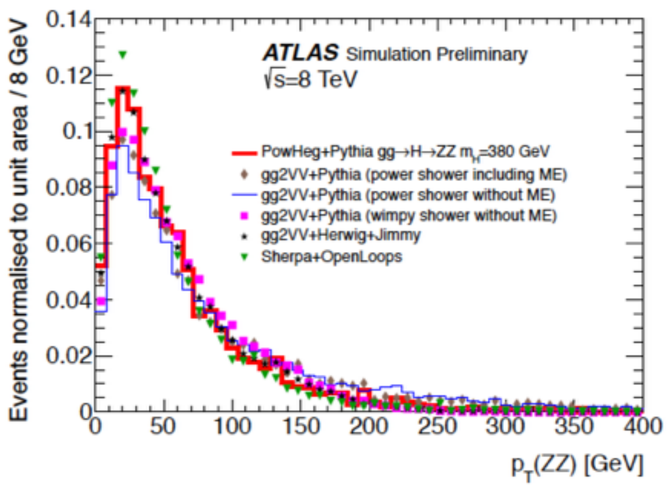

Figure 4: Generator-level distribution of $p_T(ZZ)$ for the $gg \to (H^* \to)ZZ$ process, comparing the NLO generator Powheg showered with Pythia8, the LO generator gg2VV with Pythia8 using a matrix element correction to the first jet, the power shower or the wimpy shower, the LO generator gg2VV showered with Jimmy+Herwig and a Sherpa+OpenLoops $gg \to ZZ$ sample with a matched 0-jet + 1-jet matrix element. All samples are restricted to the range $345 < m_{4\ell} < 415$ GeV in order to ensure a similar mass of the hard interaction system.

2l2v

4l

Source of systematic uncertainties	95% CL on $\mu_{\text{off-shell}}$
QCD scale for $gg \to ZZ$	7.9
QCD scale for the $gg \to (H^* \to)ZZ$ interference	7.7
QCD scale for $q\bar{q} \to ZZ$	7.6
PDF for $pp \to ZZ$	7.2
EW for $q\bar{q} \to ZZ$	7.1
Parton showering	7.1
Z BG systematic	7.4
Luminosity	7.3
Electron energy scale	7.1
Electron ID efficiency	7.1
Muon reconstruction efficiency	7.1
Jet energy scale	7.1
Sum of remaining systematic uncertainties	7.1
All systematic	9.9
No systematic	7.1

Table 6: The expected 95% CL upper limit on $\mu_{\text{off-shell}}$ in the $2\ell 2\nu$ channel, with a ranked listing of each systematic uncertainty individually, and comparing to including no systematic uncertainty or all systematic uncertainties. The upper limits are evaluated using the CL_s method, assuming $R^B_{H^*}$=1.

Source of systematic uncertainties	95% CL on $\mu_{\text{off-shell}}$
QCD scale for $gg \to ZZ$	9.5
QCD scale for the $gg \to (H^* \to)ZZ$ interference	9.2
QCD scale for $q\bar{q} \to ZZ$	8.8
PDF for $pp \to ZZ$	8.7
EW for $q\bar{q} \to ZZ$	8.7
Luminosity	8.8
electron efficiency	8.7
μ efficiency	8.7
All systematic	10.2
No systematic	8.7

Table 4: The expected 95% CL upper limit on $\mu_{\text{off-shell}}$ in the ME-based discriminant analysis in the 4ℓ channel, with a ranked listing of each systematic uncertainty individually, comparing with no systematic uncertainty or all systematic uncertainties. The upper limits are evaluated using the CL_s method, assuming $R^B_{H^*}$=1.

ΓH: Results

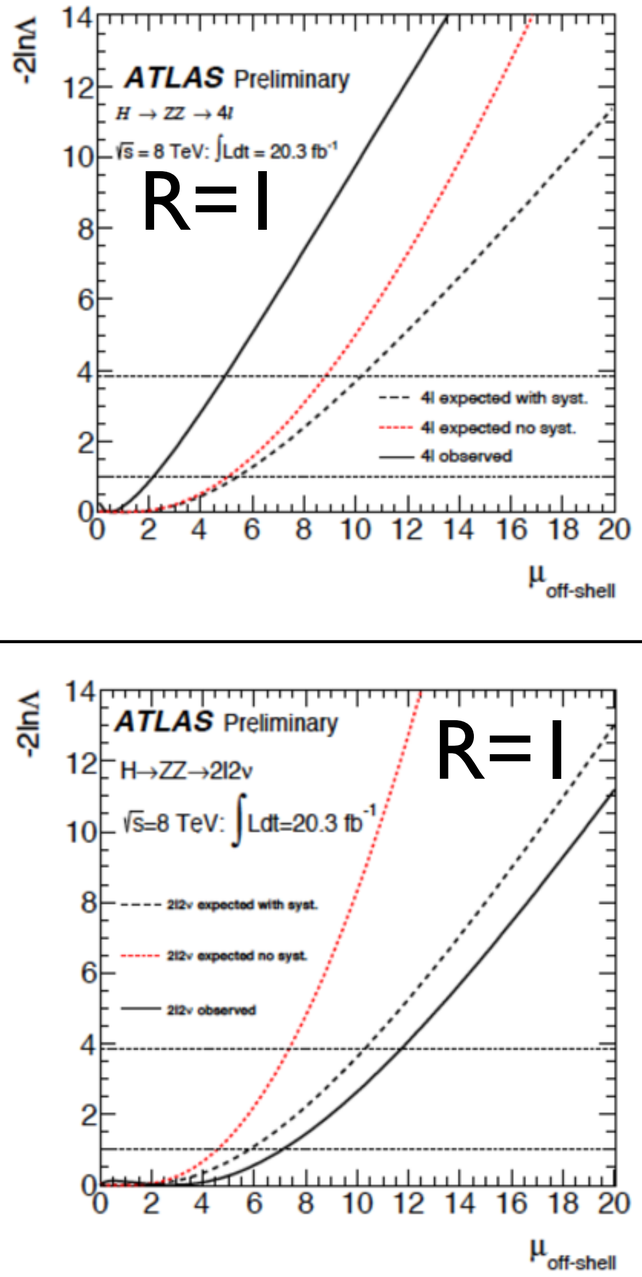

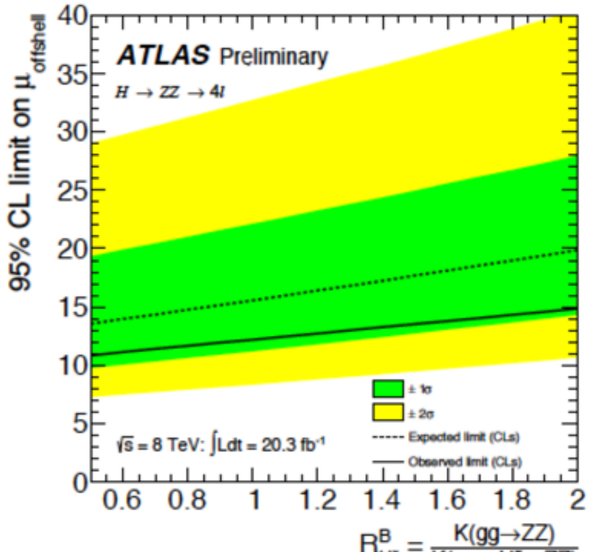

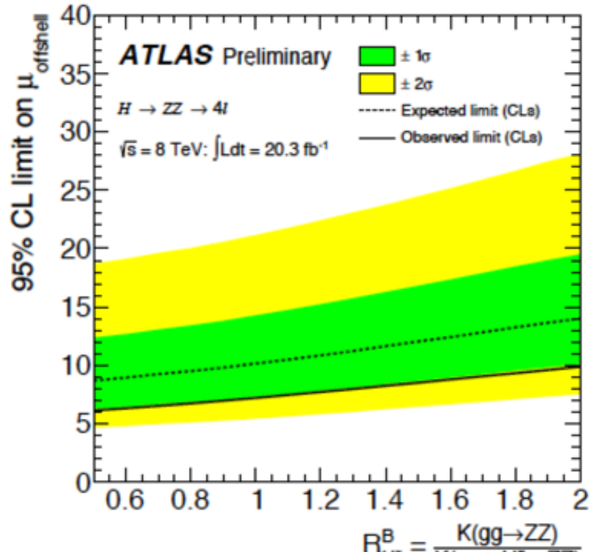

(a) Cut-based analysis (b) ME-based discriminant analysis

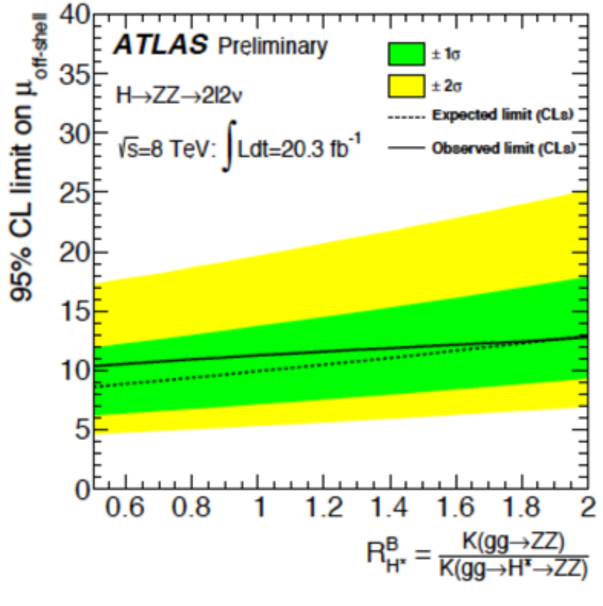

ΓH Full Result

Source of systematic uncertainties	95% CL on $\mu_{\text{off-shell}}$
QCD scale for $gg \to ZZ$	6.7
QCD scale for the $gg \to (H^* \to)ZZ$ interference	6.7
QCD scale for $q\bar{q} \to ZZ$	6.4
Z BG systematic	6.2
Luminosity	6.2
PDF for $pp \to ZZ$	6.1
Sum of remaining systematic uncertainties	6.2
No systematic	6.0
All systematic	7.9

Table 8: The expected 95% CL upper limit on $\mu_{\text{off-shell}}$ in the combination of the 4ℓ and $2\ell 2\nu$ channels, with a ranked listing of each systematic uncertainty individually, compared with no systematic uncertainty or all systematic uncertainties. The upper limits are evaluated using the CL_s method assuming $R^B_{H^*}$=1. Only the sources of systematic uncertainty that increase the limit by one significant digit are shown.

	Observed			Median expected			Alternative hypothesis
$R^B_{H^*}$	0.5	**1.0**	2.0	0.5	**1.0**	2.0	
$\mu_{\text{off-shell}}$	5.6	**6.7**	9.0	6.6	**7.9**	10.7	$R^B_{H^*} = 1, \mu_{\text{off-shell}} = 1$
$\Gamma_H/\Gamma_H^{\text{SM}}$	4.1	**4.8**	6.0	5.0	**5.8**	7.2	$R^B_{H^*} = 1, \Gamma_H/\Gamma_H^{\text{SM}} = 1, \mu_{\text{on-shell}} = 1.51$
$\Gamma_H/\Gamma_H^{\text{SM}}$	4.8	**5.7**	7.7	7.0	**8.5**	12.0	$R^B_{H^*} = 1, \Gamma_H/\Gamma_H^{\text{SM}} = 1, \mu_{\text{on-shell}} = 1$

Table 7: The observed and expected 95% CL upper limit on $\mu_{\text{off-shell}}$ and $\Gamma_H/\Gamma_H^{\text{SM}}$ within the range of $0.5 < R^B_{H^*} < 2$, combining the $ZZ \to 4\ell$ and $ZZ \to 2\ell 2\nu$ channels. The bold numbers correspond to the limit assuming $R^B_{H^*} = 1$. The upper limits are evaluated using the CL_s method, including all systematic uncertainties, with the alternative hypothesis as indicated in the last column. The two measurements of $\Gamma_H/\Gamma_H^{\text{SM}}$ differ only in the choice of the alternative hypothesis. In particular, $\mu_{\text{on-shell}}$ is treated as an auxiliary measurement in both cases in the fit and hence takes a value close to the observed value of $\mu_{\text{on-shell}} \sim 1.5$.

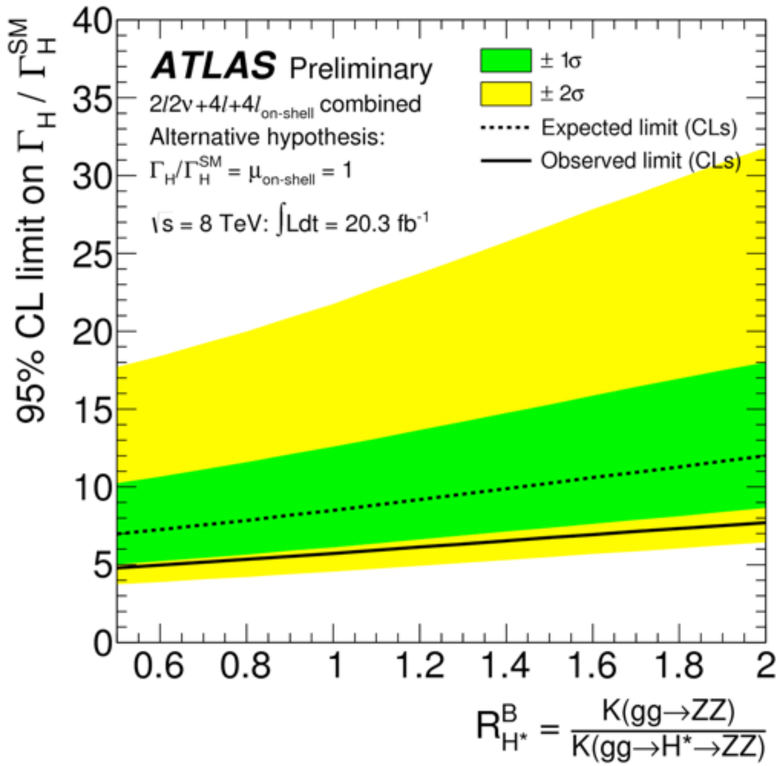

- Implemented with H→ZZ with the assumptions
  - Background insensitive to new physics modifying off-shell couplings
  - κi,on-shell = κi,off-shell (especially for κg in gg→H that is sensitive to new physics) (*)
  - use inclusive selections (NNLO/LO K-factor is known but calculated inclusively)
  - gg→ZZ background K-factors in the off-shell region unknown
    →Use signal K-factor for signal-bgr interference term but add an additional uncertainty.

H→WW

- Analysis designed to select VH(→ WW)
  - 3-lepton final state: WH→WWW→lvlvlv
    - 3 leptons, |ΣQ|=1, 0-b-tags, m_{ll}
  - 4 lepton final state: ZH→ZWW→lllvlv
    - 4 leptons, MET, 0 b-tags, m_{ll}

selection

Table 2: Selection listing for 8 TeV data. The criteria specific to $e\mu + \mu e$ and $ee + \mu\mu$ are noted as such; otherwise, they apply to both. Pre-selection applies to all N_{jet} modes. The rapidity gap is the y range spanned by the two leading jets. The $m_{\ell\ell}$ split is at 30 GeV. The modifications for the 7 TeV analysis are given in Section 6 and are not listed here. Energies, masses, and momenta are in units of GeV.

Category	$N_{\text{jet}} = 0$	$N_{\text{jet}} = 1$	$N_{\text{jet}} \geq 2$
Pre-selection	Two isolated leptons ($\ell = e, \mu$) with opposite charge Leptons with $p_{\text{T}}^{\text{lead}} > 25$ and $p_{\text{T}}^{\text{sublead}} > 15$ $e\mu + \mu e$: $m_{\ell\ell} > 10$ $ee + \mu\mu$: $m_{\ell\ell} > 12$, $\lvert m_{\ell\ell} - m_Z \rvert > 15$		
Missing transverse momentum and hadronic recoil	$e\mu + \mu e$: $E_{\text{T,rel}}^{\text{miss}} > 25$ $ee + \mu\mu$: $E_{\text{T,rel}}^{\text{miss}} > 45$ $ee + \mu\mu$: $p_{\text{T,rel}}^{\text{miss}} > 45$ $ee + \mu\mu$: $f_{\text{recoil}} < 0.05$	$e\mu + \mu e$: $E_{\text{T,rel}}^{\text{miss}} > 25$ $ee + \mu\mu$: $E_{\text{T,rel}}^{\text{miss}} > 45$ $ee + \mu\mu$: $p_{\text{T,rel}}^{\text{miss}} > 45$ $ee + \mu\mu$: $f_{\text{recoil}} < 0.2$	$e\mu + \mu e$: $E_{\text{T}}^{\text{miss}} > 20$ $ee + \mu\mu$: $E_{\text{T}}^{\text{miss}} > 45$ $ee + \mu\mu$: $E_{\text{T,STVF}}^{\text{miss}} > 35$ -
General selection	- $\lvert \Delta\phi_{\ell\ell,MET} \rvert > \pi/2$ $p_{\text{T}}^{\ell\ell} > 30$	$N_{b\text{-jet}} = 0$ - $e\mu + \mu e$: $Z/\gamma^* \to \tau\tau$ veto	$N_{b\text{-jet}} = 0$ $p_{\text{T}}^{\text{tot}} < 45$ $e\mu + \mu e$: $Z/\gamma^* \to \tau\tau$ veto
VBF topology	- - - -	- - - -	$m_{jj} > 500$ $\lvert \Delta y_{jj} \rvert > 2.8$ No jets ($p_{\text{T}} > 20$) in rapidity gap Require both ℓ in rapidity gap
$H \to WW^{(*)} \to \ell\nu\ell\nu$ topology	$m_{\ell\ell} < 50$ $\lvert \Delta\phi_{\ell\ell} \rvert < 1.8$ $e\mu + \mu e$: split $m_{\ell\ell}$ Fit m_{T}	$m_{\ell\ell} < 50$ $\lvert \Delta\phi_{\ell\ell} \rvert < 1.8$ $e\mu + \mu e$: split $m_{\ell\ell}$ Fit m_{T}	$m_{\ell\ell} < 60$ $\lvert \Delta\phi_{\ell\ell} \rvert < 1.8$ - Fit m_{T}

yields Njet=0

Table 8: Selection table for $N_{\text{jet}} = 0$ in 8 TeV data. The observed (N_{obs}) and expected (N_{exp}) yields for the signal (N_{sig}) and background (N_{bkg}) processes are shown for the (a) $e\mu + \mu e$ and (b) $ee + \mu\mu$ channels. The composition of N_{bkg} is given on the right. The requirements are imposed sequentially from top to bottom. Energies, masses, and momenta are in units of GeV. All uncertainties are statistical.

(a) $e\mu + \mu e$ channel

Selection	N_{obs}	N_{bkg}	N_{sig}	N_{WW}	N_{VV}	$N_{t\bar{t}}$	N_t	N_{Z/γ^*}	$N_{W+\text{jets}}$
$N_{\text{jet}} = 0$	9024	9000 ± 40	172 ± 2	4900 ± 20	370 ± 10	510 ± 10	310 ± 10	2440 ± 30	470 ± 10
$\lvert \Delta\phi_{\ell\ell,MET} \rvert > \frac{\pi}{2}$	8100	8120 ± 40	170 ± 2	4840 ± 20	360 ± 10	490 ± 10	310 ± 10	1690 ± 30	440 ± 10
$p_{\text{T}}^{\ell\ell} > 30$	5497	5490 ± 30	156 ± 2	4050 ± 20	290 ± 10	450 ± 10	280 ± 10	100 ± 10	320 ± 5
$m_{\ell\ell} < 50$	1453	1310 ± 10	124 ± 1	960 ± 10	110 ± 6	69 ± 3	46 ± 3	18 ± 7	100 ± 2
$\lvert \Delta\phi_{\ell\ell} \rvert < 1.8$	1399	1240 ± 10	119 ± 1	930 ± 10	107 ± 6	67 ± 3	44 ± 3	13 ± 7	88 ± 2

(b) $ee + \mu\mu$ channel

Selection	N_{obs}	N_{bkg}	N_{sig}	N_{WW}	N_{VV}	$N_{t\bar{t}}$	N_t	N_{Z/γ^*}	$N_{W+\text{jets}}$
$N_{\text{jet}} = 0$	16446	15600 ± 200	104 ± 1	2440 ± 10	190 ± 5	280 ± 6	175 ± 6	12300 ± 160	170 ± 10
$\lvert \Delta\phi_{\ell\ell,MET} \rvert > \frac{\pi}{2}$	13697	12970 ± 140	103 ± 1	2430 ± 10	190 ± 5	280 ± 6	174 ± 6	9740 ± 140	160 ± 10
$p_{\text{T}}^{\ell\ell} > 30$	5670	5650 ± 70	99 ± 1	2300 ± 10	170 ± 5	260 ± 6	167 ± 5	2610 ± 70	134 ± 4
$m_{\ell\ell} < 50$	2314	2390 ± 20	84 ± 1	760 ± 10	64 ± 3	53 ± 3	42 ± 3	1410 ± 20	62 ± 3
$p_{\text{T,rel}}^{\text{miss}} > 45$	1032	993 ± 10	63 ± 1	650 ± 10	42 ± 2	47 ± 3	39 ± 3	200 ± 5	19 ± 2
$\lvert \Delta\phi_{\ell\ell} \rvert < 1.8$	1026	983 ± 10	63 ± 1	640 ± 10	41 ± 2	46 ± 3	39 ± 3	195 ± 5	18 ± 2
$f_{\text{recoil}} < 0.05$	671	647 ± 7	42 ± 1	520 ± 10	30 ± 2	19 ± 2	22 ± 2	49 ± 3	12 ± 1

Table 9: Selection table for $N_{\text{jet}} = 1$ in 8 TeV data. More details are given in the caption of Table 8.

yields Njet=1

(a) $e\mu + \mu e$ channel

Selection	N_{obs}	N_{bkg}	N_{sig}	N_{WW}	N_{VV}	$N_{t\bar{t}}$	N_t	N_{Z/γ^*}	$N_{W+\text{jets}}$
$N_{\text{jet}} = 1$	9527	9460 ± 40	97 ± 1	1660 ± 10	270 ± 10	4980 ± 30	1600 ± 20	760 ± 20	195 ± 5
$N_{b\text{-jet}} = 0$	4320	4240 ± 30	85 ± 1	1460 ± 10	220 ± 10	1270 ± 10	460 ± 10	670 ± 10	160 ± 4
$Z \to \tau\tau$ veto	4138	4020 ± 30	84 ± 1	1420 ± 10	220 ± 10	1220 ± 10	440 ± 10	580 ± 10	155 ± 4
$m_{\ell\ell} < 50$	886	830 ± 10	63 ± 1	270 ± 4	69 ± 5	216 ± 6	80 ± 4	149 ± 5	46 ± 2
$\lvert \Delta\phi_{\ell\ell} \rvert < 1.8$	728	650 ± 10	59 ± 1	250 ± 4	60 ± 4	204 ± 6	76 ± 4	28 ± 3	34 ± 2

(b) $ee + \mu\mu$ channel

Selection	N_{obs}	N_{bkg}	N_{sig}	N_{WW}	N_{VV}	$N_{t\bar{t}}$	N_t	N_{Z/γ^*}	$N_{W+\text{jets}}$
$N_{\text{jet}} = 1$	8354	8120 ± 90	54 ± 1	820 ± 10	140 ± 10	2740 ± 20	890 ± 10	3470 ± 80	60 ± 10
$N_{b\text{-jet}} = 0$	5192	4800 ± 80	48 ± 1	720 ± 10	120 ± 10	720 ± 10	260 ± 10	2940 ± 70	40 ± 10
$m_{\ell\ell} < 50$	1773	1540 ± 20	38 ± 1	195 ± 4	35 ± 2	166 ± 5	65 ± 3	1060 ± 10	20 ± 2
$p_{\text{T,rel}}^{\text{miss}} > 45$	440	420 ± 10	21 ± 1	148 ± 3	21 ± 1	128 ± 5	52 ± 3	64 ± 4	5.1 ± 0.8
$\lvert \Delta\phi_{\ell\ell} \rvert < 1.8$	430	410 ± 10	20 ± 1	143 ± 3	20 ± 1	125 ± 5	51 ± 3	63 ± 4	4.5 ± 0.7
$f_{\text{recoil}} < 0.2$	346	320 ± 10	16 ± 1	128 ± 3	17 ± 1	97 ± 4	44 ± 3	25 ± 2	3.1 ± 0.6

H→WW

yields Njet>=2

Table 10: Selection table for $N_{\text{jet}} \geq 2$ in 8 TeV data. More details are given in the caption of Table 8. In this table, the $N_{\text{sig,ggF}}$ is included in N_{bkg}; the $N_{\text{sig},VH}$ is included in $N_{\text{sig,VBF}}$, but the contributions are negligible after the VBF-related criteria. The y gap is described in Table 2.

(a) $e\mu + \mu e$ channel

Selection	N_{obs}	N_{bkg}	$N_{\text{sig,VBF}}$	$N_{\text{sig,ggF}}$	N_{WW}	N_{VV}	$N_{t\bar{t}}$	N_t	N_{Z/γ^*}	$N_{W+\text{jets}}$
$N_{\text{jet}} \geq 2$	48723	47740 ± 80	43 ± 1	67 ± 1	940 ± 10	300 ± 20	41800 ± 70	2370 ± 20	1800 ± 30	440 ± 10
$N_{b\text{-jet}} = 0$	5852	5690 ± 30	31 ± 1	49 ± 1	690 ± 10	200 ± 10	2930 ± 20	350 ± 10	1300 ± 20	171 ± 5
$p_{\text{T}}^{\text{tot}} < 45$	4790	4620 ± 30	27 ± 1	41 ± 1	590 ± 10	160 ± 10	2320 ± 20	290 ± 10	1100 ± 20	126 ± 4
$Z \to \tau\tau$ veto	4007	3840 ± 30	25 ± 1	38 ± 1	540 ± 10	140 ± 10	2150 ± 20	260 ± 10	600 ± 20	108 ± 4
$\lvert\Delta y_{jj}\rvert > 2.8$	696	680 ± 10	12 ± 0.2	9.5 ± 0.3	100 ± 2	25 ± 3	380 ± 10	55 ± 3	95 ± 5	19 ± 2
$m_{jj} > 500$	198	170 ± 4	7.5 ± 0.1	2.9 ± 0.2	34 ± 1	5.6 ± 0.6	93 ± 3	11 ± 1	19 ± 2	4.4 ± 0.7
No jets in y gap	92	77 ± 2	6.3 ± 0.1	1.7 ± 0.2	25 ± 1	2.8 ± 0.4	30 ± 2	5.2 ± 0.8	9 ± 1	3.1 ± 0.6
Both ℓ in y gap	78	59 ± 2	6.1 ± 0.1	1.6 ± 0.1	19 ± 1	2.1 ± 0.3	22 ± 1	4.3 ± 0.7	7 ± 1	2.4 ± 0.5
$m_{\ell\ell} < 60$	31	16 ± 1	5.5 ± 0.1	1.5 ± 0.1	3.8 ± 0.4	0.7 ± 0.2	4.5 ± 0.7	0.7 ± 0.3	4.4 ± 0.8	1.0 ± 0.4
$\lvert\Delta\phi_{\ell\ell}\rvert < 1.8$	23	12 ± 1	5.1 ± 0.1	1.3 ± 0.1	3.5 ± 0.4	0.6 ± 0.2	3.7 ± 0.7	0.7 ± 0.3	1.9 ± 0.5	0.6 ± 0.3

(b) $ee + \mu\mu$ channel

Selection	N_{obs}	N_{bkg}	$N_{\text{sig,VBF}}$	$N_{\text{sig,ggF}}$	N_{WW}	N_{VV}	$N_{t\bar{t}}$	N_t	N_{Z/γ^*}	$N_{W+\text{jets}}$
$N_{\text{jet}} \geq 2$	32877	32300 ± 100	26 ± 0.7	40 ± 1	540 ± 6	180 ± 10	24540 ± 60	1390 ± 20	5420 ± 90	190 ± 10
$N_{b\text{-jet}} = 0$	65388	6370 ± 80	19 ± 0.6	30 ± 1	390 ± 5	130 ± 10	1750 ± 20	200 ± 10	3810 ± 80	58 ± 4
$p_{\text{T}}^{\text{tot}} < 45$	4903	4830 ± 70	17 ± 0.5	24 ± 1	340 ± 4	92 ± 5	1370 ± 10	170 ± 10	2790 ± 70	43 ± 3
$\lvert\Delta y_{jj}\rvert > 2.8$	958	930 ± 30	8.1 ± 0.2	6.2 ± 0.3	61 ± 2	12 ± 1.3	252 ± 6	35 ± 2	560 ± 30	6 ± 1
$m_{jj} > 500$	298	245 ± 6	5.5 ± 0.1	2.1 ± 0.2	23 ± 1	4.1 ± 1.1	62 ± 3	9 ± 1	142 ± 5	1.4 ± 0.6
No jets in y gap	147	119 ± 4	4.7 ± 0.1	1.1 ± 0.1	17 ± 1	2.8 ± 1.1	19 ± 1	4.1 ± 0.7	74 ± 3	0.7 ± 0.4
Both ℓ in y gap	108	85 ± 3	4.5 ± 0.1	0.9 ± 0.1	12 ± 1	2.3 ± 1.1	14 ± 1	3.1 ± 0.6	51 ± 3	0.3 ± 0.3
$m_{\ell\ell} < 60$	52	40 ± 2	4.0 ± 0.1	0.8 ± 0.1	3.2 ± 0.3	1.6 ± 1.1	3.7 ± 0.6	0.8 ± 0.3	30 ± 2	0.1 ± 0.2
$\lvert\Delta\phi_{\ell\ell}\rvert < 1.8$	42	34 ± 2	3.7 ± 0.1	0.7 ± 0.1	2.8 ± 0.3	1.6 ± 1.1	3.3 ± 0.5	0.7 ± 0.3	25 ± 2	0.1 ± 0.2

Table 11: Summary selection table for 8 TeV data for events in the m_{T} range noted in Section 3.5. The uncertainty on N_{bkg} accounts for the correlations among the sources. More details are given in the caption of Table 7.

N_{jet}	N_{obs}	N_{bkg}	N_{sig}	N_{WW}	N_{VV}	$N_{t\bar{t}}$	N_t	N_{Z/γ^*}	$N_{W+\text{jets}}$
$= 0$	831	739 ± 39	97 ± 20	551 ± 41	58 ± 8	23 ± 3	16 ± 2	30 ± 10	61 ± 21
$= 1$	309	261 ± 28	40 ± 13	108 ± 40	27 ± 6	68 ± 18	27 ± 10	12 ± 6	20 ± 5
≥ 2	55	36 ± 4	10.6 ± 1.4	4.1 ± 1.5	1.9 ± 0.4	4.6 ± 1.7	0.8 ± 0.4	22 ± 3	0.7 ± 0.2

systematics

Table 12: Leading systematic uncertainties on the expected event yields for the 8 TeV analysis. The first four rows are calculated for inclusive N_{jet} modes and redistributed to exclusive ones (Section 5). The QCD scale uncertainties on the inclusive ggF cross sections are anti-correlated between the exclusive N_{jet} modes. Some uncertainties are grouped differently with respect to Table 11 to reflect the treatment of correlations; most experimental ones are correlated between the signal and background. Sources contributing less than 4% to any column, and individual entries below 1%, are omitted.

	Signal processes (%)			Background processes (%)		
Source	$N_{\text{jet}} = 0$	$N_{\text{jet}} = 1$	$N_{\text{jet}} \geq 2$	$N_{\text{jet}} = 0$	$N_{\text{jet}} = 1$	$N_{\text{jet}} \geq 2$
Theoretical uncertainties						
QCD scale for ggF signal for $N_{\text{jet}} \geq 0$	13	-	-	-	-	-
QCD scale for ggF signal for $N_{\text{jet}} \geq 1$	10	27	-	-	-	-
QCD scale for ggF signal for $N_{\text{jet}} \geq 2$	-	15	4	-	-	-
QCD scale for ggF signal for $N_{\text{jet}} \geq 3$	-	-	4	-	-	-
Parton shower and UE model (signal only)	3	10	5	-	-	-
PDF model	8	7	3	1	1	1
$H \to WW$ branching ratio	4	4	4	-	-	-
QCD scale (acceptance)	4	4	3	-	-	-
WW normalisation	-	-	-	1	2	4
Experimental uncertainties						
Jet energy scale and resolution	5	2	6	2	3	7
b-tagging efficiency	-	-	-	-	7	2
f_{recoil} efficiency	1	1	-	4	2	-

H→WW VH (3/4 Yields,Selec.)

Table 1: Summary of the selection criteria defining the 3-lepton signal regions.

Signal Selections		
Cut	*Z-enriched*	*Z-depleted*
Jet multiplicity	$N_{\text{jet}} \leq 1$	
b-veto	$N_{b-\text{tag}} = 0$	
$E_{\text{T,rel}}^{\text{miss}}$ cut	$E_{\text{T,rel}}^{\text{miss}} > 40$ GeV	$E_{\text{T,rel}}^{\text{miss}} > 25$ GeV
Dilepton mass cuts	$\lvert m_{\ell\ell} - m_Z \rvert > 25$ GeV and $m_{\ell\ell} > 12$ GeV	$m_{\ell\ell} > 12$ GeV
Angular cut	$\Delta R_{\ell_0\ell_1} < 2.0$	
Overlap removal	remove overlap with $H \rightarrow WW$ analysis [6]	

Table 2: Number of expected events for the signal and the background, for an integrated luminosity of 20.7 fb^{-1}, and number of events observed in the data, as a function of the selection requirement (see Table 1).

	VVV	*VV*	Fakes	Total Bkg.	*VH*(125)	Data
3 leptons	19.5±0.5	2410±50	930±100	3370±150	18.53±0.25	3717
Z-enriched ($eee + \mu\mu\mu$)	5.89±0.18	1228±23	380±40	1620±50	7.31±0.17	1711
Jet multiplicity and b-veto	4.79±0.19	1064±24	273±33	1350±50	4.85±0.13	1321
$E_{\text{T,rel}}^{\text{miss}}$ cut	2.51±0.13	241±6	12±7	256±12	1.72±0.07	252
Dilepton mass cuts	0.86±0.07	12.2±0.6	5±5	18±5	0.48±0.03	12
Angular cut	0.64±0.06	9.0±0.5	4±4	14±4	0.45±0.03	9
Overlap removal	0.63±0.06	8.7±0.5	4±4	14±4	0.42±0.03	8
Z-enriched ($ee\mu + \mu\mu e$)	9.54±0.29	1180±29	530±90	1730±120	9.25±0.18	1968
Jet multiplicity and b-veto	7.97±0.29	1008±29	420±90	1440±120	6.56±0.14	1490
$E_{\text{T,rel}}^{\text{miss}}$cut	4.24±0.19	219±7	12±6	235±12	2.37±0.08	247
Dilepton mass cuts	2.35±0.13	15.6±0.8	2.3±1.8	20.3±2.3	1.17±0.05	24
Angular cut	1.67±0.11	10.8±0.6	0.65±0.22	13.2±0.8	1.11±0.04	16
Overlap removal	1.56±0.11	10.1±0.6	0.50±0.20	12.2±0.7	1.04±0.04	16
Z-depleted	4.10±0.16	6.0±0.4	20±4	30±4	1.98±0.06	38
Jet multiplicity and b-veto	3.61±0.16	4.79±0.33	7±4	15±4	1.66±0.05	16
$E_{\text{T,rel}}^{\text{miss}}$ cut	2.42±0.12	1.82±0.20	0.8±0.4	5.0±0.6	1.05±0.04	12
Dilepton mass cut	2.40±0.12	1.81±0.20	0.8±0.4	5.0±0.6	1.01±0.04	12
Angular cut	1.54±0.09	0.86±0.14	0.8±0.4	3.2±0.5	0.92±0.04	10
Overlap removal	1.45±0.09	0.68±0.12	0.58±0.35	2.7±0.5	0.88±0.04	9

Table 3: Summary of the selection criteria defining the 4-lepton signal regions.

Signal Selections		
Cut		
$E_{\text{T}}^{\text{miss}}$ cut	$E_{\text{T}}^{\text{miss}} > 30$ GeV	
p_{T}^{ℓ} cuts	highest p_{T} lepton: $p_{\text{T}} > 25$ GeV second highest p_{T} lepton: $p_{\text{T}} > 20$ GeV third highest p_{T} lepton: $p_{\text{T}} > 15$ GeV fourth highest p_{T} lepton: $p_{\text{T}} > 10$ GeV	
Jet multiplicity	$N_{\text{jet}} \leq 1$	
b-veto	$N_{b-\text{tag}} = 0$	
Mass cuts	$\lvert m_{\ell_2\ell_3} - m_Z \rvert < 10$ GeV 10 GeV $< m_{\ell_0\ell_1} <$ 65 GeV	
Angular cut	$\Delta\phi_{01}^{\text{boost}} < 2.5$	
Channel separation	2SFOS	1SFOS
$p_{\text{T}4\ell}$ cut	$p_{\text{T}4\ell} > 30$ GeV	
$m_{4\ell}$ cut	$m_{4\ell} > 130$ GeV	
Overlap removal [6]	remove overlap with $H \rightarrow WW$ analysis	

Table 4: Number of expected events for the signal and the background, for an integrated luminosity of 20.7 fb^{-1}, and number of events observed in the data, as a function of the selection requirement (see Table 3).

	ZZ	*VVV*	Fakes	Total Bkg.	*VH*(125)	Data
4 leptons	164±6	1.89±0.08	8.8±5.8	175±10	0.89±0.04	182
$E_{\text{T}}^{\text{miss}}$ and p_{T}	41.8±1.6	1.65±0.07	7.8±5.3	51.3±5.6	0.71±0.03	55
Jet multiplicity and b-veto	30.8±1.1	1.30±0.06	0.31±0.11	32.5±1.2	0.52±0.02	35
Mass cuts	2.97±0.15	0.22±0.02	0.05±0.03	3.24±0.16	0.41±0.02	2
Angular cut	1.88±0.12	0.20±0.02	0.04±0.02	2.12±0.12	0.39±0.02	2
1 SFOS pair	0.24±0.04	0.08±0.01	0.00±0.01	0.33±0.05	0.19±0.01	2
Overlap removal	0.23±0.04	0.08±0.01	0.00±0.01	0.32±0.05	0.18±0.01	2
2 SFOS pairs	1.64±0.11	0.12±0.01	0.04±0.02	1.79±0.11	0.20±0.01	0
4ℓ system cuts	0.72±0.07	0.11±0.01	0.04±0.02	0.86±0.08	0.18±0.01	0
Overlap removal	0.70±0.07	0.10±0.01	0.04±0.02	0.84±0.08	0.17±0.01	0

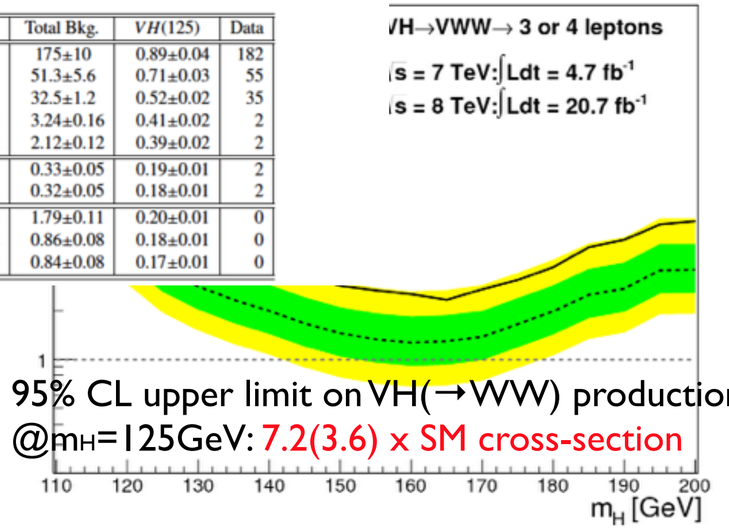

95% CL upper limit on VH(→WW) production
@m_H=125GeV: 7.2(3.6) x SM cross-section

H→WW (VH)

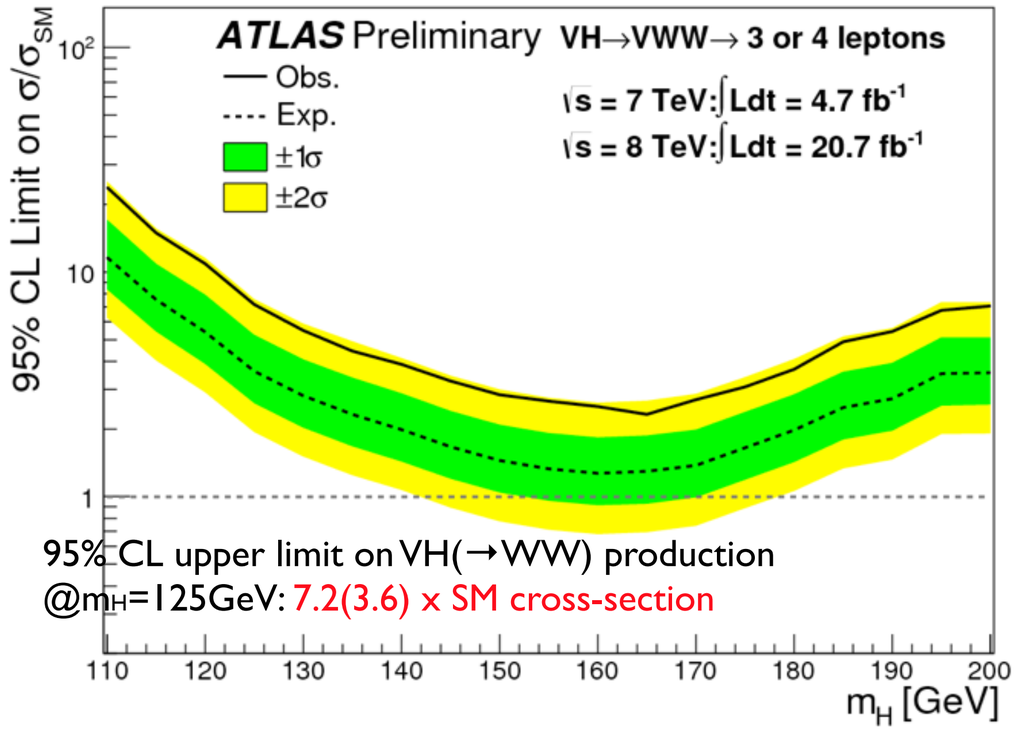
ATLAS Preliminary VH→VWW→ 3 or 4 leptons
Obs.
Exp.
±1σ
±2σ
√s = 7 TeV: ∫Ldt = 4.7 fb-1
√s = 8 TeV: ∫Ldt = 20.7 fb-1
95% CL Limit on σ/σSM
95% CL upper limit on VH(→WW) production
@mH=125GeV: 7.2(3.6) x SM cross-section
mH [GeV]

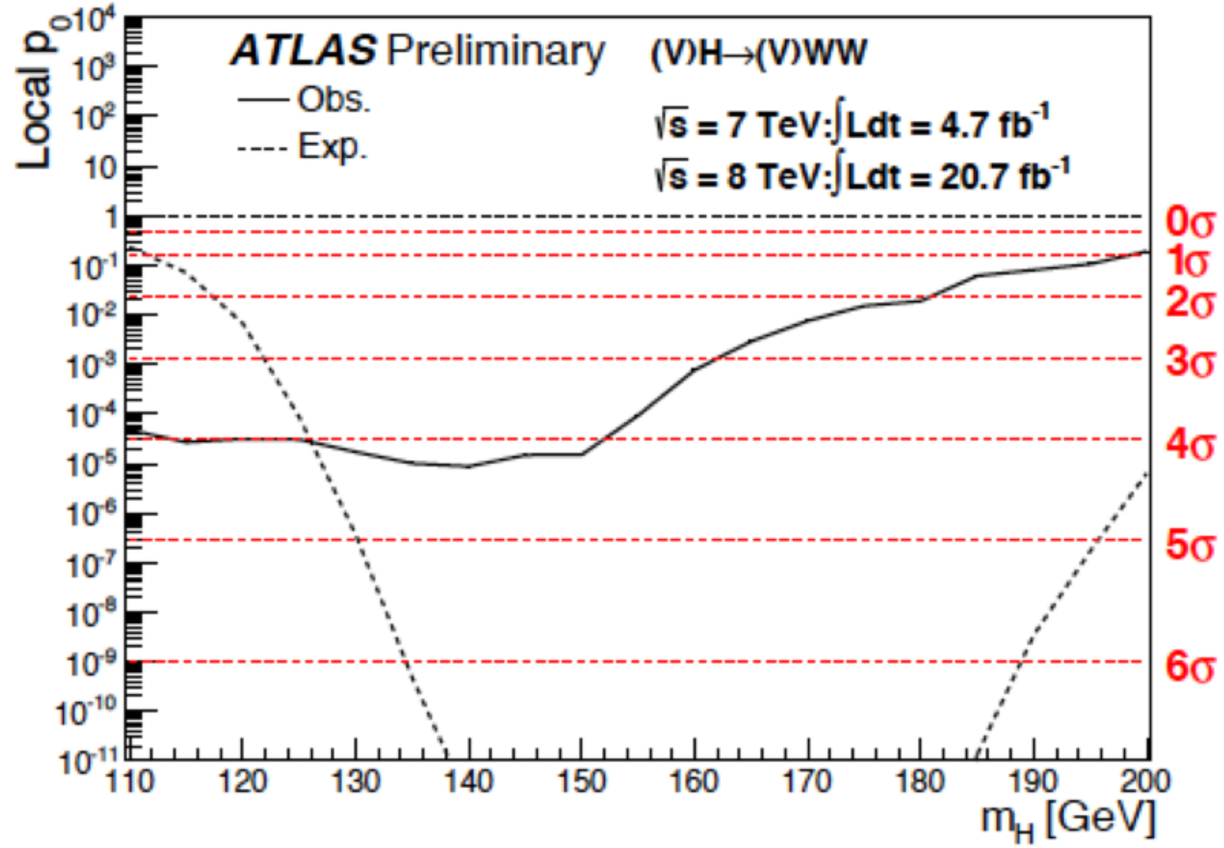
ATLAS Preliminary (V)H→(V)WW
Obs.
Exp.
√s = 7 TeV: ∫Ldt = 4.7 fb-1
√s = 8 TeV: ∫Ldt = 20.7 fb-1
Local p0
0σ
1σ
2σ
3σ
4σ
5σ
6σ
mH [GeV]

H→ττ

Trigger	p_T threshold(s) [GeV]	$\tau_{lep}\tau_{lep}$	$\tau_{lep}\tau_{had}$	$\tau_{had}\tau_{had}$
Electron	24	•	•	
Muon	24		•	
Di-electron	12 ; 12	•		
Di-muon	18 ; 8	•		
Electron + Muon	12 ; 8	•		
Electron + τ_{had}	18 ; 20		•	
Muon + τ_{had}	15 ; 20		•	
Di-τ_{had}	29 ; 20			•

Table 1: Triggers used for each channel. When more than one trigger is used, a logical OR of the triggers is taken and the trigger efficiency is calculated accordingly. The electron+τ_{had} and muon+τ_{had} triggers are used for the $\tau_{lep}\tau_{had}$ channel at preselection, but not in the VBF and boosted categories as defined in Section 7.

Category	Selection	$\tau_{lep}\tau_{lep}$	$\tau_{lep}\tau_{had}$	$\tau_{had}\tau_{had}$
VBF	$p_T(j_1)$ (GeV)	40	50	50
	$p_T(j_2)$ (GeV)	30	30	30/35
	$\Delta\eta(j_1, j_2)$	2.2	3.0	2.0
	b–jet veto for jet p_T (GeV)	25	30	-
	p_T^H (GeV)	-	-	40
Boosted	$p_T(j_1)$ (GeV)	40	-	-
	p_T^H (GeV)	100	100	100
	b–jet veto for jet p_T (GeV)	25	30	-

Table 2: Selection criteria applied in each analysis category for each channel. The numbers shown are lower thresholds. Only events that fail VBF category selection are considered for the boosted category. The $\Delta\eta(j_1, j_2)$ cut is applied on the two highest p_T jets in the event. Events in the $\tau_{lep}\tau_{had}$ VBF category must also satisfy $m_{\tau\tau}^{vis} > 40$ GeV, and those that fail this requirement are not considered for the $\tau_{lep}\tau_{had}$ boosted category. The $p_T(j_2)$ threshold in the $\tau_{had}\tau_{had}$ channel is 30 (35) GeV for jets within (outside of) $|\eta| = 2.4$.

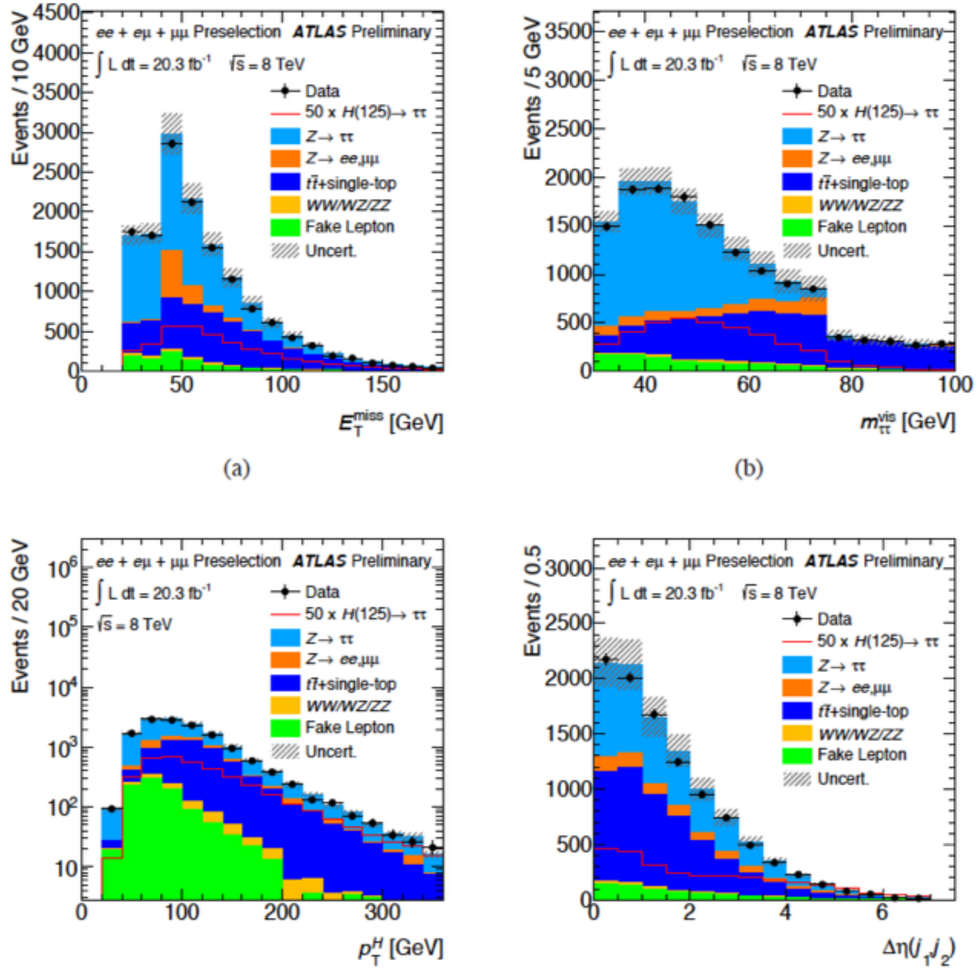

Figure 1: Kinematic distributions for the $\tau_{lep}\tau_{lep}$ channel after preselection: (a) E_T^{miss}, (b) $m_{\tau\tau}^{vis}$, (c) p_T^H, and (d) $\Delta\eta(j_1, j_2)$. The background estimate for these distributions is described in Section 9. The $m_{\tau\tau}^{vis}$ distribution shows a step at 75 GeV due to the difference in cuts between same flavour and different flavour event selection. The $\Delta\eta(j_1, j_2)$ distribution is shown for events with at least two jets. Signal shapes are shown multiplied by a factor of 50. These figures use background predictions made without the global fit defined in Section 12.

H→ττ

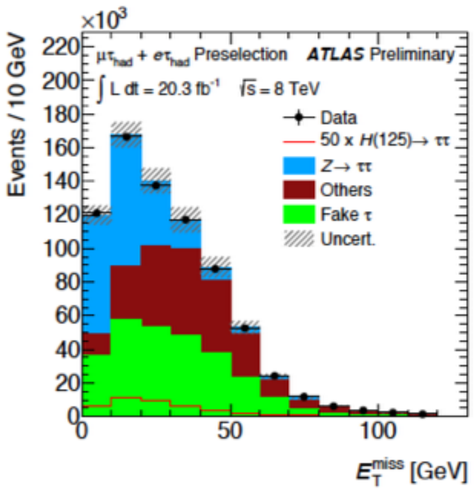

(a)

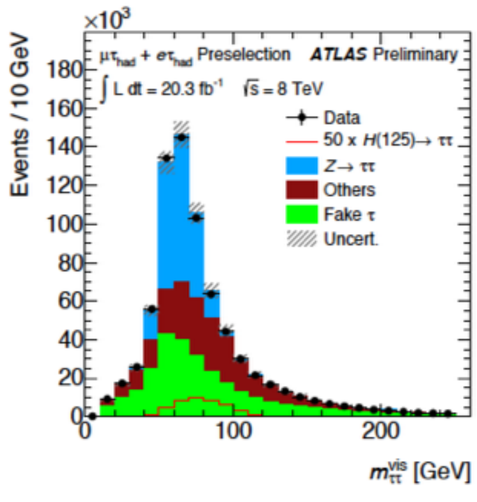

(b)

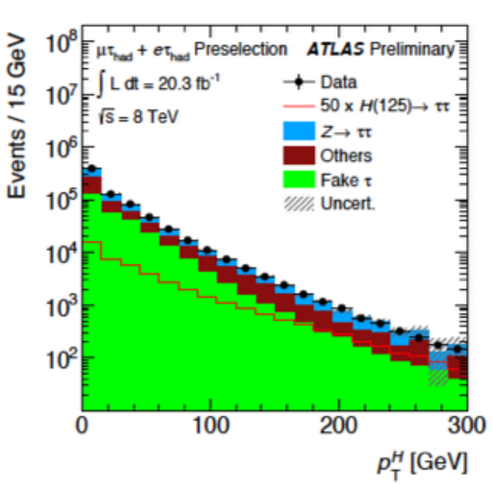

(c)

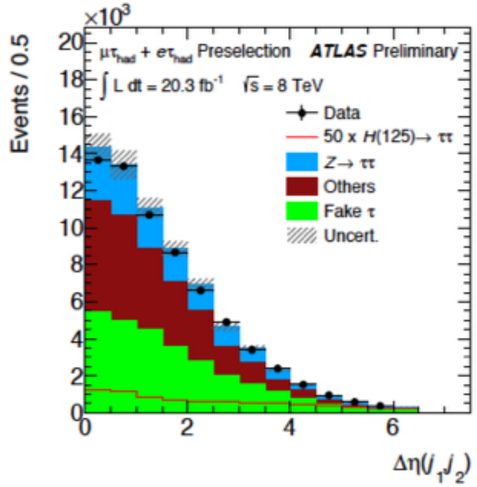

(d)

Figure 2: Kinematic distributions for the $\tau_{lep}\tau_{had}$ channel after preselection: (a) E_T^{miss}, (b) $m_{\tau\tau}^{vis}$, (c) p_T^H, and (d) $\Delta\eta(j_1, j_2)$. The background estimate for these distributions is described in Section 9. The $\Delta\eta(j_1, j_2)$ distribution is shown for events with at least two jets. Signal shapes are shown multiplied by a factor of 50. These figures use background predictions made without the global fit defined in Section 12.

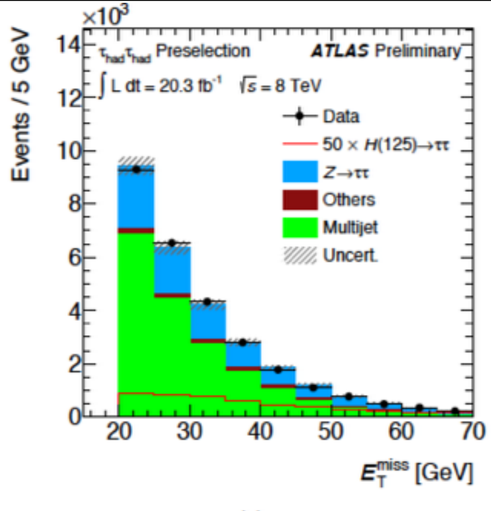

(a)

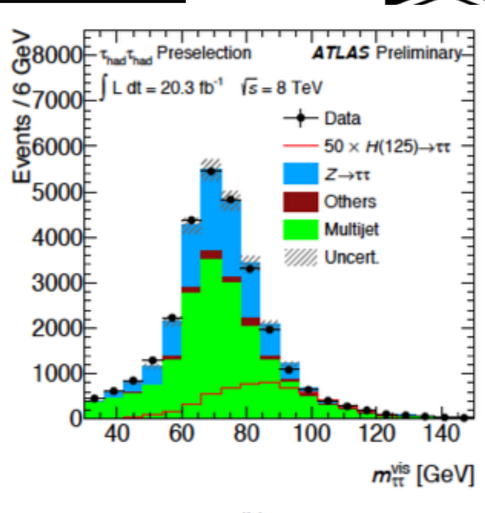

(b)

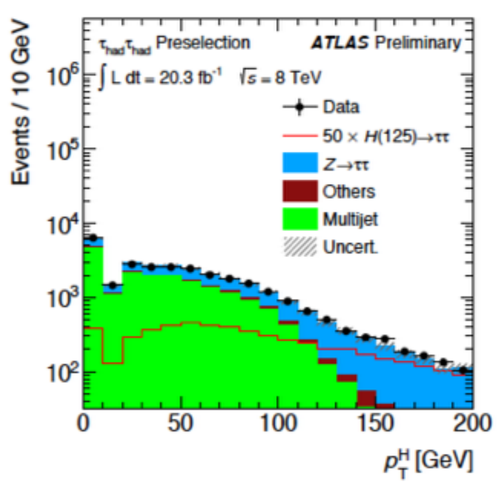

(c)

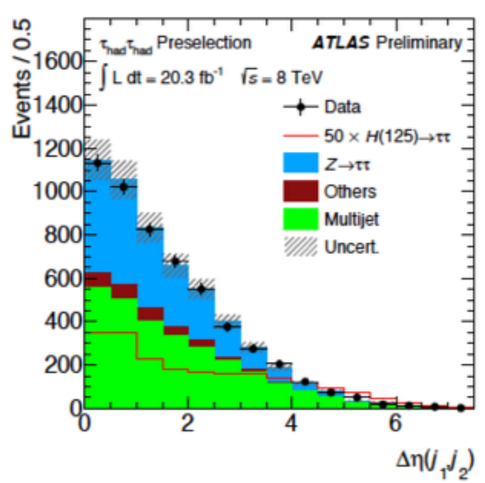

(d)

Figure 3: Kinematic distributions for the $\tau_{had}\tau_{had}$ channel after preselection: (a) E_T^{miss}, (b) $m_{\tau\tau}^{vis}$, (c) p_T^H, and (d) $\Delta\eta(j_1, j_2)$. The background estimate for these distributions is described in Section 9. The $\Delta\eta(j_1, j_2)$ distribution is shown for events with at least two jets. Signal shapes are shown multiplied by a factor of 50. These figures use background predictions made without the global fit defined in Section 12.

H→ττ

TlepTlep yields

Table 4: Predicted event yields in the $\tau_{\text{lep}}\tau_{\text{lep}}$ channel for $m_H = 125$ GeV in the three highest bins of the BDT distributions. The background normalizations, signal normalization, and uncertainties reflect the preferred values from the global fit. The uncertainties on the total background and total signal reflect the full statistical+systematic uncertainty, while the uncertainties on the individual background components reflect the full systematic uncertainty only.

Process/Category	VBF			Boosted		
BDT score bin edges	0.684-0.789	0.789-0.895	0.895-1.0	0.667-0.778	0.778-0.889	0.889-1.0
ggF	0.53 ± 0.26	0.8 ± 0.4	0.7 ± 0.4	5.3 ± 2.1	5.2 ± 2.0	1.7 ± 0.7
VBF	1.15 ± 0.35	2.0 ± 0.6	5.0 ± 1.5	1.01 ± 0.33	1.5 ± 0.5	0.67 ± 0.22
WH	< 0.05	< 0.05	< 0.05	0.71 ± 0.22	0.64 ± 0.20	0.16 ± 0.05
ZH	< 0.05	< 0.05	< 0.05	0.36 ± 0.11	0.32 ± 0.10	0.06 ± 0.02
$Z \to \tau^+\tau^-$	7.6 ± 0.8	9.0 ± 0.9	4.6 ± 0.6	97 ± 7	61.5 ± 3.2	13.6 ± 1.3
Fake	2.8 ± 0.7	5.8 ± 2.0	4.5 ± 1.7	10.1 ± 3.1	15 ± 5	0.79 ± 0.29
Top	4.0 ± 0.9	2.9 ± 0.7	1.8 ± 0.4	28 ± 7	15 ± 4	3.5 ± 0.9
Others	1.97 ± 0.26	3.3 ± 0.4	2.7 ± 0.4	24.7 ± 1.9	8.8 ± 0.6	2.34 ± 0.24
Total Background	16.3 ± 1.5	20.9 ± 2.4	13.5 ± 2.4	160 ± 7	101 ± 4	20.2 ± 1.8
Total Signal	1.7 ± 0.5	2.9 ± 0.9	5.7 ± 1.7	7.4 ± 2.4	7.7 ± 2.5	2.6 ± 0.8
S/B	0.10	0.14	0.42	0.05	0.08	0.13
Data	23	28	19	156	128	20

TlepThad yields

Table 5: Predicted event yields in the $\tau_{\text{lep}}\tau_{\text{had}}$ channel for $m_H = 125$ GeV in the three highest bins of the BDT distributions. The background normalizations, signal normalization, and uncertainties reflect the preferred values from the global fit. The uncertainties on the total background and total signal reflect the full statistical+systematic uncertainty, while the uncertainties on the individual background components reflect the full systematic uncertainty only.

Process/Category	VBF			Boosted		
BDT score bin edges	0.5-0.667	0.667-0.833	0.833-1.0	0.6-0.733	0.733-0.867	0.867-1.0
ggF	2.2 ± 0.9	3.5 ± 1.5	1.2 ± 0.6	7.7 ± 2.9	6.3 ± 2.3	5.5 ± 2.1
VBF	4.1 ± 1.2	9.2 ± 2.7	7.5 ± 2.2	1.7 ± 0.5	1.5 ± 0.5	1.3 ± 0.4
WH	< 0.05	< 0.05	< 0.05	0.95 ± 0.29	0.85 ± 0.26	0.81 ± 0.25
ZH	< 0.05	< 0.05	< 0.05	0.42 ± 0.13	0.47 ± 0.14	0.41 ± 0.12
$Z \to \tau^+\tau^-$	28.6 ± 1.4	25.0 ± 1.6	2.41 ± 0.35	48.3 ± 3.4	26.1 ± 2.7	18.4 ± 2.0
Fake	37.7 ± 1.8	27.9 ± 2.1	3.5 ± 0.5	27 ± 4	10.8 ± 1.8	5.8 ± 1.4
Top	6.5 ± 0.7	4.1 ± 0.8	1.5 ± 0.4	7.0 ± 0.9	5.7 ± 0.8	2.23 ± 0.33
Diboson	2.9 ± 0.4	3.0 ± 0.5	0.23 ± 0.04	4.8 ± 0.5	4.0 ± 0.5	1.69 ± 0.23
$Z \to \ell\ell(j \to \tau_{\text{had}})$	8.7 ± 1.7	3.3 ± 0.5	0.40 ± 0.10	3.8 ± 0.5	0.71 ± 0.07	< 0.05
$Z \to \ell\ell(\ell \to \tau_{\text{had}})$	2.8 ± 1.2	1.9 ± 1.2	0.7 ± 0.6	9.4 ± 1.9	4.9 ± 1.1	3.8 ± 1.2
Total Background	87.2 ± 2.7	65 ± 5	8.7 ± 2.5	101 ± 6	52 ± 4	32 ± 4
Total Signal	6.3 ± 1.8	12.7 ± 3.5	8.7 ± 2.4	10.7 ± 3.3	9.2 ± 2.8	8.0 ± 2.5
S/B	0.07	0.20	1.0	0.11	0.18	0.25
Data	90	80	18	103	64	34

ThadThad yields

Table 6: Predicted event yields in the $\tau_{\text{had}}\tau_{\text{had}}$ channel for $m_H = 125$ GeV in the three highest bins of the BDT distributions. The background normalizations, signal normalization, and uncertainties reflect the preferred values from the global fit. The uncertainties on the total background and total signal reflect the full statistical+systematic uncertainty, while the uncertainties on the individual background components reflect the full systematic uncertainty only.

Process/Category	VBF			Boosted		
BDT score bin edges	0.85-0.9	0.9-0.95	0.95-1.0	0.85-0.9	0.9-0.95	0.95-1.0
ggF	0.39 ± 0.17	0.35 ± 0.16	2.0 ± 0.9	2.2 ± 0.8	2.5 ± 1.0	2.3 ± 0.9
VBF	0.57 ± 0.18	0.72 ± 0.22	5.9 ± 1.8	0.55 ± 0.17	0.61 ± 0.19	0.57 ± 0.17
WH	< 0.05	< 0.05	< 0.05	0.34 ± 0.11	0.40 ± 0.12	0.44 ± 0.14
ZH	< 0.05	< 0.05	< 0.05	0.22 ± 0.07	0.22 ± 0.07	0.22 ± 0.07
$Z \to \tau^+\tau^-$	3.2 ± 0.6	3.4 ± 0.7	5.3 ± 1.0	15.7 ± 1.7	12.3 ± 1.8	9.7 ± 1.6
Multijet	3.3 ± 0.6	2.9 ± 0.6	5.9 ± 0.9	5.2 ± 0.6	3.7 ± 0.5	1.40 ± 0.22
Others	0.38 ± 0.09	0.49 ± 0.12	0.64 ± 0.13	1.49 ± 0.27	2.8 ± 0.5	0.07 ± 0.02
Total Background	6.9 ± 1.3	6.8 ± 1.3	11.8 ± 2.6	22.4 ± 2.5	18.8 ± 2.8	11.2 ± 1.9
Total Signal	0.97 ± 0.29	1.09 ± 0.31	8.0 ± 2.2	3.3 ± 1.0	3.8 ± 1.2	3.6 ± 1.1
S/B	0.14	0.16	0.67	0.15	0.2	0.32
Data	6	6	19	20	16	15

systematics

Source of Uncertainty	Uncertainty on μ
Signal region statistics (data)	0.30
$Z \to \ell\ell$ normalization ($\tau_{\text{lep}}\tau_{\text{had}}$ boosted)	0.13
ggF $d\sigma/dp_T^H$	0.12
JES η calibration	0.12
Top normalization ($\tau_{\text{lep}}\tau_{\text{had}}$ VBF)	0.12
Top normalization ($\tau_{\text{lep}}\tau_{\text{had}}$ boosted)	0.12
$Z \to \ell\ell$ normalization ($\tau_{\text{lep}}\tau_{\text{had}}$ VBF)	0.12
QCD scale	0.07
di-τ_{had} trigger efficiency	0.07
Fake backgrounds ($\tau_{\text{lep}}\tau_{\text{lep}}$)	0.07
τ_{had} identification efficiency	0.06
$Z \to \tau^+\tau^-$ normalization ($\tau_{\text{lep}}\tau_{\text{had}}$)	0.06
τ_{had} energy scale	0.06

Table 7: The important sources of uncertainty on the measured signal strength parameter μ, given as absolute uncertainties on μ.

H→ττ BDTs Inputs

definitions

- $p_{\mathrm{T}}^{\mathrm{Total}}$: Magnitude of vector sum of the visible components of the τ decay products, the two leading jets and the $E_{\mathrm{T}}^{\mathrm{miss}}$.
- sum p_{T}: Scalar sum of p_{T} of the visible components of the τ decay products and of the jets.
- $E_{\mathrm{T}}^{\mathrm{miss}}\phi$ centrality: A variable that quantifies the relative angular position of the $E_{\mathrm{T}}^{\mathrm{miss}}$ with respect to the τ decay products in the transverse plane. The transverse plane is transformed such that the direction of the τ decay products are orthogonal, and that the smaller ϕ angle between the τ decay products defines the positive quadrant of the transformed plane. $E_{\mathrm{T}}^{\mathrm{miss}}\phi$ centrality is defined as the sum of the x and y components of the $E_{\mathrm{T}}^{\mathrm{miss}}$ unit vector in this transformed plane.
- sphericity: A variable that describes the isotropy of energy flow. It is based on the quadratic momentum tensor:

$$S^{\alpha\beta} = \frac{\sum_i p_i^\alpha p_i^\beta}{\sum_i |\vec{p}_i^{\,2}|}. \quad (2)$$

Both leptons and the selected jets are considered in the computation. In this equation, α and β are the indices of the tensor, and the summation is performed over the momenta of the leptons and the jets in the event. The sphericity of the event is then defined in terms of the two largest eigenvalues of this tensor, λ_2 and λ_3:

$$S = \frac{3}{2}(\lambda_2 + \lambda_3). \quad (3)$$

- object η centrality: A variable that quantifies the η position of an object (a τ_{had} candidate or an isolated lepton) with respect to the two leading jets in the event. It is defined as

$$C_{\eta_1,\eta_2}(\eta) = \exp\left[\frac{-4}{(\eta_1-\eta_2)^2}\left(\eta - \frac{\eta_1+\eta_2}{2}\right)^2\right] \quad (4)$$

where η_1 and η_2 are the pseudorapidities of the two leading jets. This variable has value 1 when the object is halfway between the two jets, $1/e$ when the object is aligned with one of the jets, and $< 1/e$ when the object is outside the jets. This variable is used for the following BDT inputs: $\ell_1 \times \ell_2$ η centrality (product of the two η centralities), ℓ η centrality, j_3 η centrality and $\tau_{1,2}$ η centrality (η centrality of each τ_{had}). When j_3 η centrality is used, events with only two jets are assigned a dummy value of -0.5.

only VBF as signal

VBF,ggf,VH as signal

Variable	VBF			Boosted		
	$\tau_{\mathrm{lep}}\tau_{\mathrm{lep}}$	$\tau_{\mathrm{lep}}\tau_{\mathrm{had}}$	$\tau_{\mathrm{had}}\tau_{\mathrm{had}}$	$\tau_{\mathrm{lep}}\tau_{\mathrm{lep}}$	$\tau_{\mathrm{lep}}\tau_{\mathrm{had}}$	$\tau_{\mathrm{had}}\tau_{\mathrm{had}}$
$m_{\tau\tau}^{\mathrm{MMC}}$	•	•	•	•	•	•
$\Delta R(\tau,\tau)$	•	•	•		•	•
$\Delta\eta(j_1, j_2)$	•	•	•			
m_{j_1,j_2}	•	•	•			
$\eta_{j_1} \times \eta_{j_2}$		•	•			
$p_{\mathrm{T}}^{\mathrm{Total}}$		•	•			
sum p_{T}					•	•
$p_{\mathrm{T}}(\tau_1)/p_{\mathrm{T}}(\tau_2)$					•	•
$E_{\mathrm{T}}^{\mathrm{miss}}\phi$ centrality		•	•	•	•	•
$x_{\tau 1}$ and $x_{\tau 2}$						•
$m_{\tau\tau,j_1}$				•		
m_{ℓ_1,ℓ_2}				•		
$\Delta\phi_{\ell_1,\ell_2}$				•		
sphericity				•		
$p_{\mathrm{T}}^{\ell_1}$				•		
$p_{\mathrm{T}}^{j_1}$				•		
$E_{\mathrm{T}}^{\mathrm{miss}}/p_{\mathrm{T}}^{\ell_2}$				•		
m_{T}		•			•	
$\min(\Delta\eta_{\ell_1\ell_2,\mathrm{jets}})$	•					
j_3 η centrality	•					
$\ell_1 \times \ell_2$ η centrality	•					
ℓ η centrality		•				
$\tau_{1,2}$ η centrality			•			

Table 3: Discriminating variables used for each channel and category. The filled circles identify which variables are used in each decay mode. Note that variables such as $\Delta R(\tau,\tau)$ are defined either between the two leptons, between the lepton and τ_{had}, or between the two τ_{had} candidates, depending on the decay mode.

VH→bb

event selection

Table 1: The basic event selection for the three channels.

Object	0-lepton	1-lepton	2-lepton
Leptons	0 loose leptons	1 tight lepton + 0 loose leptons	1 medium lepton + 1 loose lepton
Jets	2 b-tags $p_{\mathrm{T}}^{\mathrm{jet}_1} > 45$ GeV $p_{\mathrm{T}}^{\mathrm{jet}_2} > 20$ GeV + ≤ 1 extra jets		
Missing E_T	$E_{\mathrm{T}}^{\mathrm{miss}} > 120$ GeV $p_{\mathrm{T}}^{\mathrm{miss}} > 30$ GeV $\Delta\phi(\boldsymbol{E}_{\mathrm{T}}^{\mathrm{miss}}, \boldsymbol{p}_{\mathrm{T}}^{\mathrm{miss}}) < \pi/2$ $\min[\Delta\phi(\boldsymbol{E}_{\mathrm{T}}^{\mathrm{miss}}, \mathrm{jet})] > 1.5$ $\Delta\phi(\boldsymbol{E}_{\mathrm{T}}^{\mathrm{miss}}, b\bar{b}) > 2.8$	$E_{\mathrm{T}}^{\mathrm{miss}} > 25$ Gev	$E_{\mathrm{T}}^{\mathrm{miss}} < 60$ GeV
Vector Boson	-	$m_{\mathrm{T}}^{W} < 120$ GeV	$83 < m_{\ell\ell} < 99$ GeV

Table 2: Further topological criteria in p_{T}^{V} intervals. The 0-lepton channel does not use the lowest two p_{T}^{V} intervals.

	p_{T}^{V} [GeV]	0-90	90-120	120-160	160-200	>200
All Channels	$\Delta R(b,\bar{b})$	0.7-3.4	0.7-3.0	0.7-2.3	0.7-1.8	<1.4
1-lepton	$E_{\mathrm{T}}^{\mathrm{miss}}$ [GeV]	>25				>50
	m_{T}^{W} [GeV]	40-120			<120	

σ x BR (3 channels)

Table 3: The cross section × branching ratio (BR) and acceptance for the three channels at both 7 and 8 TeV. The branching ratios are calculated considering only decays to muons and electrons for $Z \to \ell\ell$, decays to all three lepton flavours for $W \to \ell\nu$ and decays to neutrinos for $Z \to \nu\nu$. The acceptance is calculated as the fraction of events remaining in the 2-tag signal regions after the full event selection.

$m_H = 125$ GeV at 7 TeV				
$(W/Z)(H \to b\bar{b})$	Cross-section × BR [fb]	Acceptance [%]		
		0-lepton	1-lepton	2-lepton
$Z \to \ell\ell$	12.3	0.0	0.7	8.2
$W \to \ell\nu$	107.1	0.2	3.5	-
$Z \to \nu\nu$	36.4	2.2	-	-
$m_H = 125$ GeV at 8 TeV				
$(W/Z)(H \to b\bar{b})$	Cross-section × BR [fb]	Acceptance [%]		
		0-lepton	1-lepton	2-lepton
$Z \to \ell\ell$	15.3	0.0	0.9	8.4
$W \to \ell\nu$	130.2	0.2	3.3	-
$Z \to \nu\nu$	45.5	2.5	-	-

VH→bb

~~yields~~

Table 5: The fitted numbers of signal and background events and the observed numbers of events, for each lepton channel and in p_T^V intervals for $90 < m_{bb} < 150$ GeV. These numbers are for the combined 7 TeV and 8 TeV datasets, corresponding to integrated luminosities of 4.7 and 20.3 fb^{-1}, respectively. The fitted numbers of signal events are shown for WH and ZH production separately for $m_H = 125$ GeV. The quoted errors on the total background correspond to one standard deviation of the fitted nuisance parameters incorporating both the systematic and statistical uncertainties.

2-jet, 2-tag sample													
	0-lepton			1-lepton					2-lepton				
Process	E_T^{miss} [GeV]			p_T^W [GeV]					p_T^Z [GeV]				
	120-160	160-200	>200	0-90	90-120	120-160	160-200	> 200	0-90	90-120	120-160	160-200	>200
$Z \to \nu\nu$	1.6	0.9	1.0	<0.1	<0.1	<0.1	<0.1	<0.1	<0.1	<0.1	<0.1	<0.1	<0.1
$Z \to \ell\ell$	<0.1	<0.1	<0.1	0.2	<0.1	<0.1	<0.1	<0.1	2.1	0.5	0.4	0.2	0.2
$W \to \ell\nu$	0.4	0.2	0.2	7.6	1.7	1.2	1.0	1.1	<0.1	<0.1	<0.1	<0.1	<0.1
VH total	2.0	1.1	1.1	7.8	1.8	1.2	1.1	1.1	2.1	0.5	0.4	0.2	0.2
VH expected	11	5.8	6.1	42	9.5	6.6	5.6	6.1	11	2.7	2.2	1.1	1.2
Top	159	33	8	2763	729	359	113	40	166	32	8.0	0.5	<0.1
W+c, light	21	5.3	2.7	616	65	27	12	7.8	<0.1	<0.1	<0.1	<0.1	<0.1
W+b	30	10	6.1	909	106	49	25	19	<0.1	<0.1	<0.1	<0.1	<0.1
Z+c, light	23	8.1	5.2	22	2.1	0.5	0.3	0.1	91	12	5.6	1.6	1.0
Z+b	226	71	39	97	13	3.9	1.8	0.5	938	146	64	14	8.3
WW	0.5	0.1	0.1	11	1.0	0.7	0.3	0.2	<0.1	<0.1	<0.1	<0.1	<0.1
VZ	26	11	10	145	20	12	7.6	6.5	60	8.6	4.5	2.2	2.1
Multijet	4.8	1.1	0.7	1306	45.6	8.7	4.8	0.4	<0.1	<0.1	<0.1	<0.1	<0.1
Total Bkg.	491 ± 10	141 ± 3	72 ± 2	5869 ± 64	981 ± 16	460 ± 9	165 ± 4	74 ± 3	1255 ± 24	199 ± 4	82 ± 2	18 ± 1	11.4 ± 0.5
Data	502	143	90	5916	990	458	162	79	1282	204	70	22	6
S/B	0.004	0.008	0.02	0.001	0.002	0.003	0.006	0.02	0.002	0.003	0.005	0.01	0.02

3-jet, 2-tag sample													
	0-lepton			1-lepton					2-lepton				
Process	E_T^{miss} [GeV]			p_T^W [GeV]					p_T^Z [GeV]				
	120-160	160-200	>200	0-90	90-120	120-160	160-200	> 200	0-90	90-120	120-160	160-200	>200
$Z \to \nu\nu$	0.4	0.2	0.3	<0.1	<0.1	<0.1	<0.1	<0.1	<0.1	<0.1	<0.1	<0.1	<0.1
$Z \to \ell\ell$	<0.1	<0.1	<0.1	0.1	<0.1	<0.1	<0.1	<0.1	0.9	0.3	0.2	0.1	0.1
$W \to \ell\nu$	0.1	0.1	<0.1	2.1	0.6	0.5	0.5	0.6	<0.1	<0.1	<0.1	<0.1	<0.1
VH total	0.5	0.3	0.4	2.2	0.6	0.5	0.5	0.6	0.9	0.3	0.2	0.1	0.1
VH expected	2.7	1.6	1.9	12	3.2	2.6	2.8	3.4	4.9	1.4	1.1	0.6	0.7
Top	169	44	13	4444	1171	592	238	121	114	22	5.5	0.3	<0.1
W+c, light	7.1	2.1	1.2	189	23	11.7	6.8	5.4	<0.1	<0.1	<0.1	<0.1	<0.1
W+b	12	4.7	3.3	318	36	21	14	12	<0.1	<0.1	<0.1	<0.1	<0.1
Z+c, light	6.3	2.8	2.5	8.8	0.9	0.4	0.2	0.1	53	9.6	4.5	1.4	1.2
Z+b	59	26	17	56	6.9	2.5	1.4	0.7	509	91	45	12	7.6
WW	0.2	0.1	0.1	4.0	0.5	0.3	0.1	0.1	<0.1	<0.1	<0.1	<0.1	<0.1
VZ	3.7	1.8	2.3	31	4.7	3.1	2.5	3.7	20.1	3.1	1.6	0.9	1.2
Multijet	3.1	0.6	0.4	425	17	5.5	3.0	0.8	<0.1	<0.1	<0.1	<0.1	<0.1
Total Bkg.	260 ± 6	82 ± 2	40 ± 1	5476 ± 57	1260 ± 17	637 ± 11	266 ± 7	143 ± 5	696 ± 16	125 ± 3	57 ± 2	15 ± 1	10 ± 1
Data	287	59	40	5523	1233	639	249	154	734	119	56	13	9
S/B	0.002	0.004	0.009	0.0004	0.0005	0.0008	0.002	0.004	0.001	0.002	0.004	0.008	0.01

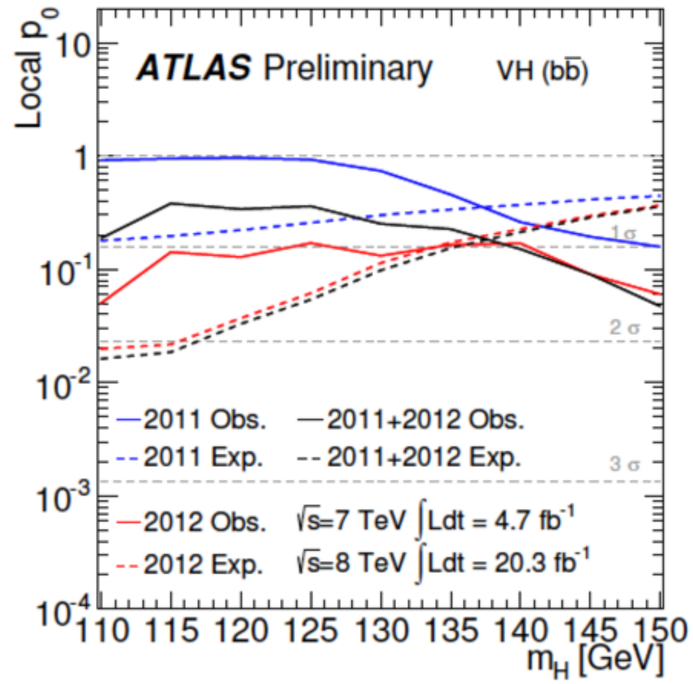

Figure 17: The observed local p_0 as a function of the Higgs boson mass. The dashed curves show the expected local p_0 under the hypothesis of a SM Higgs boson signal at that mass. Results are shown separately for the 7 TeV data (blue), the 8 TeV data (red), and the full dataset (black).

VH->bb

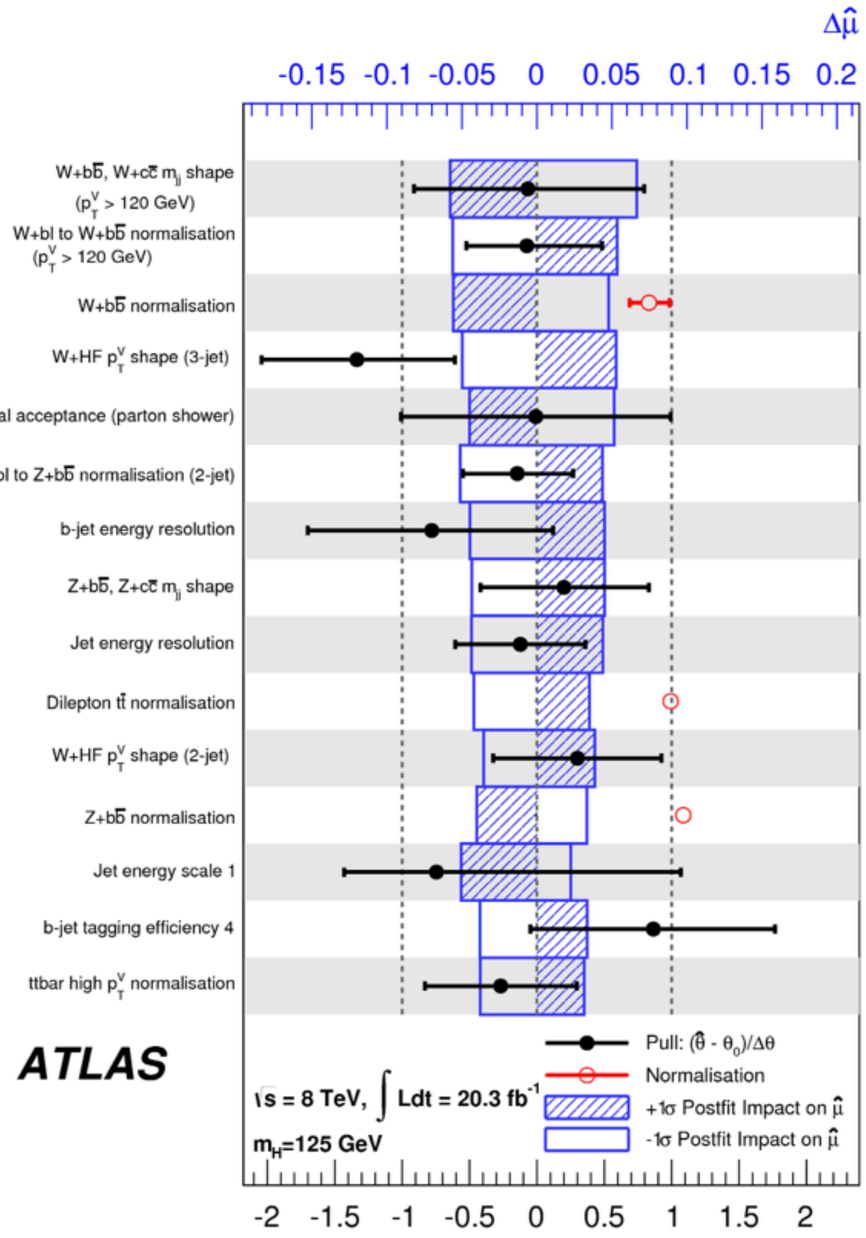
$\Delta\hat{\mu}$
-0.15 -0.1 -0.05 0 0.05 0.1 0.15 0.2
W+bb̄, W+cc̄ m_jj shape (p_T^V > 120 GeV)
W+bl to W+bb̄ normalisation (p_T^V > 120 GeV)
W+bb̄ normalisation
W+HF p_T^V shape (3-jet)
Signal acceptance (parton shower)
Z+bl to Z+bb̄ normalisation (2-jet)
b-jet energy resolution
Z+bb̄, Z+cc̄ m_jj shape
Jet energy resolution
Dilepton tt̄ normalisation
W+HF p_T^V shape (2-jet)
Z+bb̄ normalisation
Jet energy scale 1
b-jet tagging efficiency 4
ttbar high p_T^V normalisation
ATLAS
√s = 8 TeV, ∫ Ldt = 20.3 fb^-1
m_H=125 GeV
Pull: (θ̂ - θ_0)/Δθ
Normalisation
+1σ Postfit Impact on μ̂
-1σ Postfit Impact on μ̂
-2 -1.5 -1 -0.5 0 0.5 1 1.5 2

ATLAS-HIGG-2013-07

H→μμ

- Clean signature with BR~21.9e-05 for m_H=125GeV
- Signature: 2 high-p_T (25(15) GeV) muons of opposite charge at least 1 muon identified in ΔR<0.15
- Categories: Mutually exclusive categories based on η, $p_{T\mu\mu}$ and VBF existence (2 forward high-p_T jets with little hadronic activity)
- Backgrounds: irreducible Z/γ*→μμ, st, ttbar
- Discriminant: $m_{\mu\mu}$ distribution

$\sqrt{s}$ [TeV]	Category	N_S	$\frac{N_S}{\sqrt{N_B}}$	FWHM [GeV]	χ^2/ndof
8	non-cen. low $p_T^{\mu^+\mu^-}$	6.1	0.07	6.6	49.8/48
8	cen. low $p_T^{\mu^+\mu^-}$	2.6	0.06	5.5	52.8/48
8	non-cen. medium $p_T^{\mu^+\mu^-}$	10.4	0.15	6.6	45.1/48
8	cen. medium $p_T^{\mu^+\mu^-}$	4.7	0.13	5.6	36.7/48
8	non-cen. high $p_T^{\mu^+\mu^-}$	5.5	0.13	7.2	26.7/48
8	cen. high $p_T^{\mu^+\mu^-}$	2.6	0.10	6.0	32.3/48
8	VBF	0.8	0.09	7.0	18.6/19
7	non-cen. low $p_T^{\mu^+\mu^-}$	1.0	0.03	6.8	42.0/48
7	cen. low $p_T^{\mu^+\mu^-}$	0.5	0.03	5.3	43.5/48
7	non-cen. medium $p_T^{\mu^+\mu^-}$	1.8	0.06	6.9	41.2/48
7	cen. medium $p_T^{\mu^+\mu^-}$	0.8	0.05	5.5	34.4/48
7	non-cen. high $p_T^{\mu^+\mu^-}$	0.9	0.05	7.5	60.0/48
7	cen. high $p_T^{\mu^+\mu^-}$	0.5	0.05	5.9	56.2/48
7	VBF	0.1	0.05	6.9	6.2/19

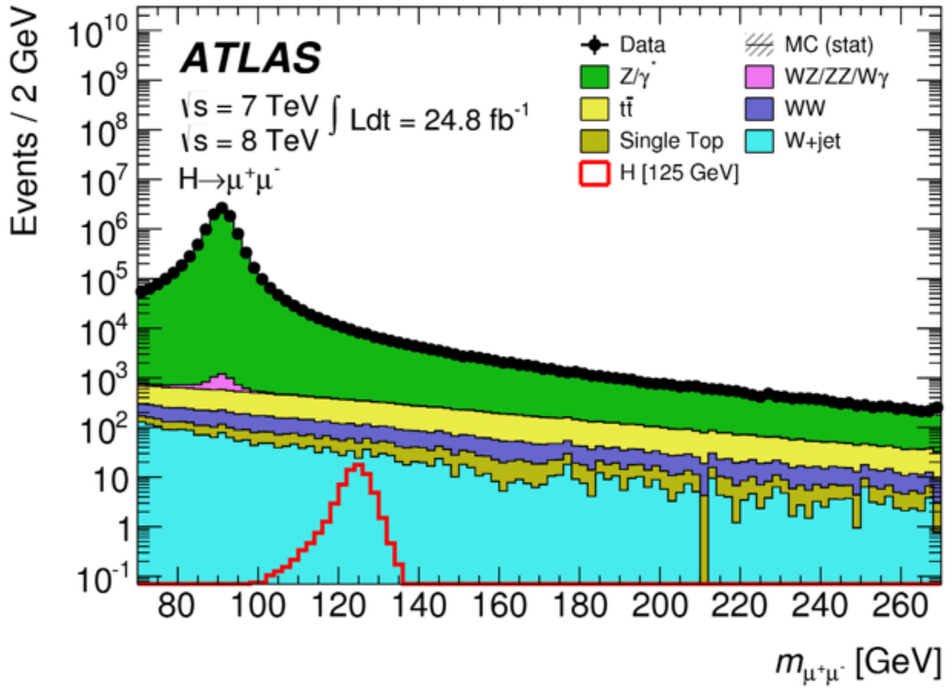

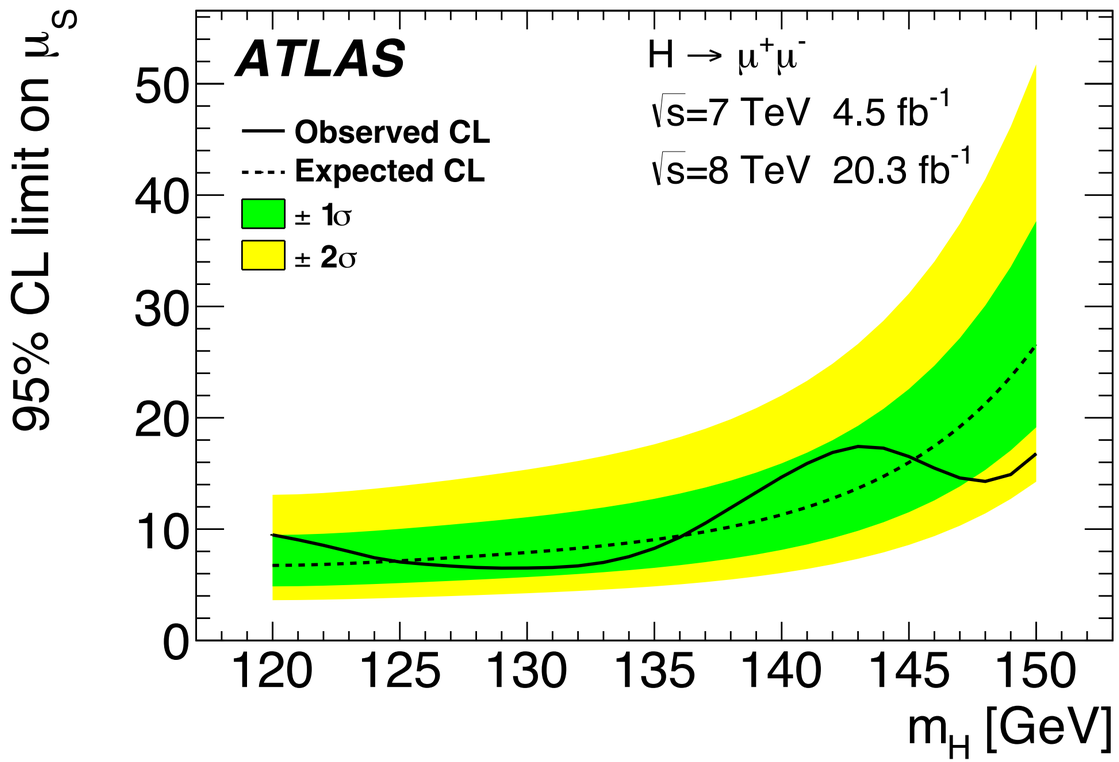

for mH=125.5GeV

95% upper limit on μs

7.0 (7.2) x SM

H→Zγ

- BR~1.6 e-3 for m_H=125.5GeV
  - Loop mediated Higgs decay, *sensitive to New Physics*
- Narrow peak at llγ invariant mass.
- Signature: ee/μμ + γ
  - One photon & two OS SF leptons & one primary vertex
  - signal efficiency eeγ (μμγ) : 27% (33%)
- Backgrounds:
  - Z+γ continuum + radiative Z→llγ (82%)
  - Z+jets (17%)
  - ttbar, WZ (~ 1%)
- Discriminant: $m_{ll\gamma}$ distribution, after correction
  - on photon pseudorapidity and E_T
  - muon momenta corrected for collinear FSR
  - lepton momenta recalculation by means of Z-mass constrained fit

$\sqrt{s}$ [TeV]	ℓ	Category	N_S	N_B	N_D	$\frac{N_S}{\sqrt{N_B}}$	FWHM [GeV]
8	μ	high p_{Tt}	2.3	310	324	0.13	3.8
8	μ	low p_{Tt}, low $\Delta\eta$	3.7	1600	1587	0.09	3.8
8	μ	low p_{Tt}, high $\Delta\eta$	0.8	600	602	0.03	4.1
8	e	high p_{Tt}	1.9	260	270	0.12	3.9
8	e	low p_{Tt}, low $\Delta\eta$	2.9	1300	1304	0.08	4.2
8	e	low p_{Tt}, high $\Delta\eta$	0.6	430	421	0.03	4.5
7	μ	high p_{Tt}	0.4	40	40	0.06	3.9
7	μ	low p_{Tt}	0.6	340	335	0.03	3.9
7	e	high p_{Tt}	0.3	25	21	0.06	3.9
7	e	low p_{Tt}	0.5	240	234	0.03	4.0

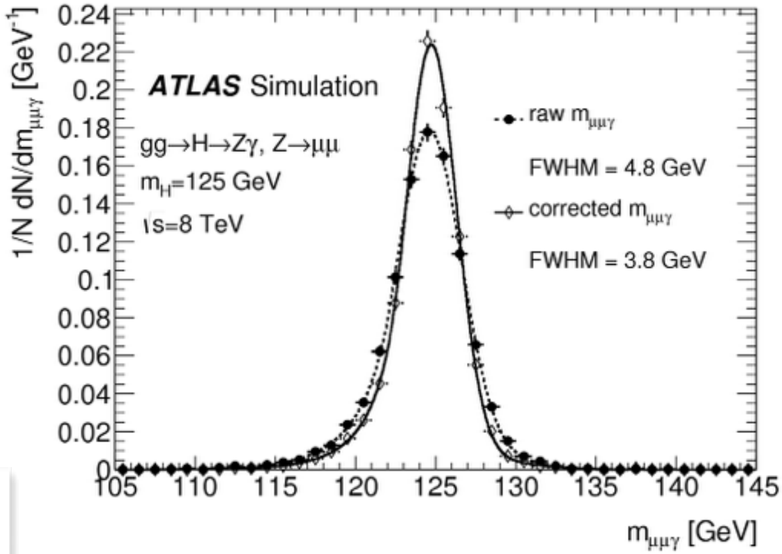

Phys. Lett. B 732(2014), pp.8-27

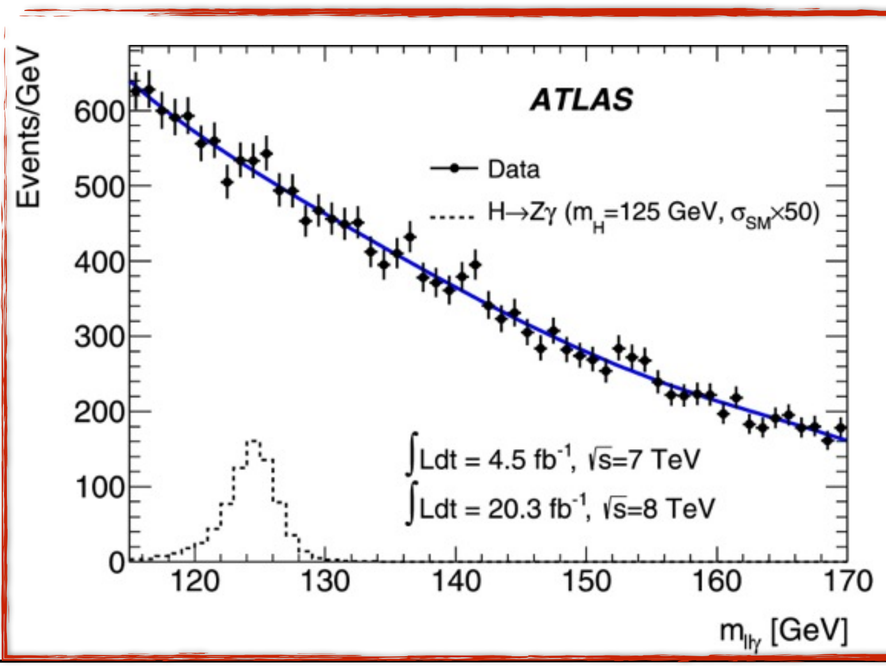

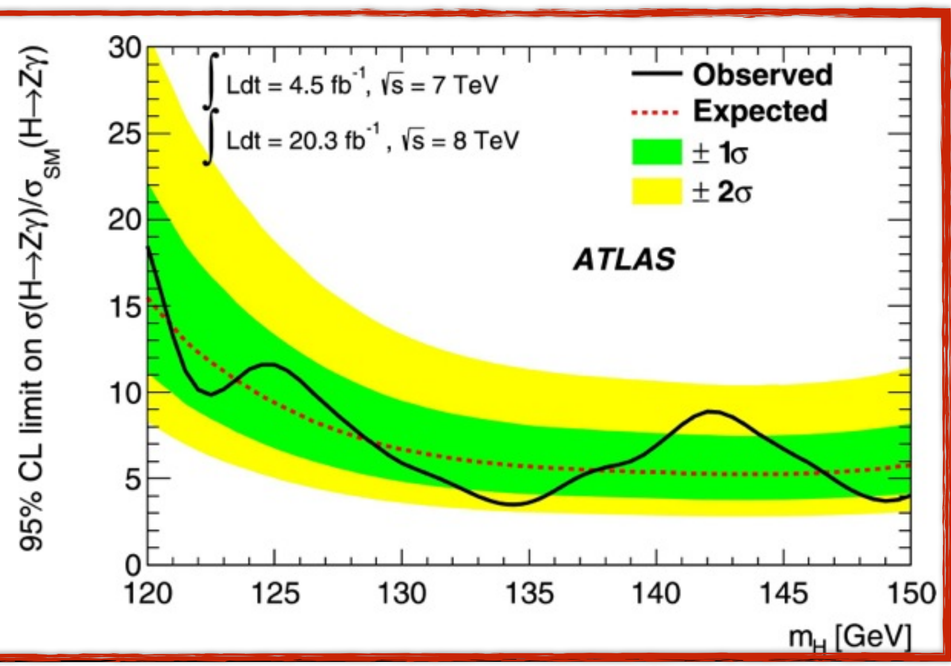

For mH=125.5GeV

0.2σ (0.6σ) significance

95% CLs upper limit:
11(9) x SM

Couplings: Beyond SM

- Contributions from new particles (in loops or final states) are probed
- Assumption: All SM coupling scale factors fixed at 1
- For H→γγ and gg→H vertices κg, κγ are introduced

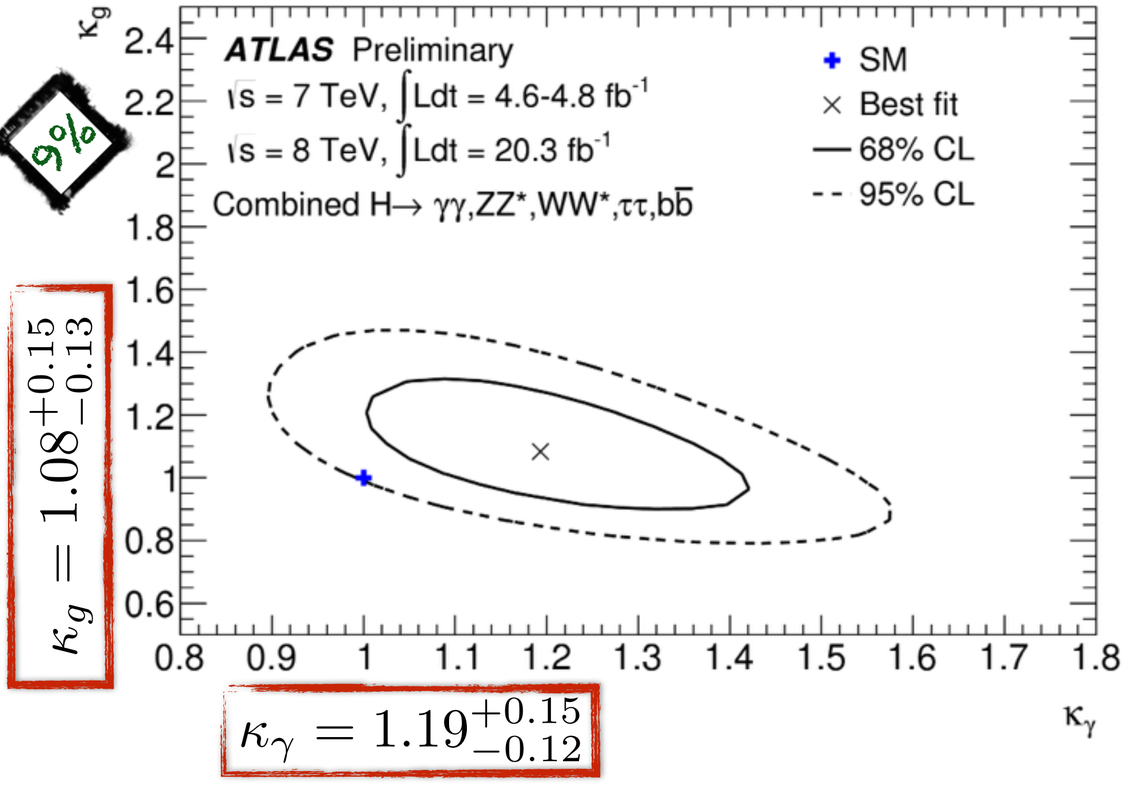

9%

$\kappa_g = 1.08^{+0.15}_{-0.13}$

$\kappa_\gamma = 1.19^{+0.15}_{-0.12}$

ATLAS-CONF-2014-009

18%

Potential new particles contributions to H→γγ and gg→H loops

- Possible contributions to the total width through direct invisible decays or non-distinguishable from background final states

- Releasing the assumption parametrization of Γ_H with the BRi.,u.

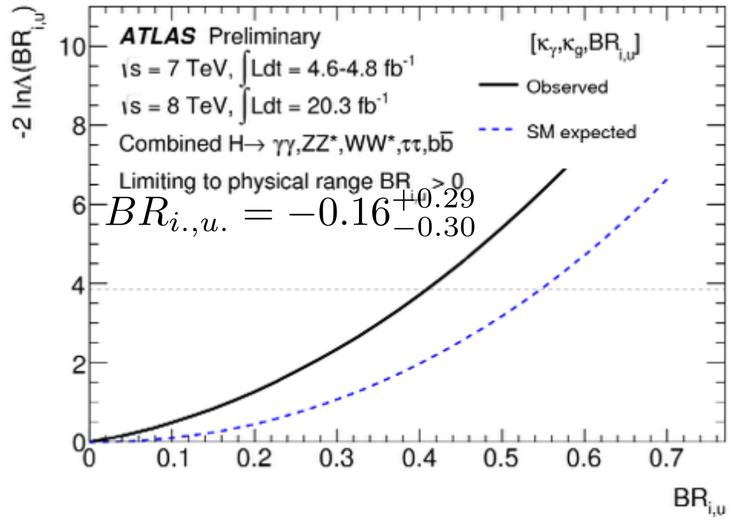

$BR_{i.,u.} = -0.16^{+0.29}_{-0.30}$

$$\Gamma_H = \frac{\kappa_H^2(\kappa_i)}{(1-BR_{i.,u.})}\Gamma_H$$

using the physical BR>0 upper limit at 95% CL:
BRi.,u.<0.41 (0.55)

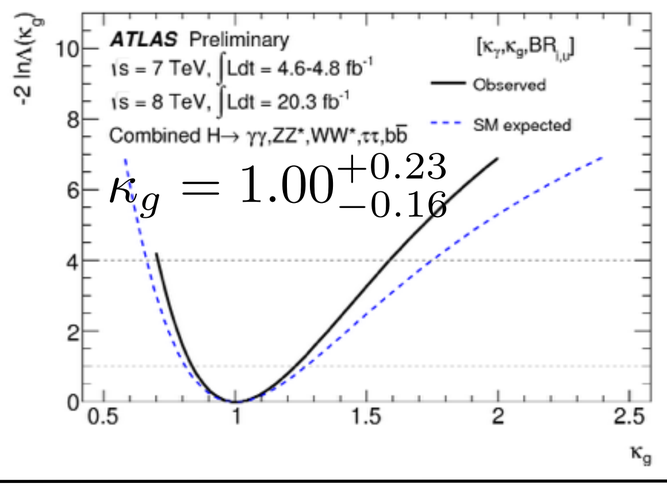

$\kappa_g = 1.00^{+0.23}_{-0.16}$

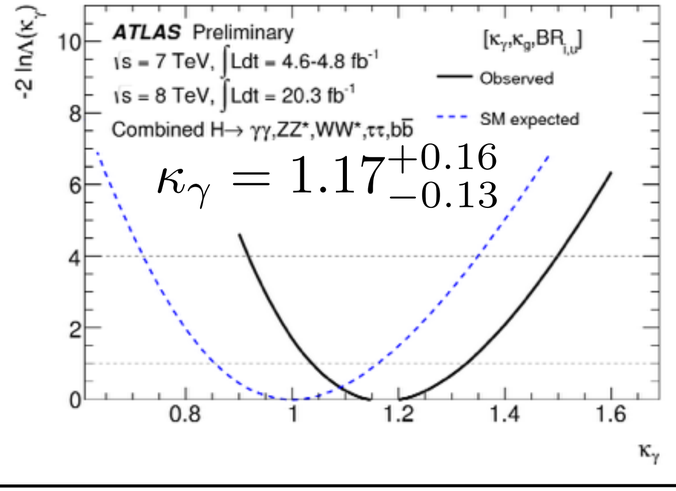

$\kappa_\gamma = 1.17^{+0.16}_{-0.13}$

Couplings: Summary

- κW, κZ, κ

ATLAS-CONF-2014-009

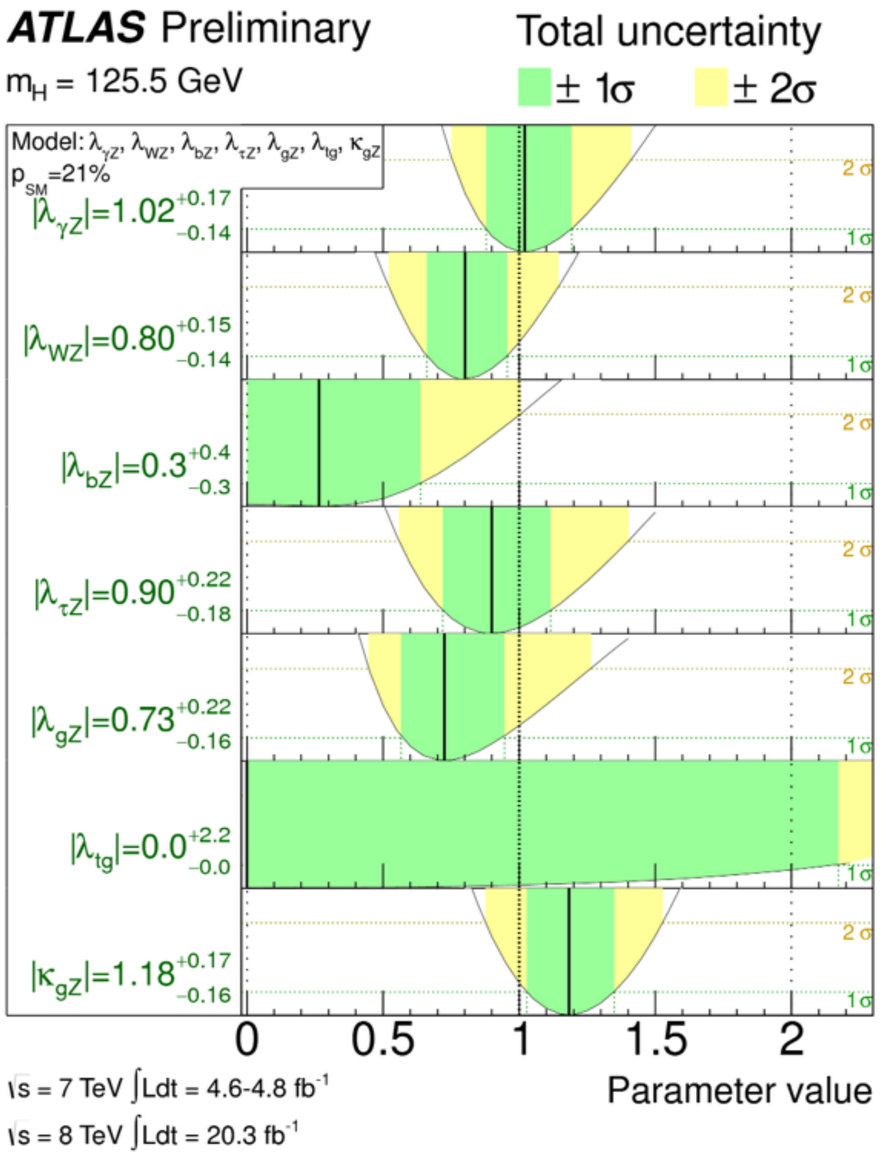

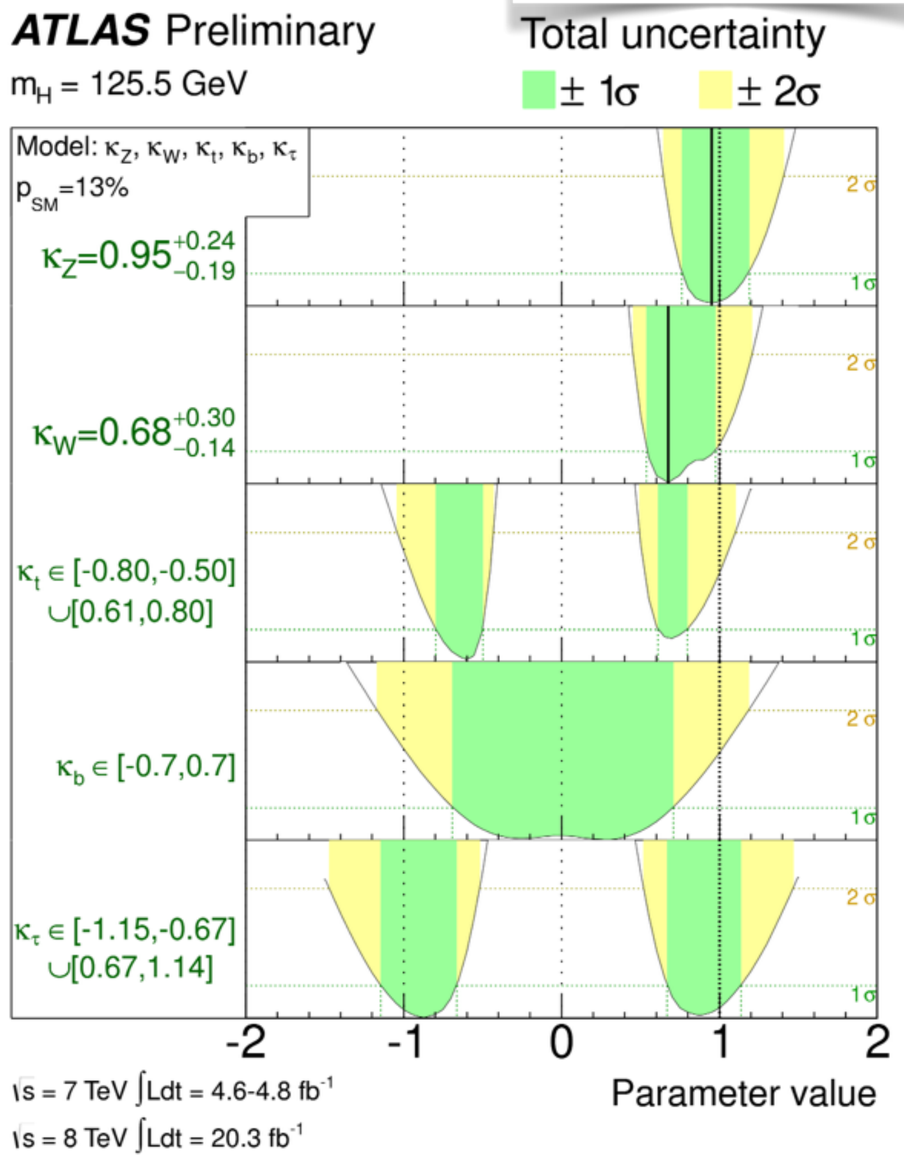

Spin: H→γγ

ATLAS-CONF-2013-029

Table 2: Systematic uncertainties on the relative yields in each bin of $|\cos\theta^*|$ (in %) for the spin-0 signal (from the interference between $gg \to H \to \gamma\gamma$ and $gg \to \gamma\gamma$) and for the spin-2 signal produced via gluon fusion (from the uncertainty on the p_T spectrum).

$\lvert\cos\theta^*\rvert$	0.05	0.15	0.25	0.35	0.45	0.55	0.65	0.75	0.85	0.95
Spin-0 (%)	−0.4	−0.4	−0.3	−0.2	−0.1	0.1	0.4	0.7	1.0	5.4
Spin-2, gg (%)	−1.2	−1.8	−2.1	−2.7	−3.4	−4.1	−3.5	−1.2	27	46

- Discriminating variable:
polar angle of γ wrt z-axis of the Collins-Soper frame (minimize effect of ISR)
- Analysis similar to "rate/mass" analysis
  - $p_{T\gamma 1}$>0.35 $m_{\gamma\gamma}$ and $p_{T\gamma 2}$>0.25 $m_{\gamma\gamma}$
  [Minimize $m_{\gamma\gamma}$ and cosθ* correlations for background]
- H→γγ is a low S/B final state (inclusive ~3%)
  - Simultaneous fit
    $m_{\gamma\gamma}$ and |cosθ*| in signal region
    $m_{\gamma\gamma}$ in side-bands

Phys.Rev.Lett.90:252001,2003 We write the fractional interference correction to the resonance, for polarized gluons and photons, as

$$\delta \equiv \frac{\delta\hat{\sigma}}{\hat{\sigma}} = 2m_H\Gamma_H \,\mathrm{Im}\left[\frac{\mathcal{A}^{(1)}_{\mathrm{cont}}}{\mathcal{A}^{(1)}_{gg\to H}\mathcal{A}^{(1)}_{H\to\gamma\gamma}} \times \left(1 + \frac{\mathcal{A}^{(2)}_{\mathrm{cont}}}{\mathcal{A}^{(1)}_{\mathrm{cont}}} - \frac{\mathcal{A}^{(2)}_{gg\to H}}{\mathcal{A}^{(1)}_{gg\to H}} - \frac{\mathcal{A}^{(2)}_{H\to\gamma\gamma}}{\mathcal{A}^{(1)}_{H\to\gamma\gamma}}\right)\right]$$

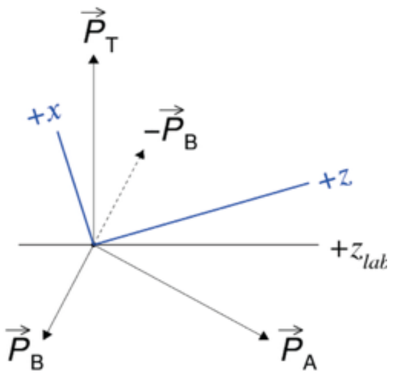

- Particles A,B are gluons that fuse into Higgs
- z-axis is the bisection of P_A and $-P_B$
- x-axis is "away"-vector of P_A+P_B and also direction of Higgs in lab frame

Spin/CP: H→γγ spin

- H→γγ contributes in the spin-2 exclusion,
  - Due to the decay into two photons, the spin-1 hypothesis is strongly disfavored (Landay-Yang theorem)
- Main background: non-resonant γγ → between spin-0 & spin-2
- Discriminant: $|\cos\theta^*|$ in the Collins-Soper frame and mγγ (min. ISR)

$$|cos\theta^*| = \frac{|sinh(\Delta\eta^{\gamma\gamma})|}{\sqrt{1+(\frac{p_T^{\gamma\gamma}}{m_{\gamma\gamma}})^2}} \cdot \frac{2p_T^{\gamma 1}p_T^{\gamma 2}}{m_{\gamma\gamma}^2}$$

Negligible effect of correlations for $|\cos\theta^*|<0.8$, ~10% for =1 Corrected and taken as systematic uncertainty

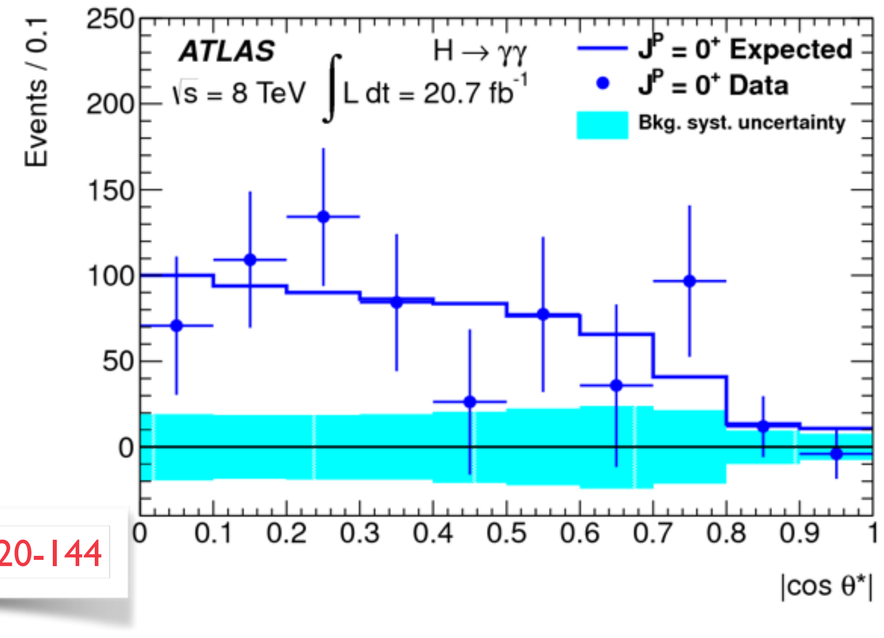

Phys. Lett. B 726(2013), pp.120-144

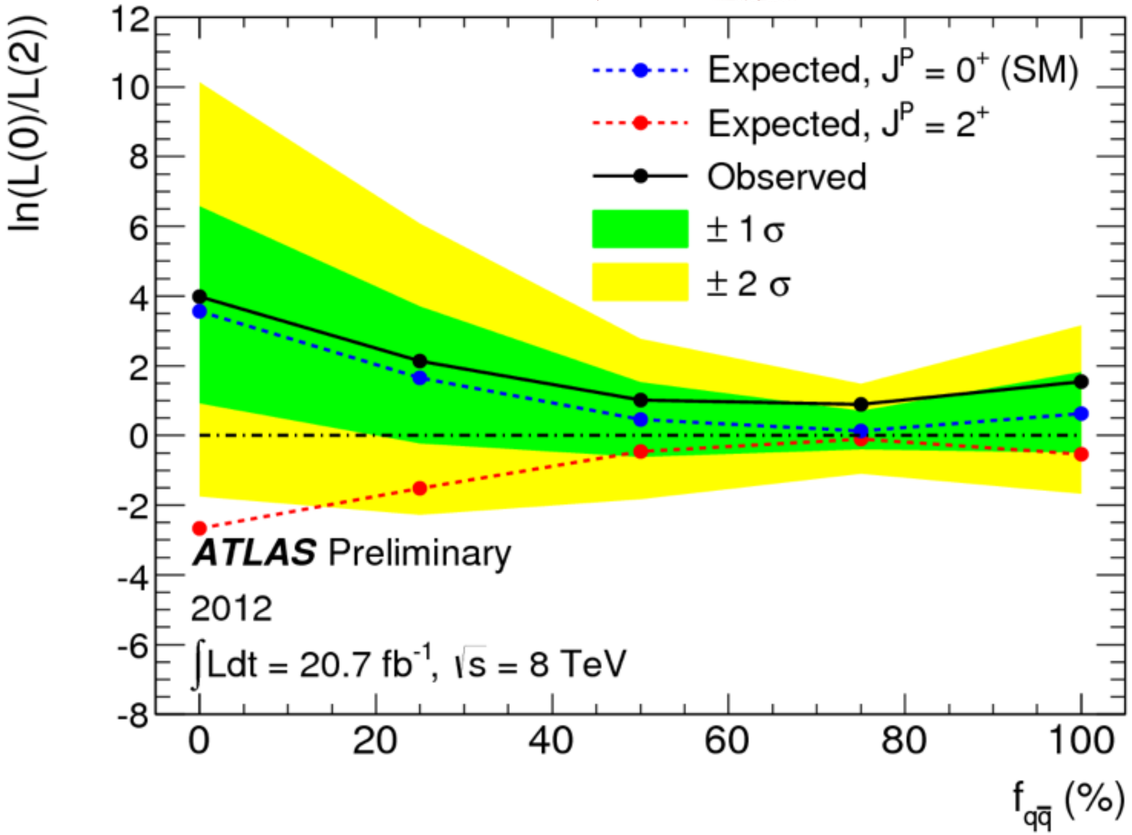

$f_{q\bar{q}}$	$CL(J^P = 2^+)$
100%	0.124
75%	0.337
50%	0.260
25%	0.054
0%	0.007

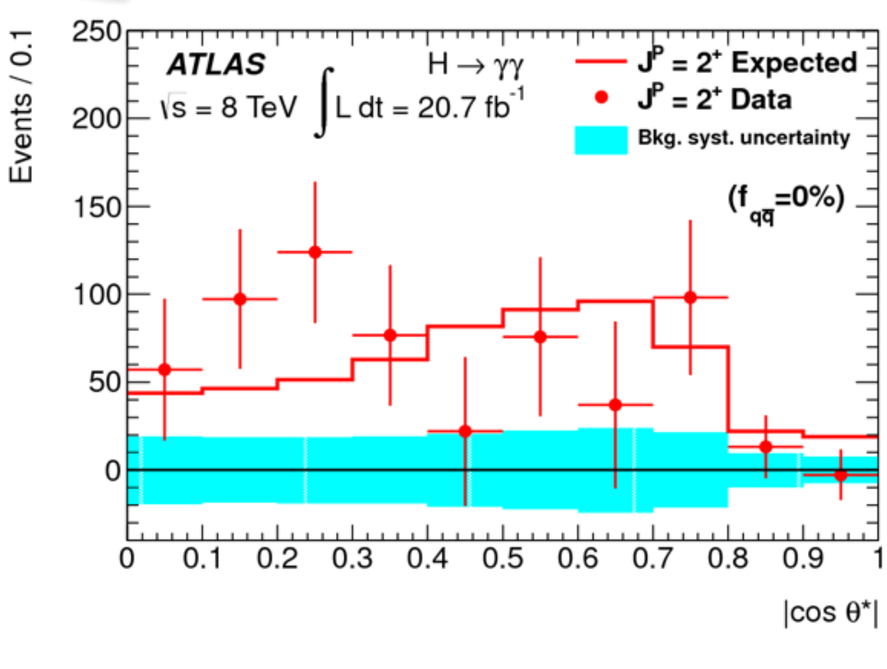

Spin: H→ZZ

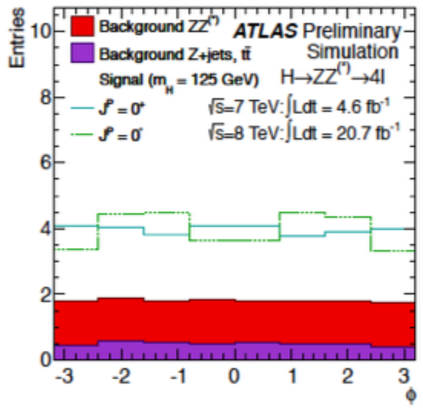

(a)

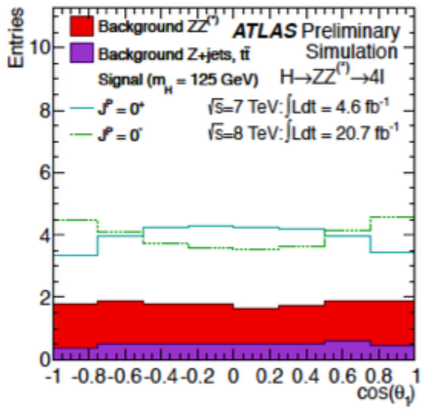

(b)

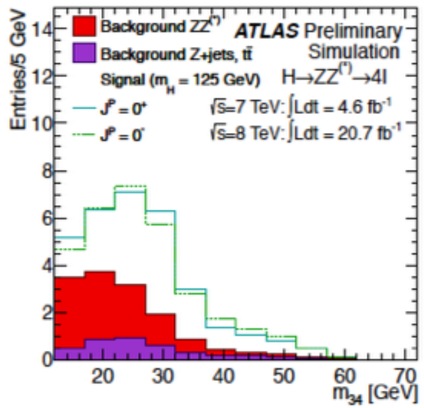

(c)

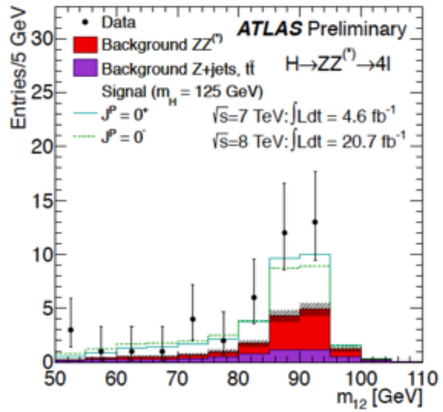

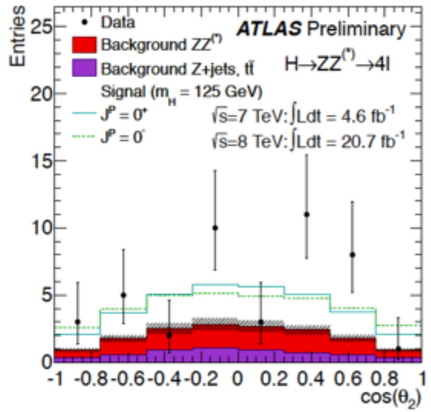

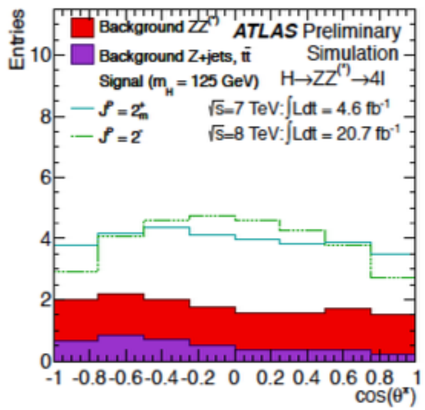

(d)

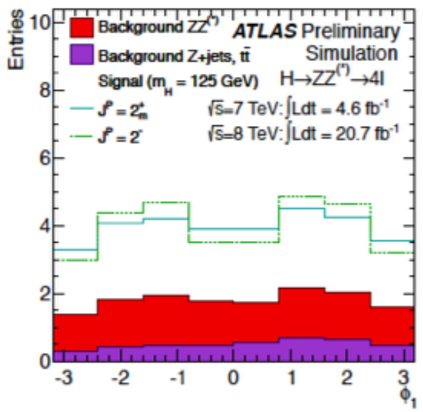

(e)

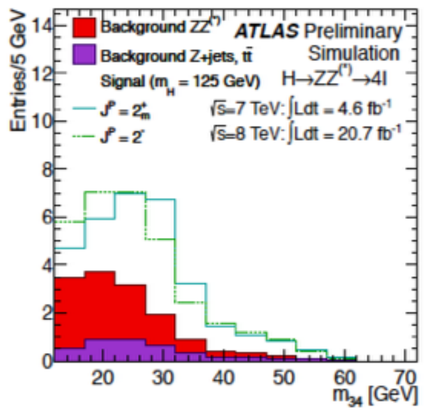

(f)

ATLAS-CONF-2013-013

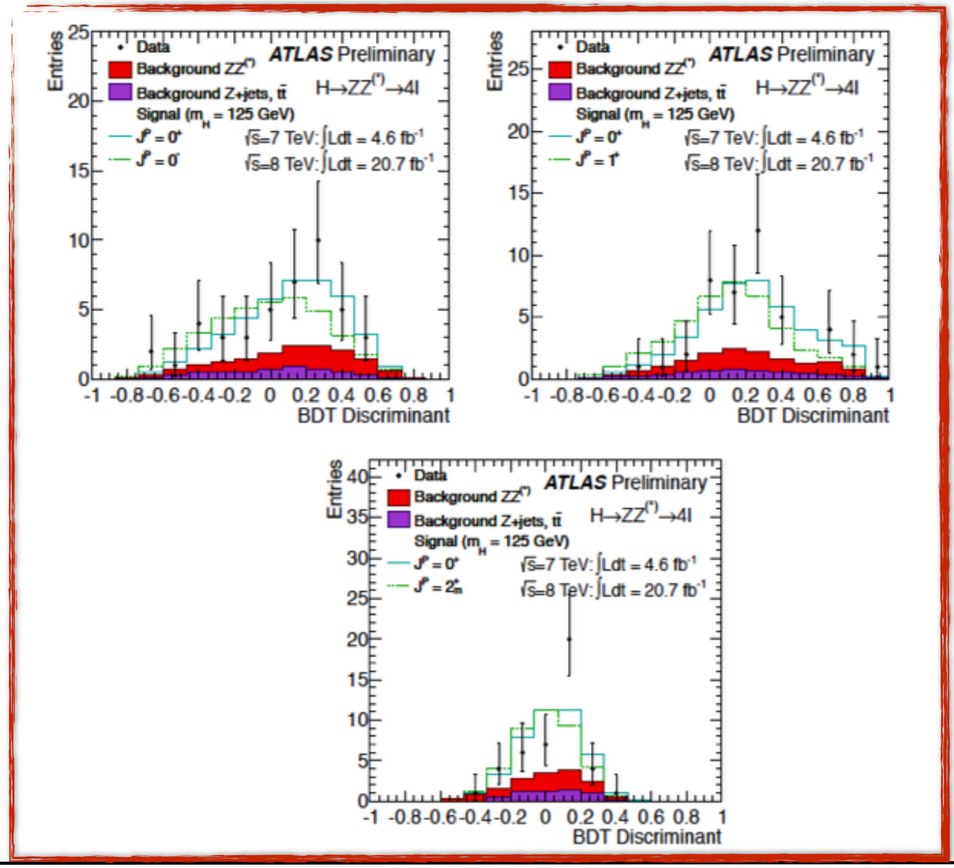

Phys. Lett. B 726(2013), pp.120-144
ATLAS-CONF-2013-031

Spin: H→WW

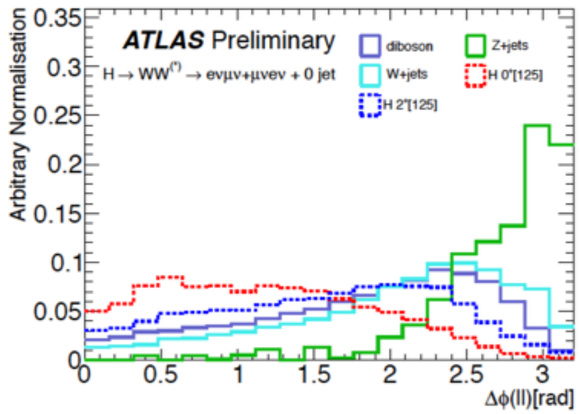

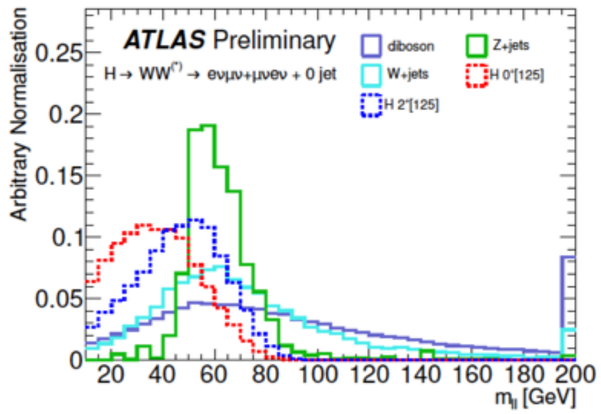

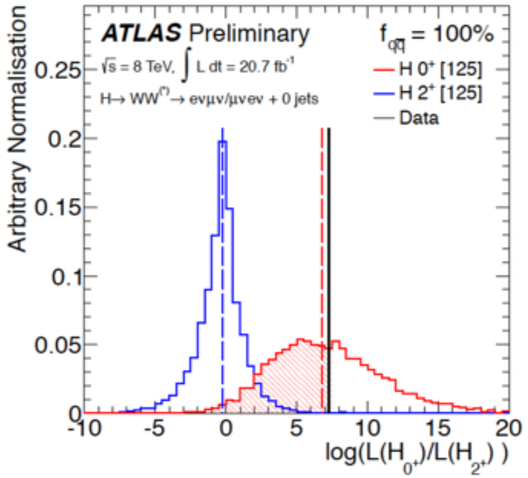

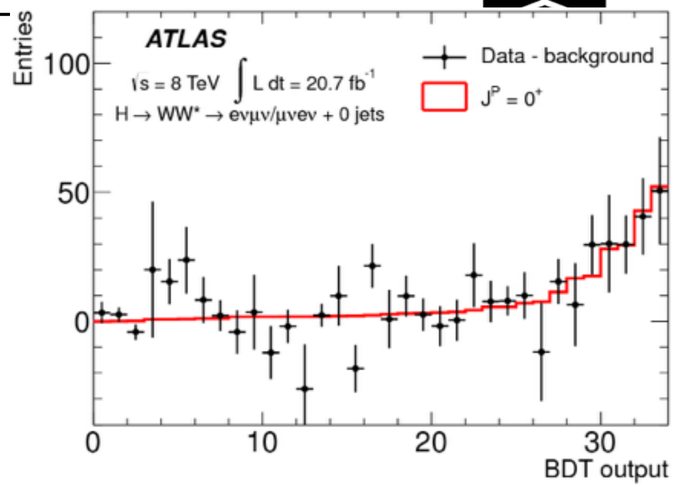

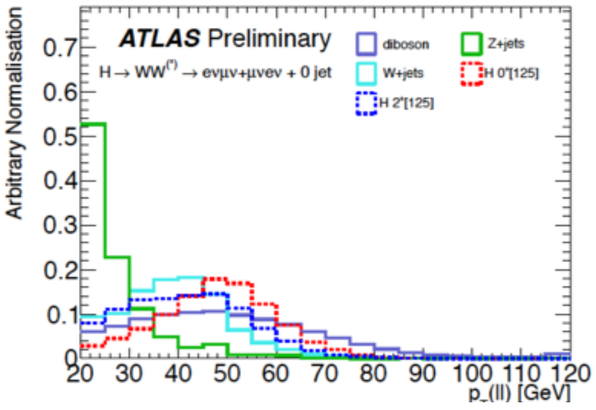

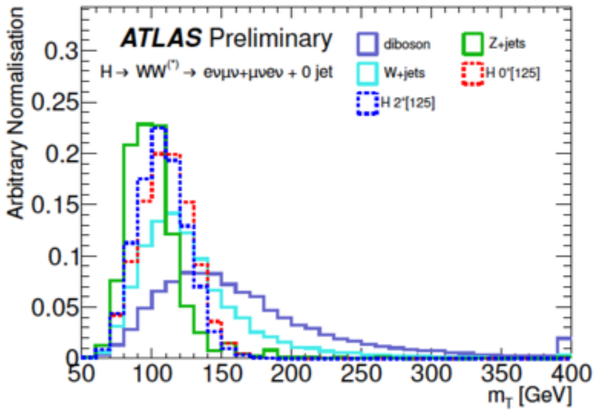

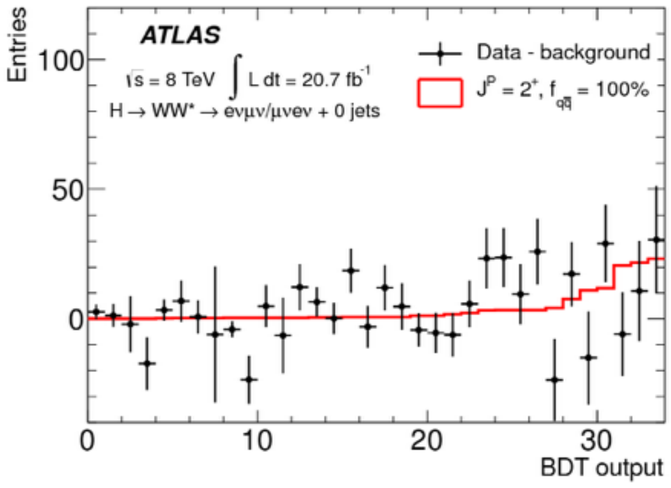

Source	Uncertainty (%)
Jet energy scale & resolution	± 9
WW normalisation, theory	± 9
W+jets fake factor	± 8
Lepton scale & resolution	± 6
Other backgrounds, theory	± 5
Pileup modelling	± 4
PDF model	± 4
$E_{\mathrm{T}}^{\mathrm{miss}}$ scale & resolution	± 3

$f_{q\bar{q}}$	$N_{\mathrm{fit}}(0^+)$	$N_{\mathrm{fit}}(2^+_m)$	exp. $p_0(0^+)$	exp. $p_0(2^+_m)$	obs. $p_0(0^+)$	obs. $p_0(2^+_m)$	1-CL_S (2^+_m)
100%	270^{+100}_{-80}	110^{+110}_{-90}	0.013	0.005	0.543	0.005	0.99
75%	250^{+100}_{-80}	170^{+110}_{-100}	0.034	0.007	0.591	0.005	0.99
50%	250^{+100}_{-80}	230^{+140}_{-100}	0.035	0.012	0.619	0.007	0.98
25%	260^{+110}_{-80}	260^{+130}_{-110}	0.048	0.019	0.613	0.010	0.97
0%	260^{+100}_{-80}	320^{+130}_{-110}	0.091	0.057	0.725	0.014	0.95